



Executive summary

A Flight Dynamics Helicopter UAV Model For A Single Pitch-Lag-Flap Main Rotor

Modeling & Simulations

Problem area

The main objective of this paper is twofold, first we derive the coupled flap-lag equations of motion for a rigid articulated Pitch-Lag-Flap (P-L-F) rotor, with hinge springs and viscous dampers, for both CW and CCW rotating main rotors, with all hinges physically separated. The equations are obtained by the Lagrangian method. The flap-lag equations of motion are valid for small flap, lag, and pitch angles. Further the exact tangential and perpendicular blade velocity expressions are used, hence full coupling between vehicle and blade dynamics is modeled. Second the purpose of this work is to present a UAV helicopter flight dynamics model for a single articulated (P-L-F) main rotor with rigid blades, for both CW and CCW main rotor rotations, valid for a range of flight conditions, including the VRS, and applicable for high bandwidth control specifications. The model

includes the two most relevant helicopter components, i.e. the main and tail rotors; other components such as the fuselage and tail may be added at a later stage. The paper outlines also a detailed review of all assumptions made in deriving the model, i.e. structural, aerodynamics, and dynamical simplifications.

Results and conclusions

Simulation results show that the nonlinear UAV model is in good agreement with an equivalent nonlinear FLIGHTLAB model, for static (trim) conditions, and for dynamic conditions from hover to approximately 10 m/s.

Applicability

The present model could potentially be used to investigate UAV flight in the VRS, additionally a simplified version of this model is currently being exploited for the development of nonlinear optimal control schemes.

Report no.

NLR-TP-2010-286-PT-1

Author(s)

S. Taamallah

Report classification

UNCLASSIFIED

Date

July 2011

Knowledge area(s)

Helikoptertechnologie

Descriptor(s)

Unmanned Aerial Vehicle (UAV)
Helicopter flight dynamics
Main rotor flap-lag
Dynamic inflow
Vortex-Ring-State (VRS)

UNCLASSIFIED

**A Flight Dynamics Helicopter UAV Model
For A Single Pitch-Lag-Flap Main Rotor**
Modeling & Simulations

Nationaal Lucht- en Ruimtevaartlaboratorium, National Aerospace Laboratory NLR

Anthony Fokkerweg 2, 1059 CM Amsterdam,
P.O. Box 90502, 1006 BM Amsterdam, The Netherlands
Telephone +31 20 511 31 13, Fax +31 20 511 32 10, Web site: www.nlr.nl

UNCLASSIFIED



NLR-TP-2010-286-PT-1

A Flight Dynamics Helicopter UAV Model For A Single Pitch-Lag-Flap Main Rotor

Modeling & Simulations


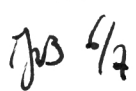
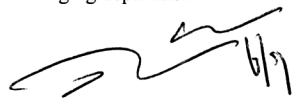
S. Taamallah

This report is based on a paper (with same title) accepted for publication at the 36th European Rotorcraft Forum, Paris, September 7-9, 2010.

The contents of this report may be cited on condition that full credit is given to NLR and the authors. This publication has been refereed by the Advisory Committee AEROSPACE SYSTEMS & APPLICATIONS and AEROSPACE VEHICLES.

Customer	National Aerospace Laboratory NLR
Contract number	----
Owner	National Aerospace Laboratory NLR
Division NLR	Aerospace Systems and Applications
Distribution	Unlimited
Classification of title	Unclassified
	July 2011

Approved by:

Author 	Reviewer  6/7	Managing department  6/7
---	---	--

A Flight Dynamics Helicopter UAV Model For A Single Pitch-Lag-Flap Main Rotor

Skander Taamallah*[†]

Keywords: Unmanned Aerial Vehicle (UAV), helicopter flight dynamics; main rotor flap-lag; dynamic inflow; vortex-ring-state (VRS)

Abstract: We present a UAV helicopter flight dynamics nonlinear model for a flybarless articulated Pitch-Lag-Flap (P-L-F) main rotor with rigid blades, applicable for high bandwidth control specifications, for both Clock-Wise (CW) and Counter-ClockWise (CCW) main rotor rotation, and valid for a range of flight conditions including autorotation and the Vortex-Ring-State (VRS). The model includes the main and tail rotors. Additionally, the paper reviews all assumptions made in deriving the model, i.e. structural, aerodynamics, and dynamical simplifications. Simulation results show that the match between this model and an equivalent nonlinear FLIGHTLAB[®] model is very good for static (trim) conditions, is good for dynamic conditions from hover to medium speed flight, and is fair to good for dynamic conditions at high speed. Hence, this model could potentially be used to simulate and investigate the flight dynamics of a flybarless UAV helicopter, including in autorotation and VRS conditions.

1 Introduction

In the past twenty years the availability of increasingly miniaturized, high performance, reliable, and accurate sensors, together with advances in computing power, has allowed for sustained research and development effort in robotics¹, flying robots, and hence Unmanned Aerial Vehicles (UAVs)².

*Avionics Systems Department, National Aerospace Laboratory (NLR), Anthony Fokkerweg 2, 1059 CM Amsterdam, The Netherlands (staamall@nlr.nl).

[†]Delft Center for Systems and Control (DCSC), Faculty of Mechanical, Maritime and Materials Engineering, Delft University of Technology, Mekelweg 2, 2628 CD Delft, The Netherlands.

¹Robotics is a science of integration, requiring a framework for theories of traditional disciplines and experimentation to interact [113]

²Note that industry and the regulators have now adopted UAS rather than UAV as the preferred term for Unmanned Aircraft, as UAS encompasses all aspects of deploying these vehicles and not just the platform itself [163]

1.1 Unmanned Aerial Vehicles

A UAV, whether fixed- or rotary-wing, is often defined as an unmanned, powered aerial vehicle, that uses aerodynamic forces to generate lift, flies either autonomously or under remote control, and which carries a lethal or non-lethal payload [62].

Over the years, UAVs have been developed for both civilian and military purposes. Their *raison d'être* stems from a need for real-time information. The nature of this information spans a broad spectrum of domains: visual, electromagnetic, physical, nuclear, biological, chemical, and meteorological. Typically the benefits of unmanned systems have been associated with the so-called *DDD* tasks: Dull (e.g. long duration), Dirty (e.g. sampling for hazardous materials), and Dangerous (e.g. extreme exposure to hostile action) [62].

Further many of the civilian or military missions may require deployment, operation, and recovery from unprepared or confined sites such as within a city and between buildings, from a naval ship, or inside a forest. Now due to the helicopter's versatility in maneuverability (such as hovering, vertical takeoff/landing, and longitudinal/lateral flight), it is a particularly attractive solution for flying in and out of such restricted areas.

1.2 Helicopter flight dynamics

A helicopter is a complex system, and understanding helicopter flight has been a continuous endeavor. Certainly helicopter nonlinear flight dynamics³ modeling has seen considerable development over the past forty years. We refer here to the important contributions of the 1970s in [61, 93, 90, 43], of the 1980s in [7, 92, 158, 133, 74, 170, 88, 20, 84, 50, 178], of the 1990s in [31, 156, 79, 80, 142, 121, 3], and for the last decade in [29, 166, 14, 67].

For a single main rotor, and briefly summarized, helicopter flight dynamics include the rigid-body responses combined with higher-frequency modes, see for example the associated frequency range for a full-size vehicle in Fig. 1. These higher-frequency modes are generated by the main rotor system, and its interaction with the fuselage and other vehicle components. For flight mechanics and control development purposes, the three most important aspects of these higher order rotor dynamics are blade flapping, which allows

³Without considering aspects related to Inverse Simulation, Higher Harmonic Control (HHC), and Individual Blade Control (IBC)

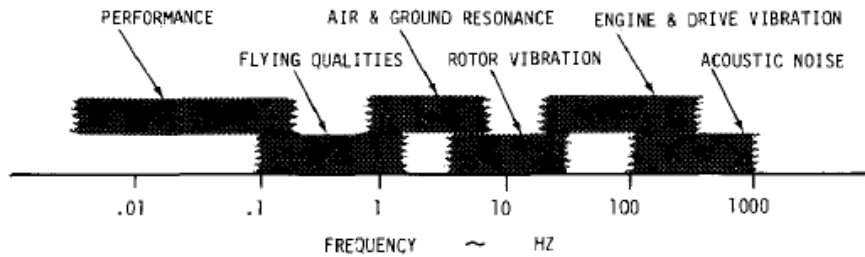


Figure 1: Helicopter frequency spectrum (from [33])

the blade to move in a plane containing the blade and the shaft, blade lead-lag, which allows the blade to move in the plane of rotation, and rotor inflow, which is the flow field induced by the rotor at the rotor disk.

Already since the early 1950s it had been known that including flapping dynamics in a helicopter flight model could produce limitations in rate and attitude feedback gains [63]. In fact blade flapping motion has three natural modes, i.e. coning, advancing, and regressing. The regressing flapping mode is the most important concerning the effect of rotor dynamics on the handling characteristics of a helicopter, it is the lowest frequency mode of the three, and it has a tendency to couple into the fuselage modes [76, 116, 44, 49, 54, 37, 55].

Concerning blade lead-lag dynamics, it was found that for helicopter directional axis control, lead-lag motion ought to be considered for control system design [114]. In particular it was found that blade lead-lag produced increased phase lag at high frequency, in the same frequency range where flapping effects occur [54], and that control rate gains were primarily limited by lead-lag-body coupling [54, 161].

Regarding the induced rotor flow, this latter contributes to the local blade incidence and dynamic pressure. It was found that it played a key role in destabilizing the flapping mode, which may result in a large initial overshoot in the vertical acceleration response, to an abrupt input in the collective pitch [48, 54]. In fact for full-size helicopters, frequencies of inflow dynamics are of the same order of magnitude as those of rotor blade flapping and lead-lag modes. Hence inflow dynamics can have a significant influence on the performance of a main rotor system [48, 54]. Additionally wake bending during maneuvering flight may significantly change inflow distribution over

		Dynamics	
		Medium Bandwidth	High Bandwidth
Validity	Hover & Low Speed (H-LS)	Level A	Level B_1
	H-LS & Aggressive Maneuvers (AM)		Level B_2
	H-LS & AM & VRS		Level C

Table 1: Helicopter UAV - Model Complexity

the rotor, giving rise to a sign reversal in the off-axis response [138]. This phenomenon is known as the off-axis response [99].

For manned helicopters, extensive discussions covering the various levels of required model complexity can be found in [12, 121]. In [50], a general definition of helicopter model sophistication was also formulated, which we have slightly modified and adapted in this paper, see Table 1, to conveniently describe helicopter (mini-)UAV model complexity, by the following two factors

- **Dynamics.** The levels of detail in representing the dynamics of the helicopter. This factor determines the validity of the model in terms of the frequency range of applicability
- **Validity.** The levels of sophistication in calculating the helicopter forces, moments, and inflow. This factor determines the domain of validity in the flight envelope

Where the *Dynamics* field is divided into medium and high bandwidths, with *medium* and *high* defined with reference to flight dynamics for control. The *medium* level refers to models where the main inflow dynamics, blade flap and/or lag dynamics are either omitted or elementary modeled. The *high* level refers to models which do account, in a relatively detailed way, for most of those effects. Further the *Validity* field is divided into three levels: hover and low speed, aggressive/aerobatic maneuvers, and VRS flight conditions.

1.3 Helicopter UAVs

In the past fifteen to twenty years, there has been considerable worldwide activity in research related to automatic flight of (mini-)UAVs, particularly at academia and various research institutions, for both fixed- and rotary-wing aircrafts. This research effort was mainly fourfold, on modeling, model validation, navigation and data fusion, and control development. And it is probably fair to say that a significant part of this research has concentrated on the development of control design methodologies. This said, in

the area of helicopter UAV flight dynamics and modeling, one of the major contributions was undoubtedly that of B. Mettler [113]. Helicopter modeling continues to be seen as a non-trivial exercise, and as stated in [113], the development of a model that is at once sufficiently accurate and simple enough for practical control design remains a challenging task.

Additionally small-scale helicopters exhibit higher bandwidth, and higher sensitivity to control inputs and disturbances when compared to their full-size counterparts, primarily since for small-scale helicopters the stiffness of the rotor hub and blades is considerably larger than that of full-sized helicopters.

In terms of helicopter UAV modeling⁴ for control synthesis, the level *A* class (see Table 1) has undeniably provided for quick and reasonably good results. The usual robustness-performance trade-off, which guarantees high robustness in return for lower performance, allowed to demonstrate hover and low speed flight for medium bandwidth system specifications, see [122, 117, 171, 28, 52, 96, 73, 40, 167, 177, 100].

On the other hand, for higher bandwidth⁵ system specifications at conventional flying conditions, it is necessary to accurately model the higher order rotor dynamics [89, 57]. Model-based examples for the B_1 class include [68, 102, 118, 151, 51, 53, 159, 60, 153, 75, 30, 59, 39, 10], and non-model⁶-based examples include [18, 38, 120, 65], while vision based systems have been reported in [9, 149, 143, 145, 146, 22].

Some researchers have pushed the boundaries further, i.e. class B_2 , through the combination of detailed models and advanced control strategies, demonstrating model-based aggressive/aerobatic maneuvers [71, 113, 111], and for non-model-based methods see [119, 5]. Actually from a modeling point of view, the separation between classes B_1 and B_2 is rather artificial, since most of the models presented in level B_1 could potentially be used to demonstrate aerobatic maneuvers, provided adequate control strategies are implemented.

Finally for the case of high bandwidth control system specifications, the final step aims at extending the flight envelope towards unusual flight con-

⁴In the sequel, and due to time and space constraints, we only review contributions in the field of helicopter UAV flight dynamics, excluding thus system identification, navigation, and control

⁵Higher bandwidth specifications may be necessary in case higher performance, for example aggressive maneuvering, are required. Further atmospheric disturbances such as gusts act as unmeasurable input disturbances, which require high control bandwidth to be effectively rejected [113]

⁶Such as machine learning, adaptive and intelligent control

ditions, such as for high sink rates, in the vortex-ring-state (VRS)⁷, or in autorotation, see class *C*. For example, 3-D automatic autorotation of a helicopter UAV was successfully demonstrated, albeit from a non-model-based approach, in [4].

Now to the best of our knowledge, none of the previous UAV flight dynamics models are valid for flight in steep descent or the VRS.

1.4 Our research model

The purpose of our work is to present a class *C* flight dynamics model for a small-scale helicopter UAV flight dynamics model for a flybarless, i.e. without a Bell-Hiller stabilizing bar, articulated Pitch-Lag-Flap (P-L-F) main rotor with rigid blades, applicable for high bandwidth control specifications, for both ClockWise (CW) and Counter-ClockWise (CCW)⁸ main rotor rotation, and valid for a range of flight conditions including the Vortex-Ring-State (VRS). The model includes the two most relevant helicopter components, i.e. the main and tail rotors; other components such as fuselage and tail may be added at a later stage.

The nonlinear dynamic model includes the twelve-states rigid body equations of motion, the four-states/blade flap/lag angles and flap/lag rotational velocities, the three-states dynamic inflow, and the single-state main rotor Revolutions Per Minute (RPM). Thus, for a two-bladed helicopter main rotor, the full model includes twenty-four-states, while for a three-bladed helicopter main rotor, the full model includes twenty-eight-states. Besides, the model accommodates for an off-axis response correction factor, for flight in the VRS, and for deterministic⁹ wind linear velocity inputs. Static ground effect has been accounted for by a correction factor applied to the non-dimensional total velocity at the rotor disk center. Further, computation of main rotor forces is done numerically through Gaussian quadrature integration, using a low order Legendre polynomial scheme. For the tail rotor, this latter has been modeled as a Bailey type rotor. Finally the paper reviews all assumptions made in deriving the model, i.e. structural, aerodynamics, and dynamical simplifications, which are valid for stability and control investigations of helicopters up to an advance ratio limit¹⁰ of about 0.3 [148, 43, 44].

The paper presents a detailed review of all assumptions made in deriving the

⁷For a review of the VRS and autorotation see [154]

⁸ClockWise and Counter ClockWise main rotor rotation. CCW rotation is common to American, British, German, Italian, and Japanese helicopter designs. While CW rotation is standard on Chinese, French, Indian, Polish and Russian helicopters designs

⁹Stochastic atmospheric turbulence will be added at a later stage

¹⁰The flight envelope of small-scale helicopters is well within this limit

model, i.e. structural, aerodynamics, and dynamical simplifications. These assumptions are valid for stability and control investigations of helicopters up to an advance ratio of about 0.3 [148, 43, 44].

A novel contribution of this paper is the derivation of the coupled flap-lag equations of motion for a rigid articulated (P-L-F) rotor, with hinge springs and viscous dampers, for both CW and CCW rotating main rotor, with all hinges physically separated. The equations were obtained by the Lagrangian method, which requires only velocity and position terms, and is much more convenient for overall system modeling. The flap-lag equations of motion are valid for small flap, lag, and pitch angles. Further the exact tangential and perpendicular blade velocity expressions have been used, hence full coupling between vehicle and blade dynamics is modeled.

Simulation results show that the nonlinear model is in good agreement with an equivalent nonlinear FLIGHTLAB model [14], for static (trim) conditions, and for dynamic conditions in hover and low to medium speed (up to 10 m/s). Hence the present model could potentially be used to investigate UAV flight in the VRS. For the VRS case, thrust fluctuations as given in [95] could be added at a later stage, as flight test data becomes available. Finally if additional simplifications are introduced, this model could also be exploited for the development of nonlinear control schemes.

The paper is organized as follows: in Section 2, the rigid body equations of motion are expressed. In Section 3, the main rotor model is presented. In Section 4, the tail rotor model is presented. In Section 5, simulation results are discussed. Finally, conclusions and future directions are presented in Section 6.

2 Rigid body equations of motion

We present the equations that describe a vehicle motion as a rigid body with six degrees of freedom, free to move in the atmosphere. The notation and equations outlined here are derived from the comprehensive reference [34].

The nomenclature is given in Appendix A, and for a description of frames and frame transformations see Appendix C.

First we present the various assumptions made in deriving the equations.

2.1 Assumptions

We have

- The vehicle has a longitudinal plane of symmetry
- The vehicle has constant mass, inertia, and CG position, hence fuel consumption and/or payload pickup/release are neglected
- The vehicle is a rigid system, i.e. it does not contain any flexible structures, hence the time derivative of the inertia matrix is zero
- Variations of helicopter CG locations due to main rotor blades position are neglected
- The vehicle height above ground is very small compared to the earth radius, implying a gravitation independent of height and thus constant
- The center of mass and center of gravity CG are identical for a constant gravity field
- The earth is fixed and flat
- For a flat and fixed earth, there is no longer a distinction between the directions of gravitational force and the force of gravity, hence the external force becomes the force of gravity. For further details on the geoid earth and gravity see [34, 115]
- Gravity is also a function of latitude, for all practical purpose we will consider the medium latitudes of 52° giving $g = 9.812 \text{ m/s}^2$
- Finally we neglect the effect of buoyancy or Archimedes force, which is negligible with respect to all other forces

2.2 Modeling

The standard rigid body equations of motion are given by the following twelve-state set of equations [34]

$$\begin{pmatrix} \dot{x}_N \\ \dot{x}_E \\ \dot{x}_Z \end{pmatrix} = \begin{pmatrix} V_N \\ V_E \\ V_Z \end{pmatrix} \quad (1)$$

$$\begin{pmatrix} \dot{u} \\ \dot{v} \\ \dot{w} \end{pmatrix} = - \begin{pmatrix} q.w - r.v \\ r.u - p.w \\ p.v - q.u \end{pmatrix} + g \cdot \begin{pmatrix} -\sin \theta \\ \cos \theta \sin \phi \\ \cos \theta \cos \phi \end{pmatrix} + \frac{\mathbf{F}_{aero,GFus}^b}{m_{Fus}} \quad (2)$$

$$\begin{pmatrix} \dot{p} \\ \dot{q} \\ \dot{r} \end{pmatrix} = \mathbb{I}_{Fus}^{-1} \cdot \left[\mathbf{M}_{aero,GFus}^b - \begin{pmatrix} p \\ q \\ r \end{pmatrix} \times \left[\mathbb{I}_{Fus} \cdot \begin{pmatrix} p \\ q \\ r \end{pmatrix} \right] \right] \quad (3)$$

$$\begin{pmatrix} \dot{\phi} \\ \dot{\theta} \\ \dot{\psi} \end{pmatrix} = \begin{pmatrix} 1 & \sin \theta \cdot \frac{\sin \phi}{\cos \theta} & \sin \theta \cdot \frac{\cos \phi}{\cos \theta} \\ 0 & \cos \phi & -\sin \phi \\ 0 & \frac{\sin \phi}{\cos \theta} & \frac{\cos \phi}{\cos \theta} \end{pmatrix} \cdot \begin{pmatrix} p \\ q \\ r \end{pmatrix} \quad (4)$$

With $\mathbf{F}_{aero,GFus}^b$ the aerodynamic forces experienced by the fuselage CG in the body frame F_b . And $\mathbf{M}_{aero,GFus}^b$ the moments of the aerodynamic forces expressed at the fuselage CG in frame F_b .

Further we have

$$\begin{pmatrix} V_N \\ V_E \\ V_Z \end{pmatrix} = \mathbb{T}_{ob} \cdot \begin{pmatrix} u \\ v \\ w \end{pmatrix} \quad (5)$$

3 The main rotor

As stated in [110], the main rotor is the single most important helicopter module of any component-type mathematical model. Hence the sophistication and accuracy of the rotor module largely determines the sophistication and accuracy of the entire model.

In a fully articulated rotor system, each rotor blade is attached to the rotor hub through a series of hinges, which allow the blade to move independently of the others. The blades are allowed to feather (pitch), flap, and lead-lag independently of each other [98, 2].

Often small-scale helicopters have rotor hubs which include a feathering hinge close to the shaft, and a lead-lag hinge a little further away, hence a Pitch-Lag (P-L) hinge arrangement. The lead-lag hinge may have stiffness and damping, depending on the blade-lead-lag hinge attachment mechanism. Further small-scale helicopter hubs are typically not equipped with a flap hinge, the hinge may often be replaced by stiff rubber rings, hence a hingeless flap mechanism. But for the purpose of modeling, it is standard practice in helicopter theory to model a hingeless rotor and its flexible blades as a rotor having rigid blades with the blades attached to a virtual flap hinge [121], offset from the main rotor axis. Additionally the virtual hinge is modeled as a torsional spring, implying thus stiffness and damping. It is therefore by adjusting the virtual hinge offset distance, and the virtual hinge stiffness and damping constants that we can recreate the correct blade flap motion, in terms of amplitude and frequency [35, 108].

Now for the purpose of modeling a generic helicopter UAV main rotor, we have chosen to select an articulated Pitch-Lag-Flap (P-L-F) hinge arrangement, placing the virtual flap hinge outboard of the lag hinge. This configuration allows for unrestricted flap hinge displacement outboard of the lag hinge, while keeping the option of having the pitch and lag hinge offsets at their current physical values. Note also that since our UAV is not equipped with a Hiller stabilizer bar, this latter will not be included in the main rotor model.

Next we present the various assumptions made in deriving the equations.

3.1 Assumptions

These include blade element theory, momentum theory, and additional assumptions and simplifications listed hereunder. As mentioned in [148, 43, 44], these assumptions are valid for stability and control investigations of helicopters for an advance ratio $\mu < 0.3$ (the UAV maximum speed is well below this limit).

Structural simplifications

- Rotor shaft forward and lateral tilt-angles, with respect to the body frame, are zero
- Rigid rotor blade in bending. Neglecting higher modes (harmonics), since higher modes are only pronounced at high speed [121, 72]
- Blade torsion is neglected, since the helicopter UAV blades are assumed to be relatively stiff
- Blade has zero twist, constant chord, zero sweep, constant thickness ratio, and has a uniform mass distribution
- Rotor inertia between shaft and flap hinge is assumed small and thus neglected

Aerodynamics simplifications

- Vehicle flies at a low altitude, hence neglecting air density and temperature variations
- Blade element theory is used. Blade element theory calculates the forces on the blade due to its motion through the air. It is assumed that each blade section acts as a two-dimensional airfoil to produce aerodynamic forces, with the influence of the wake and the rest of the rotor contained entirely in an induced angle of attack at the blade section [98]. This method is used to compute rotor lift and drag forces

-
- Radial flow along blade span is ignored
 - Momentum theory is used. Momentum theory states that the total force acting on a control volume is equal to the rate of change of momentum, and by momentum we mean the sum of flux, i.e. mass flow, entering and leaving this control volume [98, 36]. In this case, the rotor is modeled as an infinitely¹¹ thin actuator disk over which a pressure difference exists and inducing a constant velocity along the axis of rotation [36]. This method is used to compute the uniform inflow component at the rotor shaft position
 - Pitch, lag, and flap angles are assumed to be small
 - Reversed flow region is ignored. The reverse flow region occupies a small disk inboard, on the retreating side, where the air flows actually over the blade from trailing to leading edge. Now up to moderate forward speeds $\mu < 0.3$, and since the dynamic pressure in the reverse flow region is also low, the reverse flow region may be neglected [36]
 - Compressibility effects are disregarded, which is a reasonable assumption at low forward speed [121]
 - Viscous flow effects are disregarded, which is a valid assumption for low angle of attacks and un-separated flows [150, 11]

Dynamical simplifications

- A balanced rotor is assumed. In general most of the inertial terms, contributing to main rotor moments, vanish when integrated around 2π azimuth. However these terms should be retained when evaluating rotor out-of-balance loads [90]
- Dynamic twist¹² is neglected. Hence blade CG is assumed to be located on the blade section quarter chord line¹³
- Unsteady (frequency dependent) effect for time-dependent development of blade lift and pitching moment, due to changes in local incidence are ignored. For example dynamic stall, due to rapid pitch changes, is ignored

¹¹Equivalent to considering an infinite number of blades of zero thickness, hence also called the ideal rotor

¹²Any offset in blade chordwise CG or aerodynamic center position will result in a coupling of the flap and torsion DOF in blade elastic modes [121]

¹³Even though in practice the blade CG should even be forward of the blade section quarter chord line as to avoid pitch-flap flutter [36]

3.2 Position of a blade element

In the Hub-Body frame F_{HB} , see Fig. 3 and Fig. 4, the position of a blade element dm is given by

$$\begin{pmatrix} x_{dm} \\ y_{dm} \\ z_{dm} \end{pmatrix}^{HB} = \mathbb{T}_{(HB)6} \left\{ \mathbb{T}_{54} \left[\mathbb{T}_{32} \left(\mathbb{T}_{1(bl)} \begin{pmatrix} 0 \\ r_{dm} \\ 0 \end{pmatrix} + \begin{pmatrix} 0 \\ e_F \\ 0 \end{pmatrix} \right) + \begin{pmatrix} 0 \\ e_L \\ 0 \end{pmatrix} \right] + \begin{pmatrix} 0 \\ e_P \\ 0 \end{pmatrix} \right\} \quad (6)$$

Expanding the previous equation (and using the CW/CCW switch Γ such that $\Gamma^2 = 1$) we get the position of a blade element outboard of the flap hinge as

$$\begin{aligned} \mathbf{HP}_{dm} = \begin{pmatrix} x_{dm} \\ y_{dm} \\ z_{dm} \end{pmatrix}^{HB} &= \begin{pmatrix} -\cos \psi_{bl} \left(e_L + e_P + \cos \zeta_{bl} \left(e_F + r_{dm} \cos \beta_{bl} \right) \right) \\ -\Gamma \cos \psi_{bl} \left(\cos \theta_{bl} \sin \zeta_{bl} \left(e_F + r_{dm} \cos \beta_{bl} \right) + r_{dm} \sin \beta_{bl} \sin \theta_{bl} \right) \\ -r_{dm} \cos \theta_{bl} \sin \beta_{bl} \\ -\sin \psi_{bl} \left(\cos \theta_{bl} \sin \zeta_{bl} \left(e_F + r_{dm} \cos \beta_{bl} \right) + r_{dm} \sin \beta_{bl} \sin \theta_{bl} \right) \\ +\Gamma \sin \psi_{bl} \left(e_L + e_P + \cos \zeta_{bl} \left(e_F + r_{dm} \cos \beta_{bl} \right) \right) \\ + \left(e_F + r_{dm} \cos \beta_{bl} \right) \sin \zeta_{bl} \sin \theta_{bl} \end{pmatrix} \quad (7) \end{aligned}$$

And the inertial position of a blade element dm in the inertial frame F_I is given by

$$\mathbf{AP}_{dm} = \mathbf{AG} + \mathbf{GH} + \mathbf{HP}_{dm} = \mathbf{AG} + \begin{pmatrix} x_H \\ y_H \\ z_H \end{pmatrix} + \begin{pmatrix} x_{dm} \\ y_{dm} \\ z_{dm} \end{pmatrix} \quad (8)$$

3.3 Velocity of a blade element

The inertial velocity of a blade element dm positioned at P_{dm} , is defined as $\mathbf{V}_{I,P_{dm}}$ relative to the inertial frame F_I , using eq (8) we get

$$\mathbf{V}_{I,P_{dm}} = \frac{d\mathbf{A}\mathbf{P}_{dm}^I}{dt} = \frac{d\mathbf{A}\mathbf{G}^I}{dt} + \frac{d\mathbf{G}\mathbf{H}^I}{dt} + \frac{d\mathbf{H}\mathbf{P}_{dm}^I}{dt} \quad (9)$$

Projecting the previous expression in the Hub-Body frame F_{HB} we obtain

$$\mathbf{V}_{I,P_{dm}}^{HB} = \left(\frac{d\mathbf{A}\mathbf{G}^I}{dt} \right)^{HB} + \left(\frac{d\mathbf{G}\mathbf{H}^I}{dt} \right)^{HB} + \left(\frac{d\mathbf{H}\mathbf{P}_{dm}^I}{dt} \right)^{HB} \quad (10)$$

For the first term on the right-hand side of eq (10), and in the case of a flat and fixed earth, we have

$$\left(\frac{d\mathbf{A}\mathbf{G}^I}{dt} \right)^{HB} = \mathbb{T}_{(HB)o} \mathbf{V}_{k,G}^o = \mathbb{T}_{(HB)o} \begin{pmatrix} V_N \\ V_E \\ V_Z \end{pmatrix}^o \quad (11)$$

For the second term on the right-hand side of eq (10) we have

$$\left(\frac{d\mathbf{G}\mathbf{H}^I}{dt} \right)^{HB} = \left(\frac{d\mathbf{G}\mathbf{H}^b}{dt} \right)^{HB} + \boldsymbol{\Omega}_{bI}^{HB} \times \mathbf{G}\mathbf{H}^{HB} \quad (12)$$

Where \times denotes the cross product between two vectors.

Here the first term on the right-hand side of eq (12) is zero since the hub center H is fixed in body frame F_b . We further can express the second term on the right-hand side of eq (12) as

$$\boldsymbol{\Omega}_{bI}^{HB} \times \mathbf{G}\mathbf{H}^{HB} = \left(\mathbb{T}_{(HB)b} \boldsymbol{\Omega}_{bI}^b \right) \times \left(\mathbb{T}_{(HB)b} \mathbf{G}\mathbf{H}^b \right) \quad (13)$$

Since the earth is fixed, we obtain

$$\left(\frac{d\mathbf{G}\mathbf{H}^I}{dt} \right)^{HB} = \left(\mathbb{T}_{(HB)b} \begin{pmatrix} p \\ q \\ r \end{pmatrix} \right) \times \left(\mathbb{T}_{(HB)b} \begin{pmatrix} x_H \\ y_H \\ z_H \end{pmatrix}^b \right) \quad (14)$$

With

$$\boldsymbol{\Omega}_{bI}^b = \begin{pmatrix} p \\ q \\ r \end{pmatrix} \quad (15)$$

For the third term on the right-hand side of eq (10) we have

$$\begin{aligned} \left(\frac{d\mathbf{HP}_{dm}^I}{dt} \right)^{HB} &= \left(\frac{d\mathbf{HP}_{dm}^{HB}}{dt} \right)^{HB} + \boldsymbol{\Omega}_{(HB)I}^{HB} \times \mathbf{HP}_{dm}^{HB} \\ &= \frac{d}{dt} \begin{pmatrix} x_{dm} \\ y_{dm} \\ z_{dm} \end{pmatrix}^{HB} + \boldsymbol{\Omega}_{(HB)I}^{HB} \times \begin{pmatrix} x_{dm} \\ y_{dm} \\ z_{dm} \end{pmatrix}^{HB} \end{aligned} \quad (16)$$

With

$$\boldsymbol{\Omega}_{(HB)I}^{HB} = \boldsymbol{\Omega}_{(HB)b}^{HB} + \boldsymbol{\Omega}_{bI}^{HB} \quad (17)$$

And the first term on the right-hand side of eq (17) is zero since frame F_{HB} is fixed wrt frame F_b . Additionally we have $\boldsymbol{\Omega}_{bI}^{HB} = \mathbb{T}_{(HB)b} \boldsymbol{\Omega}_{bI}^b$

Regrouping terms, eq (11), eq (14), eq (16) eq (17), we can express the inertial velocity of a blade element dm in the Hub-Body frame F_{HB} as

$$\begin{aligned} \mathbf{V}_{I,P_{dm}}^{HB} &= \mathbb{T}_{(HB)b} \cdot \mathbb{T}_{bo} \begin{pmatrix} V_N \\ V_E \\ V_Z \end{pmatrix}^o + \frac{d}{dt} \begin{pmatrix} x_{dm} \\ y_{dm} \\ z_{dm} \end{pmatrix}^{HB} \\ &+ \left(\mathbb{T}_{(HB)b} \begin{pmatrix} p \\ q \\ r \end{pmatrix} \right) \times \left(\mathbb{T}_{(HB)b} \begin{pmatrix} x_H \\ y_H \\ z_H \end{pmatrix}^b + \begin{pmatrix} x_{dm} \\ y_{dm} \\ z_{dm} \end{pmatrix}^{HB} \right) \end{aligned} \quad (18)$$

Since rotor shaft forward and lateral tilt-angles are zero, we get $\mathbb{T}_{(HB)b} = \mathbb{I}$

Expanding eq (18) we get for the x-component of the inertial velocity of a blade element dm , in frame F_{HB}

$$\begin{aligned}
u_{I,P_{dm}}^{HB} &= u \\
&+ \Omega_{MR} \left(\sin \psi_{bl} [e_L + e_P + \cos \zeta_{bl} (e_F + r_{dm} \cos \beta_{bl})] \right. \\
&- \cos \psi_{bl} [\cos \theta_{bl} \sin \zeta_{bl} (e_F + r_{dm} \cos \beta_{bl}) + r_{dm} \sin \beta_{bl} \sin \theta_{bl}] \left. \right) \\
&+ \dot{\zeta}_{bl} (e_F + r_{dm} \cos \beta_{bl}) [\cos \psi_{bl} \sin \zeta_{bl} - \sin \psi_{bl} \cos \theta_{bl} \cos \zeta_{bl}] \\
&+ \dot{\beta}_{bl} r_{dm} [\cos \psi_{bl} \cos \zeta_{bl} \sin \beta_{bl} + \sin \psi_{bl} (\cos \theta_{bl} \sin \zeta_{bl} \sin \beta_{bl} - \cos \beta_{bl} \sin \theta_{bl})] \\
&+ \dot{\theta}_{bl} \sin \psi_{bl} [\sin \theta_{bl} \sin \zeta_{bl} (e_F + r_{dm} \cos \beta_{bl}) - r_{dm} \sin \beta_{bl} \cos \theta_{bl}] \\
&\quad + q \left(z_H - r_{dm} \cos \theta_{bl} \sin \beta_{bl} \right. \\
&\quad \left. + (e_F + r_{dm} \cos \beta_{bl}) \sin \zeta_{bl} \sin \theta_{bl} \right) \\
&- r \left(y_H - \Gamma \cos \psi_{bl} (\cos \theta_{bl} \sin \zeta_{bl} (e_F + r_{dm} \cos \beta_{bl}) \right. \\
&\quad \left. + r_{dm} \sin \beta_{bl} \sin \theta_{bl}) \right. \\
&\quad \left. + \Gamma \sin \psi_{bl} (e_L + e_P + \cos \zeta_{bl} (e_F + r_{dm} \cos \beta_{bl})) \right)
\end{aligned} \tag{19}$$

The y-component of the inertial velocity of a blade element dm , in frame F_{HB} is

$$\begin{aligned}
v_{I,P_{dm}}^{HB} = & v \\
& + \Omega_{MR}\Gamma \left((e_L + e_P) \cos \psi_{bl} + r_{dm} \sin \psi_{bl} \sin \beta_{bl} \sin \theta_{bl} \right. \\
& \left. + (e_F + r_{dm} \cos \beta_{bl})(\cos \psi_{bl} \cos \zeta_{bl} + \sin \psi_{bl} \cos \theta_{bl} \sin \zeta_{bl}) \right) \\
& - \dot{\zeta}_{bl}\Gamma(e_F + r_{dm} \cos \beta_{bl})[\cos \psi_{bl} \cos \zeta_{bl} \cos \theta_{bl} + \sin \psi_{bl} \sin \zeta_{bl}] \\
& + \dot{\beta}_{bl}r_{dm}\Gamma(\cos \psi_{bl} \cos \theta_{bl} \sin \zeta_{bl} \sin \beta_{bl} - \cos \psi_{bl} \cos \beta_{bl} \sin \theta_{bl} - \sin \psi_{bl} \cos \zeta_{bl} \sin \beta_{bl}) \\
& + \dot{\theta}_{bl}\Gamma \cos \psi_{bl}[\sin \theta_{bl} \sin \zeta_{bl}(e_F + r_{dm} \cos \beta_{bl}) - r_{dm} \sin \beta_{bl} \cos \theta_{bl}] \\
& \quad - p \left(z_H - \left(r_{dm} \cos \theta_{bl} \sin \beta_{bl} \right. \right. \\
& \quad \left. \left. - (e_F + r_{dm} \cos \beta_{bl}) \sin \zeta_{bl} \sin \theta_{bl} \right) \right) \\
& + r \left(x_H - \left(\cos \psi_{bl}(e_L + e_P + \cos \zeta_{bl}(e_F + r_{dm} \cos \beta_{bl})) \right. \right. \\
& \quad \left. \left. + \sin \psi_{bl}(\cos \theta_{bl} \sin \zeta_{bl}(e_F + r_{dm} \cos \beta_{bl}) \right. \right. \\
& \quad \left. \left. + r_{dm} \sin \beta_{bl} \sin \theta_{bl}) \right) \right)
\end{aligned} \tag{20}$$

And the z-component of the inertial velocity of a blade element dm , in frame F_{HB} is

$$\begin{aligned}
w_{I,Pdm}^{HB} = & w \\
& + \dot{\zeta}_{bl} \cos \zeta_{bl} \sin \theta_{bl} (e_F + r_{dm} \cos \beta_{bl}) \\
& - \dot{\beta}_{bl} r_{dm} (\cos \beta_{bl} \cos \theta_{bl} + \sin \beta_{bl} \sin \zeta_{bl} \sin \theta_{bl}) \\
& + \dot{\theta}_{bl} [r_{dm} \sin \theta_{bl} \sin \beta_{bl} + (e_F + r_{dm} \cos \beta_{bl}) \sin \zeta_{bl} \cos \theta_{bl}] \\
& + p \left(y_H - \Gamma \cos \psi_{bl} (\cos \theta_{bl} \sin \zeta_{bl} (e_F + r_{dm} \cos \beta_{bl}) \right. \\
& \quad \left. + r_{dm} \sin \beta_{bl} \sin \theta_{bl}) \right. \\
& \quad \left. + \Gamma \sin \psi_{bl} (e_L + e_P + \cos \zeta_{bl} (e_F + r_{dm} \cos \beta_{bl})) \right) \\
& - q \left(x_H - \cos \psi_{bl} (e_L + e_P + \cos \zeta_{bl} (e_F + r_{dm} \cos \beta_{bl})) \right. \\
& \quad \left. - \sin \psi_{bl} (\cos \theta_{bl} \sin \zeta_{bl} (e_F + r_{dm} \cos \beta_{bl}) \right. \\
& \quad \left. + r_{dm} \sin \beta_{bl} \sin \theta_{bl}) \right)
\end{aligned} \tag{21}$$

These expressions are valid for both CW and CCW rotating main rotor, through the switch Γ .

3.4 Flap-Lag equations of motion

Coupled flap-lag equations of motion for (F-L-P)¹⁴, (F-P-L), and (L-F-P) hinge arrangements, with hinge springs and viscous dampers, have been described for a CCW rotor in [45]. A novel contribution of this paper is the derivation of the coupled flap-lag equations of motion for a rigid articulated (P-L-F) rotor, with hinge springs and viscous dampers, for both CW and CCW rotating main rotor, with all hinges physically separated.

The presented flap-lag equations of motion are valid for small flap, lag, and pitch angles. Further the exact tangential and perpendicular blade velocity expressions have been used, hence full coupling between vehicle and blade dynamics is modeled. Additionally main rotor RPM variation was allowed, since it is known that the effective helicopter vertical damping and low frequency rigid-body modes may be affected by main rotor RPM [47, 91].

¹⁴Flap-Lag-Pitch

The equations were obtained by the Lagrangian method [172], which requires only velocity and position terms, and is much more convenient for overall system modeling. For an in-depth review of the flap-lag equations of motion, through the Lagrangian method, see [45, 179, 89].

From the Lagrangian method we have

$$\frac{d}{dt} \left(\frac{\partial K_E}{\partial \dot{\zeta}_{bl}} \right) - \frac{\partial K_E}{\partial \zeta_{bl}} = Q_{\zeta_{bl}} \quad (22a)$$

$$\frac{d}{dt} \left(\frac{\partial K_E}{\partial \dot{\beta}_{bl}} \right) - \frac{\partial K_E}{\partial \beta_{bl}} = Q_{\beta_{bl}} \quad (22b)$$

With K_E the kinetic energy of a single rotor blade, ζ_{bl} the blade lag angle, β_{bl} the blade flap angle, and $Q_{\zeta_{bl}}$, $Q_{\beta_{bl}}$ the generalized forces. These generalized forces include the effect of gravity, aerodynamic forces, and forces due to spring damping and stiffness.

$$Q_{\zeta_{bl}} = Q_{\zeta_{bl},G} + Q_{\zeta_{bl},A} + Q_{\zeta_{bl},D} + Q_{\zeta_{bl},S} \quad (23a)$$

$$Q_{\beta_{bl}} = Q_{\beta_{bl},G} + Q_{\beta_{bl},A} + Q_{\beta_{bl},D} + Q_{\beta_{bl},S} \quad (23b)$$

The kinetic energy of a single rotor blade is given by

$$K_E = \frac{1}{2} \int_0^{R_{bl}} \mathbf{V}_{I,P_{dm}}^{HB} \cdot \mathbf{V}_{I,P_{dm}}^{HB} dm \quad (24)$$

Where the limits of integration are from the flap hinge, i.e. 0 , to the blade tip, i.e. R_{bl} . The kinetic energy associated with the blade segment inboard of the flap hinge is neglected.

Determination of the generalized forces requires first the calculation the virtual work of an individual contributing external force, associated with its respective virtual flapping and lead-lag displacements. Let $F_{X_i}, F_{Y_i}, F_{Z_i}$ be the components of the i th external force \mathbf{F}_i , acting on the blade element dm in frame F_{HB} . Then the resulting elemental virtual work done by this external force due to the virtual flapping and lag displacements $\partial\beta_{bl}$ and $\partial\zeta_{bl}$ is given by

$$dW_i = F_{X_i} dx_{dm} + F_{Y_i} dy_{dm} + F_{Z_i} dz_{dm} \quad (25)$$

Where dx_{dm} , dy_{dm} , dz_{dm} are given by

$$dx_{dm} = \frac{\partial x_{dm}}{\partial \beta_{bl}} \partial \beta_{bl} + \frac{\partial x_{dm}}{\partial \zeta_{bl}} \partial \zeta_{bl} \quad (26a)$$

$$dy_{dm} = \frac{\partial y_{dm}}{\partial \beta_{bl}} \partial \beta_{bl} + \frac{\partial y_{dm}}{\partial \zeta_{bl}} \partial \zeta_{bl} \quad (26b)$$

$$dz_{dm} = \frac{\partial z_{dm}}{\partial \beta_{bl}} \partial \beta_{bl} + \frac{\partial z_{dm}}{\partial \zeta_{bl}} \partial \zeta_{bl} \quad (26c)$$

Now, summing up the elemental virtual work over the appropriate blade span results in the total virtual work W_i due to external force \mathbf{F}_i

$$W_i = \int_0^{R_{bl}} \left(F_{X_i} \frac{\partial x_{dm}}{\partial \beta_{bl}} + F_{Y_i} \frac{\partial y_{dm}}{\partial \beta_{bl}} + F_{Z_i} \frac{\partial z_{dm}}{\partial \beta_{bl}} \right) \partial \beta_{bl} \\ + \int_0^{R_{bl}} \left(F_{X_i} \frac{\partial x_{dm}}{\partial \zeta_{bl}} + F_{Y_i} \frac{\partial y_{dm}}{\partial \zeta_{bl}} + F_{Z_i} \frac{\partial z_{dm}}{\partial \zeta_{bl}} \right) \partial \zeta_{bl} \quad (27)$$

Which is equivalent to

$$W_i = Q_{\beta_{bl},i} \cdot \partial \beta_{bl} + Q_{\zeta_{bl},i} \cdot \partial \zeta_{bl} \quad (28)$$

3.4.1 Inertia dynamics

We can rewrite the first term on the left-hand side of eq (22a) as

$$\frac{d}{dt} \left(\frac{\partial K_E}{\partial \dot{\zeta}_{bl}} \right) = \frac{d}{dt} \left(\frac{\partial}{\partial \dot{\zeta}_{bl}} \frac{1}{2} \int_0^{R_{bl}} \mathbf{V}_{I,P_{dm}}^{HB} \cdot \mathbf{V}_{I,P_{dm}}^{HB} dm \right) \quad (29)$$

And since the limits of integration are constant, with Leibniz integral rule, the former expression is equal to

$$\frac{1}{2} \int_0^{R_{bl}} \frac{d}{dt} \frac{\partial}{\partial \dot{\zeta}_{bl}} \left(\mathbf{V}_{I,P_{dm}}^{HB} \cdot \mathbf{V}_{I,P_{dm}}^{HB} \right) dm \quad (30)$$

Eq (30) is equivalent to

$$\int_0^{R_{bl}} \frac{d}{dt} \left(\mathbf{V}_{I,P_{dm}}^{HB} \cdot \frac{\partial}{\partial \dot{\zeta}_{bl}} \mathbf{V}_{I,P_{dm}}^{HB} \right) dm = \int_0^{R_{bl}} \left[\mathbf{V}_{I,P_{dm}}^{HB} \cdot \frac{d}{dt} \frac{\partial}{\partial \dot{\zeta}_{bl}} \mathbf{V}_{I,P_{dm}}^{HB} + \frac{d}{dt} (\mathbf{V}_{I,P_{dm}}^T) \cdot \frac{\partial}{\partial \dot{\zeta}_{bl}} \mathbf{V}_{I,P_{dm}}^{HB} \right] dm \quad (31)$$

With

$$\frac{d}{dt} \frac{\partial}{\partial \dot{\zeta}_{bl}} \mathbf{V}_{I,P_{dm}}^{F_I} = \frac{d}{dt} \frac{\partial}{\partial \dot{\zeta}_{bl}} \mathbf{V}_{I,P_{dm}}^{HB} + \boldsymbol{\Omega}_{(HB)I} \times \frac{\partial}{\partial \dot{\zeta}_{bl}} \mathbf{V}_{I,P_{dm}} \quad (32)$$

We can rewrite the second term on the left-hand side of eq (22a) as

$$-\frac{\partial K_E}{\partial \dot{\zeta}_{bl}} = -\frac{\partial}{\partial \dot{\zeta}_{bl}} \frac{1}{2} \int_0^{R_{bl}} \mathbf{V}_{I,P_{dm}}^{HB} \cdot \mathbf{V}_{I,P_{dm}}^{HB} dm \quad (33)$$

Again since the limits of integration are constant, with Leibniz integral rule, the former expression is equal to

$$-\frac{1}{2} \int_0^{R_{bl}} \frac{\partial}{\partial \dot{\zeta}_{bl}} \left(\mathbf{V}_{I,P_{dm}}^{HB} \cdot \mathbf{V}_{I,P_{dm}}^{HB} \right) dm = - \int_0^{R_{bl}} \mathbf{V}_{I,P_{dm}}^{HB} \cdot \frac{\partial}{\partial \dot{\zeta}_{bl}} \mathbf{V}_{I,P_{dm}}^{HB} dm \quad (34)$$

Now summing the previous results we can provide an expression for the left-hand side of eq (22a), i.e. the blade lead-lag equations of motion, as

$$\begin{aligned} \frac{d}{dt} \left(\frac{\partial K_E}{\partial \dot{\zeta}_{bl}} \right) - \frac{\partial K_E}{\partial \dot{\zeta}_{bl}} &= \int_0^{R_{bl}} \mathbf{V}_{I,P_{dm}}^{HB} \cdot \frac{d}{dt} \frac{\partial}{\partial \dot{\zeta}_{bl}} \mathbf{V}_{I,P_{dm}}^{HB} dm \\ &+ \int_0^{R_{bl}} \frac{d}{dt} (\mathbf{V}_{I,P_{dm}}^T) \cdot \frac{\partial}{\partial \dot{\zeta}_{bl}} \mathbf{V}_{I,P_{dm}}^{HB} dm - \int_0^{R_{bl}} \mathbf{V}_{I,P_{dm}}^{HB} \cdot \frac{\partial}{\partial \dot{\zeta}_{bl}} \mathbf{V}_{I,P_{dm}}^{HB} dm \end{aligned} \quad (35)$$

Similarly for the flap equations of motion, the left-hand side of eq (22b), we get

$$\begin{aligned}
\frac{d}{dt} \left(\frac{\partial K_E}{\partial \dot{\beta}_{bl}} \right) - \frac{\partial K_E}{\partial \beta_{bl}} &= \int_0^{R_{bl}} \mathbf{V}_{I,P_{dm}}^{HB \ T} \cdot \frac{d}{dt} \frac{\partial}{\partial \dot{\beta}_{bl}} \mathbf{V}_{I,P_{dm}}^{HB} dm \\
&+ \int_0^{R_{bl}} \frac{d}{dt} (\mathbf{V}_{I,P_{dm}}^T) \cdot \frac{\partial}{\partial \dot{\beta}_{bl}} \mathbf{V}_{I,P_{dm}}^{HB} dm - \int_0^{R_{bl}} \mathbf{V}_{I,P_{dm}}^{HB \ T} \cdot \frac{\partial}{\partial \beta_{bl}} \mathbf{V}_{I,P_{dm}}^{HB} dm
\end{aligned} \tag{36}$$

Where the components of the velocity vector $\mathbf{V}_{I,P_{dm}}^{HB}$ have been computed in eq (19), eq (20), and eq (21).

We can now reformulate eq (22), using eq (35) and eq (36), to give the four-state nonlinear flap-lag equations of motion as follows

$$\frac{d}{dt} \begin{pmatrix} \dot{\beta}_{bl} \\ \dot{\zeta}_{bl} \\ \beta_{bl} \\ \zeta_{bl} \end{pmatrix} = \mathbb{A}^{-1} \cdot \left(-\mathbb{B} \cdot \begin{pmatrix} \dot{\beta}_{bl} \\ \dot{\zeta}_{bl} \\ \beta_{bl} \\ \zeta_{bl} \end{pmatrix} - \begin{bmatrix} F_1 \\ F_2 \\ 0 \\ 0 \end{bmatrix} + \begin{bmatrix} Q_{\beta_{bl}} \\ Q_{\zeta_{bl}} \\ 0 \\ 0 \end{bmatrix} \right) \tag{37}$$

With the following matrices

$$\mathbb{A} = \begin{bmatrix} I_\beta & 0 & 0 & 0 \\ 0 & (e_F^2 \cdot M_{bl} + 2e_F \cdot C_0 + I_\beta) & 0 & 0 \\ 0 & 0 & 1 & 0 \\ 0 & 0 & 0 & 1 \end{bmatrix} \tag{38}$$

$$\mathbb{B} = \begin{bmatrix} 0 & B_{12} & 0 & 0 \\ B_{21} & 0 & 0 & 0 \\ -1 & 0 & 0 & 0 \\ 0 & -1 & 0 & 0 \end{bmatrix} \tag{39}$$

With M_{bl} , C_0 , and I_β defined in Appendix D, and matrix components B_{12} , B_{21} , F_1 , and F_2 defined in Appendix E. Note that these last four terms are also functions of $(\dot{\zeta}_{bl} \ \beta_{bl} \ \zeta_{bl})$. The generalized forces $Q_{\beta_{bl}}$ and $Q_{\zeta_{bl}}$ are given next in eq (49), eq (50), eq (51), eq (52), eq (53), eq (54), eq (68), and eq (71).

3.4.2 Flap angle as a Fourier series

Blade motion is 2π periodic around the azimuth and may hence be expanded as an infinite Fourier series [72, 98].

For the flap angle, this gives

$$\beta_{bl}(\psi_{bl}) = \beta_0 + \beta_{1c} \cos \psi_{bl} + \beta_{1s} \sin \psi_{bl} + \beta_{2c} \cos 2\psi_{bl} + \beta_{2s} \sin 2\psi_{bl} + \dots \quad (40)$$

For full-scale helicopters, it is well known that the magnitude of the flap second harmonic are less than 10% the magnitude of the flap first harmonic [113, 72]. We assume that this is also the case for small-scale helicopters. Therefore we neglect second and higher harmonics in the Fourier series, we get

$$\beta_{bl}(\psi_{bl}) \simeq \beta_0 + \beta_{1c} \cos \psi_{bl} + \beta_{1s} \sin \psi_{bl} \quad (41)$$

The first harmonic representation of the blade motion defines the rotor tip-path-plane (TPP). This type of motion results in a cone-shaped rotor, with the top of the cone being the TPP. The non-periodic term β_0 describes the so-called coning angle, and the coefficients of the first harmonic β_{1c} and β_{1s} describe the tilting of the rotor TPP, in the longitudinal and lateral directions respectively.

Now in steady-state operation of the rotor, the flap coefficients β_0 , β_{1c} , β_{1s} may be considered constant over a full 2π blade revolution. Hence a steady-state periodic solution in the form of a Fourier series as given in eq (41) may be found through a least-squares solution, see for example [15]. Obviously this solution would not be adequate for transient situations such as during a maneuver [107]. Hence we compute here the instantaneous TPP angles, at each new blade azimuth. For a three-bladed rotor, one azimuth position for each blade is sufficient to find the three coefficients β_0 , β_{1c} , and β_{1s} . For a two-bladed rotor, a least-squares solution based on two azimuth positions per blade becomes then necessary.

3.4.3 Virtual displacement of a blade element

The virtual displacement, in the Hub-Body frame, of a blade element outboard of the flap hinge is obtained, using eq (26) and eq (7) as follows

$$\begin{pmatrix} dx_{dm} \\ dy_{dm} \\ dz_{dm} \end{pmatrix}^{HB} = r_{dm} \cdot \mathbf{dP}_{\beta,r}^{HB} \cdot \partial\beta_{bl} + r_{dm} \cdot \mathbf{dP}_{\zeta,r}^{HB} \cdot \partial\zeta_{bl} + \mathbf{dP}_{\zeta,\bar{r}}^{HB} \cdot \partial\zeta_{bl} \quad (42)$$

With

$$\mathbf{dP}_{\beta,r}^{HB} = \begin{pmatrix} \cos \psi_{bl} \cos \zeta_{bl} \sin \beta_{bl} + \sin \psi_{bl} \left(\cos \theta_{bl} \sin \zeta_{bl} \sin \beta_{bl} - \cos \beta_{bl} \sin \theta_{bl} \right) \\ \Gamma \left(\cos \psi_{bl} \left(\cos \theta_{bl} \sin \zeta_{bl} \sin \beta_{bl} - \cos \beta_{bl} \sin \theta_{bl} \right) - \sin \psi_{bl} \cos \zeta_{bl} \sin \beta_{bl} \right) \\ - \cos \theta_{bl} \cos \beta_{bl} - \sin \zeta_{bl} \sin \theta_{bl} \sin \beta_{bl} \end{pmatrix} \quad (43)$$

$$\mathbf{dP}_{\zeta,r}^{HB} = \cos \beta_{bl} \begin{pmatrix} \left(\cos \psi_{bl} \sin \zeta_{bl} - \sin \psi_{bl} \cos \theta_{bl} \cos \zeta_{bl} \right) \\ -\Gamma \left(\cos \psi_{bl} \cos \theta_{bl} \cos \zeta_{bl} + \sin \psi_{bl} \sin \zeta_{bl} \right) \\ \cos \zeta_{bl} \sin \theta_{bl} \end{pmatrix} \quad (44)$$

$$\mathbf{dP}_{\zeta,\bar{r}}^{HB} = e_F \begin{pmatrix} \left(\cos \psi_{bl} \sin \zeta_{bl} - \sin \psi_{bl} \cos \theta_{bl} \cos \zeta_{bl} \right) \\ -\Gamma \left(\cos \psi_{bl} \cos \theta_{bl} \cos \zeta_{bl} + \sin \psi_{bl} \sin \zeta_{bl} \right) \\ \cos \zeta_{bl} \sin \theta_{bl} \end{pmatrix} \quad (45)$$

3.4.4 Generalized forces: gravity

The gravity force acting on a blade element with mass dm can be expressed in the Hub-Body frame F_{HB} as

$$\mathbf{F}_{G_{bl}}^{HB} = \mathbb{T}_{(HB)o} \begin{pmatrix} 0 \\ 0 \\ g \cdot dm \end{pmatrix}^o \quad (46)$$

Using eq (106) we get

$$\mathbf{F}_{G_{bl}}^{HB} = g \cdot dm \cdot \begin{pmatrix} A_1 \\ A_2 \\ A_3 \end{pmatrix} \quad (47)$$

Where we have used the following constants

$$\begin{aligned}
 A_1 &= -\sin \theta \\
 A_2 &= \cos \theta \sin \phi \\
 A_3 &= \cos \theta \cos \phi
 \end{aligned} \tag{48}$$

Substituting eq (47) and eq (42) into eq (27), the desired generalized forces due to gravity, outboard of the flap hinge, are obtained as follows

$$\begin{aligned}
 Q_{\beta_{bl},G} = g \cdot C_0 \cdot & \left(A_1 \cos \psi_{bl} \cos \zeta_{bl} \sin \beta_{bl} + A_1 \sin \psi_{bl} \cos \theta_{bl} \sin \zeta_{bl} \sin \beta_{bl} \right. \\
 & - A_1 \sin \psi_{bl} \cos \beta_{bl} \sin \theta_{bl} + A_2 \Gamma \cos \psi_{bl} \cos \theta_{bl} \sin \zeta_{bl} \sin \beta_{bl} \\
 & - A_2 \Gamma \cos \psi_{bl} \cos \beta_{bl} \sin \theta_{bl} - A_2 \Gamma \sin \psi_{bl} \cos \zeta_{bl} \sin \beta_{bl} \\
 & \left. - A_3 \cos \theta_{bl} \cos \beta_{bl} - A_3 \sin \zeta_{bl} \sin \theta_{bl} \sin \beta_{bl} \right) \tag{49}
 \end{aligned}$$

$$\begin{aligned}
 Q_{\zeta_{bl},G} = g \cdot \left(e_F \cdot M_{bl} + C_0 \cos \beta_{bl} \right) & \left(A_1 \cos \psi_{bl} \sin \zeta_{bl} - A_1 \sin \psi_{bl} \cos \theta_{bl} \cos \zeta_{bl} \right. \\
 & \left. - A_2 \Gamma \cos \psi_{bl} \cos \theta_{bl} \cos \zeta_{bl} - A_2 \Gamma \sin \psi_{bl} \sin \zeta_{bl} + A_3 \cos \zeta_{bl} \sin \theta_{bl} \right) \tag{50}
 \end{aligned}$$

Where M_{bl} and C_0 are defined in Appendix D.

3.4.5 Generalized forces: hub damping

We will assume here hinge springs with viscous dampers.

The generalized forces corresponding to the spring dampers can be obtained directly from the potential energy of the hub dampers dissipation functions [172, 45].

$$Q_{\beta_{bl},D} = -K_{D\beta} \cdot \dot{\beta}_{bl} \tag{51}$$

Similarly we obtain

$$Q_{\zeta_{bl},D} = -K_{D\zeta} \cdot \dot{\zeta}_{bl} \tag{52}$$

3.4.6 Generalized forces: hub spring restraints

Similarly the generalized forces corresponding to the spring restraints can be obtained directly from the potential energy of the hub springs [172, 45].

$$Q_{\beta_{bl},S} = -K_{S\beta} \cdot (\beta_{bl} - \beta_P) \quad (53)$$

Where we have subtracted the precone angle β_P , see [98]. Here an approximation is made since we have neglected the effect of the precone angle in the left-hand side of the flap-lag equations of motion.

Finally we also have

$$Q_{\zeta_{bl},S} = -K_{S\zeta} \cdot \zeta_{bl} \quad (54)$$

3.4.7 Generalized forces: aerodynamic

Blade element velocities A blade element located at a radius r_{dm} from the flap hinge is analyzed. The flow velocities perpendicular and tangential to the reference frame F_{ref} are named U_P and U_T . They represent the velocities of a blade element dm as if this element was fixed in space, while the air flows around it, see Fig. 2.

First we express the rotor hub aerodynamic velocity in the Hub-Body frame as

$$\mathbf{V}_{a,G}^{HB} = \begin{pmatrix} u_{I,P_{dm}} \\ v_{I,P_{dm}} \\ w_{I,P_{dm}} \end{pmatrix}^{HB} - \mathbb{T}_{(HB)o} \begin{pmatrix} u_w \\ v_w \\ w_w \end{pmatrix}^o \quad (55)$$

With $u_{I,P_{dm}}^{HB}$, $v_{I,P_{dm}}^{HB}$, and $w_{I,P_{dm}}^{HB}$ given in eq (19), eq (20), eq (21), and u_w^o , v_w^o , and w_w^o the components of the wind velocity vector in frame F_o .

Then we have

$$U_P = \begin{bmatrix} 0 \\ 0 \\ 1 \end{bmatrix}^T \cdot \mathbb{T}_{(ref)(HB)} \cdot \left\{ -\mathbf{V}_{a,G}^{HB} + \mathbb{T}_{(HB)(TPP)} \begin{pmatrix} 0 \\ 0 \\ v_i \end{pmatrix}^{TPP} \right\} \quad (56)$$

With v_i the rotor induced velocity defined in eq (81). And further

$$U_T = - \begin{bmatrix} 1 \\ 0 \\ 0 \end{bmatrix}^T \cdot \mathbb{T}_{(ref)(HB)} \cdot \mathbf{V}_{a,G}^{HB} \quad (57)$$

Note that we do not consider the spanwise (along axis y_{bl}) velocity.

Inflow angle The inflow angle ϕ_{bl} is presented in Fig. 2 and is defined as follows.

For the case of a CCW rotor, i.e. $\Gamma = 1$, we have

$$\begin{aligned} \phi_{bl} &= -\arctan \frac{U_P}{U_T} \quad \text{if } U_T < 0 \\ \phi_{bl} &= \text{sign}(U_P) \cdot \frac{\pi}{2} + \arctan \frac{U_T}{U_P} \quad \text{if } 0 \leq U_T \end{aligned} \quad (58)$$

For the case of a CW rotor, i.e. $\Gamma = -1$, we have

$$\begin{aligned} \phi_{bl} &= \arctan \frac{U_P}{U_T} \quad \text{if } 0 < U_T \\ \phi_{bl} &= \text{sign}(U_P) \cdot \frac{\pi}{2} - \arctan \frac{U_T}{U_P} \quad \text{if } U_T \leq 0 \end{aligned} \quad (59)$$

Elementary forces Here we consider the flow over a blade element, this is why the accompanying theory is named blade element method/theory.

The magnitude of the elementary lift force can be written as

$$dL_{bl} = K_{defic} \cdot \frac{1}{2} \rho \cdot U^2 \cdot c_{l_{bl}} \cdot c_{bl} \cdot dr_{dm} \quad (60)$$

And the magnitude of the elementary drag force can be written as

$$dD_{bl} = \frac{1}{2} \rho \cdot U^2 \cdot c_{d_{bl}} \cdot c_{bl} \cdot dr_{dm} \quad (61)$$

The flow velocity is given from Fig. 2

$$U = \sqrt{U_T^2 + U_P^2} \quad (62)$$

The blade section lift and drag coefficients $c_{l_{bl}}$ and $c_{d_{bl}}$ are given as tabulated functions¹⁵ of blade section angle of attack α_{bl} and Mach number M .

$$\alpha_{bl} = \theta_{bl} - \phi_{bl} \quad (63)$$

$$M = \frac{U}{a} \quad (64)$$

With the blade pitch θ_{bl} given as in [45]

$$\theta_{bl} = \theta_{0_{bl}} + \theta_{1_{c_{bl}}} \cos(\psi_{bl} + \psi_{PA}) + \theta_{1_{s_{bl}}} \sin(\psi_{bl} + \psi_{PA}) + \theta_{t,rdm} - K_{(\theta\beta)} \cdot \beta_{bl} - K_{(\theta\zeta)} \cdot \zeta_{bl} \quad (65)$$

We can express now the elementary lift force in frame F_{ref} as

$$d\mathbf{L}_{bl}^{ref} = \text{sign}(U_T) \cdot dL_{bl} \cdot \begin{pmatrix} \sin \phi_{bl} \\ 0 \\ \Gamma \cos \phi_{bl} \end{pmatrix} \quad (66)$$

And the elementary drag force in frame F_{ref} as

$$d\mathbf{D}_{bl}^{ref} = dD_{bl} \cdot \begin{pmatrix} -\Gamma \cos \phi_{bl} \\ 0 \\ \sin \phi_{bl} \end{pmatrix} \quad (67)$$

Generalized forces We first express here the generalized forces due to blade lead-lag contribution. We split the generalized aerodynamic force $Q_{\zeta_{bl},A}$, defined in eq (23), into two contributions, one due to lift Q_{ζ_{bl},A_L} and one due to drag Q_{ζ_{bl},A_D} such

$$Q_{\zeta_{bl},A} = Q_{\zeta_{bl},A_L} + Q_{\zeta_{bl},A_D} \quad (68)$$

Now keeping in mind eq (27), and using eq (44), and eq (45) we obtain

¹⁵Where we neglect sideslip influence

$$Q_{\zeta_{bl}, A_L} = \int_{r_c}^{B.R_{bl}} \left(\mathbb{T}_{(HB)(ref)} \mathbf{dL}_{bl}^{ref} \right)^T \cdot \left(r_{dm} \cdot \mathbf{dP}_{\zeta, r}^{HB} + \mathbf{dP}_{\zeta, \bar{r}}^{HB} \right) \cdot dr_{dm} \quad (69)$$

And

$$Q_{\zeta_{bl}, A_D} = \int_{r_c}^{R_{bl}} \left(\mathbb{T}_{(HB)(ref)} \mathbf{dD}_{bl}^{ref} \right)^T \cdot \left(r_{dm} \cdot \mathbf{dP}_{\zeta, r}^{HB} + \mathbf{dP}_{\zeta, \bar{r}}^{HB} \right) \cdot dr_{dm} \quad (70)$$

For the drag force contribution, the integration is performed from the blade root cutout r_c , measured from the flap hinge, to the blade tip R_{bl} . For the lift contribution, the integration is performed from the blade root cutout to a value denoted as $B.R_{bl}$, which accounts for blade tip loss. Indeed at blade tip, a trailed vortex is formed which produces a high local inflow over the tip region, effectively reducing the local lift capability [107]. Similar equations can be derived for the lift and drag forces inboard of the flap hinge.

For the generalized forces due to the blade flap contribution, we get

$$Q_{\beta_{bl}, A} = Q_{\beta_{bl}, A_L} + Q_{\beta_{bl}, A_D} \quad (71)$$

With

$$Q_{\beta_{bl}, A_L} = K_{(\beta, defic)} \cdot \int_{r_c}^{B.R_{bl}} \left(\mathbb{T}_{(HB)(ref)} \mathbf{dL}_{bl}^{ref} \right)^T \cdot \mathbf{dP}_{\beta, r}^{HB} \cdot r_{dm} \cdot dr_{dm} \quad (72)$$

And

$$Q_{\beta_{bl}, A_D} = \int_{r_c}^{R_{bl}} \left(\mathbb{T}_{(HB)(ref)} \mathbf{dD}_{bl}^{ref} \right)^T \cdot \mathbf{dP}_{\beta, r}^{HB} \cdot r_{dm} \cdot dr_{dm} \quad (73)$$

Where we have added an empirical deficiency factor $K_{(\beta, defic)}$ for the lift component.

Now providing analytical expressions for the previous four integrals represents a rather tedious task, even more so for twisted blades¹⁶ for which the blade pitch will also be function of the distance r_{dm} . We have therefore opted for a numerical evaluation of these integrals, as is often done in flight dynamics codes [156]. Here Gaussian quadrature integration was implemented, using a low order (fifth order) Legendre polynomial scheme [1].

¹⁶Although in our case we have assumed zero twist

3.5 Rotor forces

To find the total rotor forces denoted by the vector \mathbf{F}_{MR} , the general procedure is to integrate the elementary lift and drag forces $d\mathbf{L}_{bl}$ and $d\mathbf{D}_{bl}$ over the blade span, then average (integrate) the result over one revolution, and finally multiply the obtained expression by the total number of blades. Here a numerical procedure is implemented, similar to the one implemented to obtain the generalized forces in the preceding section.

Using eq (66) and eq (67) we get

$$\mathbf{F}_{MR}^{HB} = \frac{N_b}{2\pi} \left[\int_0^{2\pi} \int_{r_c}^{R_{bl}} \mathbb{T}_{(HB)(ref)} d\mathbf{L}_{bl}^{ref} \cdot dr_{dm} \cdot d\psi_{bl} + \int_0^{2\pi} \int_{r_c}^{R_{bl}} \mathbb{T}_{(HB)(ref)} d\mathbf{D}_{bl}^{ref} \cdot dr_{dm} \cdot d\psi_{bl} \right] \quad (74)$$

3.6 Rotor moments

The total rotor moments include contributions from four different sources: due to aerodynamic forces (moment arms with respect to fuselage CG due to lift \mathbf{M}_{aeroL}^{HB} , and due to drag \mathbf{M}_{aeroD}^{HB}), due to inertial loads $\mathbf{M}_{inertial}^{HB}$, due to flap hinge stiffness \mathbf{M}_{flap}^{HB} and finally due to lag hinge damping \mathbf{M}_{lag}^{HB} . We further neglect any additional blade aerodynamic moments, and moments due to airfoil camber.

We have

$$\mathbf{Mom}_{MR}^{HB} = \mathbf{M}_{aeroL}^{HB} + \mathbf{M}_{aeroD}^{HB} + \mathbf{M}_{inertial}^{HB} + \mathbf{M}_{flap}^{HB} + \mathbf{M}_{lag}^{HB} \quad (75)$$

3.6.1 Moment due to inertial loads

The expression is derived from [98].

$$\mathbf{M}_{inertial}^{HB} = -\frac{N_b}{2} \cdot M_{bl} \cdot (e_P + e_L + e_F) \cdot y_{G_{bl}} \cdot \Omega_{MR}^2 \begin{pmatrix} \Gamma \beta_{1s} \\ \beta_{1c} \\ 0 \end{pmatrix} \quad (76)$$

3.6.2 Moment due to flap hinge stiffness

The expression is derived from [98].

$$\mathbf{M}_{flap}^{HB} = -\frac{1}{1 - \frac{e_P + e_L + e_F}{R_{rot}}} \cdot \frac{N_b \cdot K_{S\beta}}{2} \begin{pmatrix} \Gamma \beta_{1s} \\ \beta_{1c} \\ 0 \end{pmatrix} \quad (77)$$

3.6.3 Moment due to lag hinge damping

$$\mathbf{M}_{lag}^{HB} = -\frac{N_b}{\frac{T_s}{\Omega_{MR}/(2\pi)}} \cdot (e_P + e_L) \cdot K_{D\zeta} \begin{pmatrix} 0 \\ 0 \\ \Gamma \dot{\zeta}_{bl} \end{pmatrix} \quad (78)$$

3.7 Inflow model

The rotor inflow is the name given to the flow field induced by the rotor at the rotor disk, thus contributing to the local blade incidence and dynamic pressure [121]. For flight dynamics analysis we shall assume that it is sufficient to consider the normal component of inflow at the rotor, i.e. the rotor induced downwash [121].

Inflow models can be divided into two categories, static and dynamic models. For low-bandwidth maneuvering applications, such as trim calculations or flying-qualities investigations, the dynamic effects of the interaction of the airmass with the airframe and rotor may be expected to be negligible, therefore static inflow models may be acceptable [46]. In a higher frequency range than that of the rigid-body modes, dynamic interactions between the inflow dynamics and the blade motion must be considered. For a review of research results obtained prior to the 1990s, see [8, 152, 41, 58, 87, 46], and for a recent review see [165].

Additionally dynamic models can be divided into two sub-categories, on one hand the so-called Pitt-Peters dynamic inflow theory [134, 135, 69, 126, 70], and on the other the Peters-He finite-state wake model [124, 128, 129].

The theory of dynamic inflow is an unsteady¹⁷ wake model that treats the wake degrees of freedom as dynamic states [126]. It is a means of accounting for the low-frequency wake effects under unsteady or transient conditions

¹⁷Unsteady aerodynamic effects (i.e. frequency dependent) can be categorized in two fields: the first one involves the calculation of the response of the rotor blade lift and pitching moment to changes in local incidence, the second one involves the calculation of the unsteady local incidence due to the time variations of the rotor wake velocities [121]

[70].

The finite-state wake model is a more comprehensive theory than dynamic inflow, not limited in harmonics and allowing to account for non linear radial inflow distributions. Actually the theory of dynamic inflow can be thought of as a special case of the finite-state wake model, with only three inflow expansion terms (uniform, side-to-side gradient, and fore-to-aft gradient) [128, 129].

Both dynamic and finite-state models have a proven track record as unsteady inflow models, while using a finite number of states, therefore very appropriate for flight dynamics analysis and control design. This said, it should be noted that recent advances in computing power and methodology have made it foreseeable for highly detailed free-wake¹⁸ models to be run in real-time, for flight dynamics simulation applications [103, 106, 165], hence potentially replacing in the future the dynamic inflow and finite-state wake models.

The sophisticated and complex finite-state Peters-He model is attractive when rotor vibration and blade aeroelasticity (e.g. elastic deformation) need to be analyzed [77]. For flight dynamics applications, it was found in [77] that the Peters-He model was not remarkably better than the three-state Pitt-Peters formulation. Since in our case we are not interested in vibration analysis or aeroelasticity, we have chosen to implement the more straightforward Pitt-Peters model [135, 126].

As a final note, we have added a pseudo-harmonic term to the induced velocity, so as to model the thrust fluctuations in the VRS, as presented in [95].

3.7.1 Static ground effect

A helicopter hovering close to the ground requires considerably less power than when it is hovering high above it [139]. One of the first theories for helicopter ground effects was presented in [85]. Early low-speed results were presented in [141], and in forward flight in [86], further wind-tunnel tests for a tail rotor in ground effect were presented in [94, 174, 64], and main rotor induced velocity modeling (e.g. image rotor method) in [42, 97, 83, 140, 137, 180, 26, 132].

¹⁸A free wake analysis is a versatile, yet complex, tool for modeling rotor vortical wake structure. Compared with momentum inflow or prescribed wake methods, free wake analysis directly captures the self-induced wake distortion without any pre-assumed wake geometries [138]

Additionally it was also reported that the type of the underlying surface has an important role in the ground effect. Indeed many pilots have reported that if the ground surface is water or tall grass instead of solid surfaces, the ground effect is diminished [139].

In this model, we chose to implement a simple formulation as presented in [15].

3.7.2 Off-axis response

It is well known that the average Tip-Path-Plane (TPP) reference for wake geometry is not suitable for transient flight modeling, where an instantaneous response is required [81]. In maneuvering flight the rotor wake distortion can be described in terms of global and local distortions. The global distortion is due to the motion of the rotor TPP (due to hub rotation during the maneuver), while the local distortion is due to the self-induced velocities of the wake [81].

Wake distortion is the primary source of the so-called off-axis response problem, observed in maneuvering flight, especially in hover and the low speed forward flight region¹⁹. Indeed wake bending during maneuvering flight significantly changes inflow distribution over the rotor, giving rise to a sign reversal in the off-axis response [138]. Further the larger the pitch rate, the greater the wake distortion [81].

It was also noted that flap hinge offset from main rotor shaft had two main effects on the off-axis coupling response: it increased the off-axis response magnitude, and it also gradually decreased the wake curvature effect [136].

Researchers have tried to improve the correlation of the off-axis response, through several methods. We provide here a short, non-exhaustive, list

- Aerodynamic interaction between helicopter rotor and body in [21]
- Including a virtual inertia effect associated with the swirl in the rotor wake in [168]
- Introducing an aerodynamic phase lag in flapping and dynamic inflow equations, and using system identification techniques in [157, 109, 66, 162, 147]
- Free wake modeling in [144, 160, 16]

¹⁹The effect of wake distortion on the first harmonic inflow variation diminishes quickly as forward speed is increased [17], e.g. for rotor advance ratios larger than 0.1 [81], where the rotor wake becomes flat

- Dynamic vortex ring modeling in [24, 27, 25]
- Extended momentum modeling in [99, 56, 13]
- Augmented Pitt-Peters dynamic inflow model in [23, 104, 105, 138, 176, 175]
- Augmented Peters-He finite state inflow model in [81]²⁰ and [81, 136, 176, 175]

Note that some of the methods outlined above, such as [99, 104, 23, 109], have utilized constant wake distortion coefficients across sometimes different flight conditions. This methodology of using constant coefficients could result in errors for low lift, or descending flight conditions [81, 27].

In this model we will use a constant coefficients method, i.e. the extended momentum model approach of [99], as it is simple to implement and has a proven track record [51, 78, 29].

3.7.3 Inflow Modeling

We derive first useful velocity expressions. Using eq (55), the velocity of the hub in the TPP frame, with respect to the air, i.e. holding the vehicle fixed in space and letting the air flow around it (hence the minus sign), is given by

$$\mathbf{V}_{air}^{TPP} = -\mathbb{T}_{(TPP)(HB)} \cdot \mathbf{V}_{a,G}^{HB} \quad (79)$$

Now we denote by V_{airX}^{TPP} the x-component of \mathbf{V}_{air}^{TPP} , we denote by V_{airY}^{TPP} the y-component of \mathbf{V}_{air}^{TPP} , and V_{airZ}^{TPP} the z-component of \mathbf{V}_{air}^{TPP} .

We also define the advance ratios, see Fig. 5 Fig. 6

$$\mu_1 = \frac{V_{airX}^{TPP}}{V_{ref}} \quad (80a)$$

$$\mu_2 = \frac{V_{airY}^{TPP}}{V_{ref}} \quad (80b)$$

$$\mu_3 = \frac{V_{airZ}^{TPP}}{V_{ref}} \quad (80c)$$

$$\mu = \sqrt{\mu_1^2 + \mu_2^2} \quad (80d)$$

Now the induced velocity in the TPP is given by [135]

²⁰This approach can be toggled on/off in FLIGHTLAB

$$v_i = V_{ref} \cdot \left(\lambda_0 + \lambda_s \cdot \frac{r_{dm}}{R_{rot}} \cdot \sin \psi_{bl} + \lambda_c \cdot \frac{r_{dm}}{R_{rot}} \cdot \cos \psi_{bl} \right) + \sum_{i=1}^n A_i \cdot \cos(\omega_i \cdot t + \phi_i) \quad (81)$$

Where the last term on the right-hand side of eq (81) has been added to empirically model the induced velocity fluctuations in the VRS, and hence thrust fluctuations, as presented in [95].

The VRS region is defined as follows $V_{tr}/v_h < V_{airZ}^{TPP}/v_h < -0.4$, with the value -0.4 from [173] and $V_{tr}/v_h \in [-1.9, -1.6]$ see [154]. In the VRS region, or even on a subset²¹ of this region given by $-0.8 \leq V_{airZ}^{TPP}/v_h < -0.6$ [173], the amplitudes A_i and frequencies ω_i can be tabulated²² as a function of the advance ratios μ and μ_3 , while the phase ϕ_i can be chosen randomly. Outside this region, the amplitude coefficients can be set to follow an exponential decrease towards zero.

And the rotor inflows are derived from the TPP wind axes

$$\begin{pmatrix} \lambda_s \\ \lambda_c \\ \lambda_0 \end{pmatrix}^{TPP} = \mathbb{T}_{(TPP)(TPPw)} \begin{pmatrix} \lambda_s \\ \lambda_c \\ \lambda_0 \end{pmatrix}^{TPPw} \quad (82)$$

In the TPP wind axes, we have the three-state dynamic inflow

$$\frac{d}{dt} \begin{pmatrix} \lambda_s \\ \lambda_c \\ \lambda_0 \end{pmatrix}^{TPPw} = \mathbb{M}^{-1} \cdot \left[-\mathbb{L}^{-1} \cdot \begin{pmatrix} \lambda_s \\ \lambda_c \\ \lambda_0 \end{pmatrix}^{TPPw} + \mathbf{F}_{dyninfl}^{TPPw} + \mathbb{L}^{-1} \cdot \begin{pmatrix} \Gamma \cdot K_p \cdot p \\ K_q \cdot q \\ 0 \end{pmatrix} \right] \quad (83)$$

Where the last term on the right-hand side of eq (83) models the off-axis response. It is however unclear whether the term $\mathbb{M}^{-1} \cdot \mathbb{L}^{-1}$ should pre-multiply the off-axis term as shown above.

The forcing function $\mathbf{F}_{dyninfl}^{TPPw}$ is given as

$$\mathbf{F}_{dyninfl}^{TPPw} = \mathbb{T}_{(TPPw)(TPP)} \begin{pmatrix} \Gamma \cdot C_{LMR} \\ C_{MMR} \\ -C_{TMR} \end{pmatrix}_{aero}^{TPP} \quad (84)$$

²¹Most turbulent region

²²In order to match flight test results

Where the subscript "aero" implies that only aerodynamic contributions are considered. Also a minus sign was added in front of C_{TMR} to have a positive induced velocity for a rotor lift vector oriented upwards (in the TPP frame the z-axis is oriented downwards).

The inflow gain and apparent mass matrices are presented next.

$$\mathbb{L} = \begin{pmatrix} \frac{-4}{V_M \cdot (1 + \cos \chi)} & 0 & 0 \\ 0 & \frac{-4 \cos \chi}{V_M \cdot (1 + \cos \chi)} & \frac{15\pi}{64V_T} \cdot \tan \frac{\chi}{2} \\ 0 & \frac{15\pi}{64V_M} \cdot \tan \frac{\chi}{2} & \frac{1}{2V_T} \end{pmatrix} \quad (85)$$

$$\mathbb{M} = \begin{pmatrix} \frac{-16}{45\pi} & 0 & 0 \\ 0 & \frac{-16}{45\pi} & 0 \\ 0 & 0 & \frac{8}{3\pi} \end{pmatrix} \quad (86)$$

The total velocity through the rotor, including ground effect correction, is given by [127]

$$V_T = G_{eff} \cdot \sqrt{(\lambda_m + \mu_3)^2 + \mu^2 + \left(\frac{v_h}{V_{ref}}\right)^2 \cdot f(\bar{\mu}) \cdot g(\bar{\lambda})} \quad (87)$$

And the momentum theory mass flow parameter is derived²³ from [126]

$$V_M = G_{eff}^2 \cdot \frac{\mu^2 + (2\lambda_m + \mu_3) \cdot (\lambda_m + \mu_3) + \left(\frac{v_h}{V_{ref}}\right)^2 \cdot f(\bar{\mu}) \cdot \left[g(\bar{\lambda}) + \frac{1}{2} \frac{\lambda_m}{V_{ref}} \cdot \dot{g}(\bar{\lambda})\right]}{V_T} \quad (88)$$

Where G_{eff} is introduced to model the static ground effect. The ground effect correction factor is given from [15] as

$$G_{eff} = \frac{1}{1 - \frac{(\lambda_m + \mu_3)^2}{16(h_H/R_{rot})^2 \cdot [(\lambda_m + \mu_3)^2 + \mu^2]}} \quad (89)$$

²³It does not exactly match the expression given in [127]

And we have the following expressions from [127]

$$f(\bar{\mu}) = 1 - 2\bar{\mu}^2 \text{ for } \bar{\mu} \in [0, 0.707] \quad (90a)$$

$$f(\bar{\mu}) = 0 \text{ otherwise} \quad (90b)$$

$$g(\bar{\lambda}) = \frac{1}{(2 + \bar{\lambda})^2} - \bar{\lambda}^2 + (1 + \bar{\lambda}) \cdot [0.109 + 0.217(\bar{\lambda} - 0.15)^2] \text{ for } \bar{\lambda} \in [-1, 0.6378] \quad (91a)$$

$$g(\bar{\lambda}) = 0 \text{ otherwise} \quad (91b)$$

$$\dot{g}(\bar{\lambda}) = \frac{-2}{(2 + \bar{\lambda})^3} + 0.049 - 1.696\bar{\lambda} + 0.651\bar{\lambda}^2 \text{ for } \bar{\lambda} \in [-1, 0.6378] \quad (92a)$$

$$\dot{g}(\bar{\lambda}) = 0 \text{ otherwise} \quad (92b)$$

Further from momentum theory the induced inflow λ_m in climb, hover, and windmill brake state [98] is given by

$$\lambda_m^2 \cdot [(\lambda_m + \mu_3)^2 + \mu^2] = (v_h/V_{ref})^4 \text{ for } \mu_3 \geq 0 \text{ or } \mu_3 \cdot \frac{V_{ref}}{v_h} \leq -2 \quad (93)$$

In the VRS and turbulent wake state we have from [127]

$$\lambda_m^2 \cdot [(\lambda_m + \mu_3)^2 + \mu^2 + \left(\frac{v_h}{V_{ref}}\right)^2 \cdot f(\bar{\mu}) \cdot g(\bar{\lambda})] = (v_h/V_{ref})^4 \text{ for } \mu_3 \cdot \frac{V_{ref}}{v_h} \in [-2, 0] \quad (94)$$

Here λ_m can either be derived as the output of a minimization routine such as *fminbnd* in MATLAB, or from a lookup table as a function of v_h/V_{ref} , μ_3 and μ .

4 Tail rotor

The tail rotor is a powerful design solution for torque balance, directional stability and control of single main rotor helicopters. The theory we apply here is based on the work done by Bailey in [19]. The model given in this paper is a standard approach towards tail rotor modeling, implemented among others in [90, 15, 169].

Next we present the various assumptions made in deriving the equations.

4.1 Assumptions

The following assumptions have been made.

Structural simplifications

- Rigid blade, has zero twist, constant chord, zero sweep, and has constant thickness ratio
- Blade torsion is neglected

Aerodynamics simplifications

- Linear lift with constant lift curve slope, and uniform induced flow over the rotor
- Compressibility and blade stall effects are disregarded
- Sophisticated aerodynamic interference effects from main rotor are neglected
- Viscous flow effects are disregarded

Dynamical simplifications

- No blade dynamics, simplified inflow dynamics
- Unsteady effects neglected

4.2 Modeling

We present first some useful velocity expressions.

4.2.1 Tail rotor velocities

We express

$$\mathbf{V}_{a,TR}^{HB} = \begin{pmatrix} u + q \cdot z_{TR} - r \cdot y_{TR} \\ v - p \cdot z_{TR} + r \cdot x_{TR} \\ w + p \cdot y_{TR} - q \cdot x_{TR} \end{pmatrix} - \mathbb{T}_{(HB)o} \cdot \begin{pmatrix} u_w \\ v_w \\ w_w \end{pmatrix}^o \quad (95)$$

In the tail rotor TR coordinate system of [15] we have

$$\mathbf{V}_{a,TR}^{TR} = \mathbb{T}_{(TR)(HB)} \cdot \mathbf{V}_{a,TR}^{HB} \quad (96)$$

Now we denote by $V_{a,TRX}^{TR}$ the x-component of $\mathbf{V}_{a,TR}^{TR}$, we denote by $V_{a,TRY}^{TR}$ the y-component of $\mathbf{V}_{a,TR}^{TR}$, and $V_{a,TRZ}^{TR}$ the z-component of $\mathbf{V}_{a,TR}^{TR}$.

The tail rotor advance ratios are expressed as follows

$$\left[\mu_{xTR} \quad \mu_{yTR} \quad \mu_{zTR} \right]^{TR} = \frac{1}{V_{refTR}} \cdot \left[V_{a,TRX} \quad V_{a,TRY} \quad \Gamma \cdot V_{a,TRZ} \right]^{TR} \quad (97)$$

4.2.2 Rotor forces

First the tail rotor blade pitch is given by

$$\theta_{TR} = \theta_{0TR} - T_{TR} \cdot \frac{\partial \beta_{0TR}}{\partial T_{TR}} \cdot \tan \delta_{3TR} + \theta_{biasTR} \quad (98)$$

The Bailey coefficients are given by

$$t_1 = \frac{B_{TR}^2}{2} + \frac{\mu_{xTR}^2 + \mu_{yTR}^2}{4} \quad (99a)$$

$$t_2 = \frac{B_{TR}^3}{3} + \frac{B_{TR} \cdot (\mu_{xTR}^2 + \mu_{yTR}^2)}{2} \quad (99b)$$

The downwash at the tail rotor is derived using momentum theory and is given as

$$\lambda_{dw} = \frac{c_{l(0,TR)} \cdot \sigma_{TR}}{2} \cdot \left(\frac{\mu_{zTR} \cdot t_1 + \theta_{TR} \cdot t_2}{2\sqrt{\mu_{xTR}^2 + \mu_{yTR}^2 + \lambda_{TR}^2} + \frac{c_{l(0,TR)} \cdot \sigma_{TR}}{2} \cdot t_1} \right) \quad (100)$$

The tail rotor total inflow is then given by

$$\lambda_{TR} = \lambda_{dw} - \mu_{zTR} \quad (101)$$

Where it is common practice to iterate between eq (100) and eq (101) until convergence within a reasonable tolerance.

Finally the thrust is given by

$$T_{TR} = 2 \cdot k_{bl} \cdot K_{TR_{corr}} \cdot \lambda_{dw} \cdot \rho \cdot \pi \cdot \left(\Omega_{TR} \cdot R_{rot_{TR}}^2 \right)^2 \cdot \sqrt{\mu_{x_{TR}}^2 + \mu_{y_{TR}}^2 + \lambda_{TR}^2} \quad (102)$$

Finally in the Hub-Body frame we have

$$\begin{pmatrix} F_{x_{TR}} \\ F_{y_{TR}} \\ F_{z_{TR}} \end{pmatrix}^{HB} = \begin{pmatrix} 0 \\ \Gamma \cdot T_{TR} \\ 0 \end{pmatrix}^{HB} \quad (103)$$

4.2.3 Rotor moments

The tail rotor moments include a crude model for the rotor torque from [98], and additional moments generated by the rotor force times the respective moment arms. We get

$$c_{Q_{TR}} = \frac{\sigma_{TR} \cdot c_{d_{TR}}}{8} \left(1 + 4.6(\mu_{x_{TR}}^2 + \mu_{y_{TR}}^2) \right) \quad (104)$$

and

$$\begin{pmatrix} L_{TR} \\ M_{TR} \\ N_{TR} \end{pmatrix}^{HB} = \begin{pmatrix} -z_{TR} \cdot T_{TR} \\ c_{Q_{TR}} \cdot \left(\rho \cdot \pi \cdot R_{rot_{TR}}^5 \cdot (GB \cdot \Omega_{MR_{100\%}})^2 \right) \\ x_{TR} \cdot T_{TR} \end{pmatrix}^{HB} \quad (105)$$

Here the distances are algebraic expressions expressed in the Hub-Body frame (hence not always positive).

5 Simulation results

Simulation plots and comparisons with FLIGHTLAB are given in Appendix F.

5.1 Trim results

The word *trim* was adopted by the aviation community to imply the correct adjustment of aircraft controls, attitude, and cargo in order to obtain a desired steady flight condition [101]. A trim condition is thus equivalent to an equilibrium point, also called an operating point of a nonlinear helicopter model, which can be thought of as a specific flight condition [75]. Further

trim settings are a prerequisite for stability analysis, vibration studies, and control systems synthesis. In the case of linear control systems development, an accurate linear time-invariant mathematical model of the nonlinear helicopter flight dynamics is necessary. Such a model may be obtained by linearization of a nonlinear model at desired steady flights, or *trim* conditions.

Any flight vehicle should be able to maintain equilibrium during steady flight conditions. This means that the resultant forces and moments on the vehicle are equal to zero [125]. For helicopters however, the concept of trim is more complicated than of fixed-wing aircrafts [123]. A helicopter has components that rotate with respect to each other and with respect to the air mass. Hence, periodic forces and moments enter the dynamic equations, and we cannot simply eliminate them by averaging [123].

Our trim module is structured as a constrained optimization problem. At equilibrium the resultant forces and moments on the vehicle should be equal to zero, hence the objective of the trim module is to minimize the three vehicle linear accelerations and the three rotational accelerations. The variables that the algorithm is allowed to manipulate include the four control inputs and the vehicle roll and pitch states, since these latter two influence the projection of the gravity vector on the body frame. Additionally constraints are specified, i.e. by assigning fixed values to the three vehicle linear velocities, the three vehicle rotational velocities, and by setting to zero the three dynamic inflow linear accelerations. Now regarding the periodic states, i.e. blade flap and lag positions, and flap and lag velocities, these four states are handled by time-marching the nonlinear helicopter model long enough until the transients have decayed. Finally the remaining four states which include the three vehicle Cartesian position and the vehicle heading are left free, since the position of the helicopter does not influence²⁴ its dynamic behavior or stability.

The optimization is further based on a Newton iteration scheme, similar to that implemented in [169]. The Newton's method is simple to implement and is one of the most widely used [6]. But although it guarantees quadratic convergence, it guarantees only local convergence, and is also sensitive to the initial starting values. Even with good starting values, the method can exhibit erratic divergence due to for example numerical corruption [6]. Hence over the years, several other approaches have been re-

²⁴Although strictly speaking this is not true in vertical flight, due to the ground effect when trimming near the ground, and due to changes in air density when trimming with a non-zero vertical velocity; however for the case of air density variations, these may be neglected when considering UAV applications, since UAV flight altitude is generally within 200-300 m above ground

searched. For a review of helicopter trim types, and associated solution strategies see [131, 130, 125, 6, 101, 123, 112, 121].

The following sections present comparisons between the research model and FLIGHTLAB, with the following characteristics selected for the FLIGHTLAB model:

- Articulated rotor, and blade element model
- Quasi-steady airloads, based on the Peters-He three-state inflow model, and no stall delay effects
- Ideal engine

The model's simulation plots, presented in the sequel, are based on an adapted version of our baseline model. Specifically, the static expressions of the Pitt-Peters inflow model have been retained in lieu of the dynamic ones, since the former ones provide a better match with FLIGHTLAB. This unexpected result is a subject of ongoing research.

5.1.1 Trim as a function of body longitudinal velocity

A very good correlation with FLIGHTLAB can be seen for the vehicle roll and pitch angles in Fig. 7, main and tail rotor collective inputs in Fig. 8, main rotor longitudinal cyclic input in Fig. 9, main rotor Tip-Path-Plane angles in Fig. 10, and inflow uniform velocity in Fig. 11.

The correlation for the main rotor lateral cyclic input is very good until about 5 m/s, see Fig. 9, and then exhibits a bias for higher velocities. This is due to inaccuracies of the research model, probably because of unmodeled effects such as blade aerodynamic moments. Similarly the longitudinal and lateral inflow velocities exhibit some slight biases when compared to FLIGHTLAB see Fig. 11, due to inaccuracies of the research model, again probably related to the blade aerodynamic roll and pitch moments.

Note also that it is well known that for low advance ratios, the lateral tilt of the rotor disk is under-predicted when compared to experimental data [164]. Hence in the future, and in case a better fit with measurements is necessary, a model modification according to [164] may be advisable.

5.1.2 Trim as a function of body lateral velocity

Here very good correlation with FLIGHTLAB can be seen for the vehicle roll and pitch angles in Fig. 12, main and tail rotor collective inputs in Fig. 13, main rotor longitudinal and lateral cyclic inputs in Fig. 14, main

rotor Tip-Path-Plane angles in Fig. 15, and inflow uniform, longitudinal and lateral velocities in Fig. 16.

5.1.3 Trim as a function of body vertical velocity

Overall a very good correlation with FLIGHTLAB can be seen in climb, and in descent up to a descent velocity of 2 m/s. As the descent velocity increases, slight deviations between the research model and FLIGHTLAB tend to appear for the vehicle roll and pitch angles in Fig. 17, while larger deviations can be seen in main and tail rotor collective inputs in Fig. 18, and in inflow uniform and lateral velocities in Fig. 21. Other parameters exhibit good match at these higher descent rates, see Fig. 19 and Fig. 20. The deviations in main and tail rotor collective inputs may be a consequence of the deviations in inflow uniform velocity. The deviations in inflow uniform velocity may be due to different inflow models in descent flight. FLIGHTLAB implements an inflow model based on [82], while the research model has the inflow based on the more recent contribution of [127]. Now the deviations in inflow lateral velocity are due to inaccuracies of the research model, related again to the blade aerodynamic roll and pitch moments.

5.2 Dynamic results

For the validation of a model dynamic responses, we may consider two approaches. The first one consists in obtaining a linearized model which describes the small perturbation motion about a trimmed equilibrium position. The validation is then carried out by comparing the frequency response predicted by the linearized model and the frequency response from an equivalent linear FLIGHTLAB model, or from a linear model identified from flight test data.

The second approach consists in comparing the time histories of the research model and those of FLIGHTLAB (or equivalently flight test data). In this paper we provide only visual comparisons of time response data.

Further, as the helicopter is a perfect example of a MIMO system, Table 2 has been provided to better understand the impact of each input channel.

5.2.1 Hover response to main rotor collective pitch

We present the dynamic results for a 1° block input on the main rotor collective pitch, at hover, between time instants $t = 0.25 \text{ sec}$ and $t = 1.25 \text{ sec}$, see Fig. 22 and Fig. 23. Since both models are highly unstable, we have chosen to simulate responses for only three seconds.

		Response			
		Pitch	Roll	Yaw	Climb/Descent
Input Axis	Long stick	Prime	Due to lat flapping	Negligible	Desired in fwd flight
	Lat stick	Due to long flapping	Prime	Undesired in hover, desired in fwd flight	Descent with bank angle
	Rudder	Negligible	Roll due to TR thrust & sideslip	Prime (hover)	Undesired, due to power changes in hover
	Collective	Due to transient & steady long flapping	Due to transient & steady lat flapping & sideslip	Power change varies requirement for TR thrust	Prime

Table 2: Single-rotor helicopter coupling sources (from [32]). *Long* stands for Longitudinal, *Lat* for Lateral

The first figure, Fig. 22, presents the four control input values, while the second one, Fig. 23, shows the standard nine vehicle body dynamics states, i.e. three Euler angles, three linear velocities, and three rotational velocities.

Overall the match between the research model and FLIGHTLAB is good to very good.

5.2.2 Response at $u = 5 \text{ m/s}$ to main rotor lateral cyclic pitch

We present the dynamic results for a 1° block input on the main rotor lateral cyclic pitch, at $u = 5 \text{ m/s}$, between time instants $t = 0.25 \text{ sec}$ and $t = 1.25 \text{ sec}$, see Fig. 24 and Fig. 25.

Overall the match between the research model and FLIGHTLAB is fair to good.

5.2.3 Response at $u = 5$ m/s to main rotor longitudinal cyclic pitch

We present the dynamic results for a 1° block input on the main rotor longitudinal cyclic pitch, at $u = 5$ m/s, between time instants $t = 0.25$ sec and $t = 1.25$ sec, see Fig. 26 and Fig. 27.

Overall the match between the research model and FLIGHTLAB is fair to good.

5.2.4 Response at $u = 10$ m/s to tail rotor collective pitch

We present the dynamic results for a 1° block input on the tail rotor collective pitch, at $u = 10$ m/s, between time instants $t = 0.25$ sec and $t = 1.25$ sec, see Fig. 28 and Fig. 29.

Overall the match between the research model and FLIGHTLAB is fair to good.

Regarding the observed discrepancies between our model and FLIGHTLAB, especially those seen at high speed or on the yaw channel in the VRS, these may very probably be attributed to the following five items: (i) validity of the flap-lag equations of motion up to about $u = 10 - 15$ m/s, see [155], (ii) a somewhat distinct implementation of the Bailey type tail rotor, (iii) a distinct implementation of the induced rotor flow, i.e. FLIGHTLAB uses the Peters-He finite-state wake model [124, 128, 129], while our model applies the static version of the Pitt-Peters model [134, 126], (iv) a distinct implementation of the induced rotor flow in the VRS, i.e. FLIGHTLAB uses the method presented in [82], while our model utilizes a slightly adapted version of [127], and finally (v) any side-effects due to the model simplifications as presented in Section 3. This said, we believe that most of the observed differences may primarily be attributed to the first three items, namely distinct models and hence behavior of the main rotor blade flap-lag, tail rotor inflow, and main rotor inflow.

6 Conclusion

We have presented a UAV helicopter flight dynamics nonlinear model for a flybarless articulated Pitch-Lag-Flap (P-L-F) main rotor, with rigid blades, and applicable for high bandwidth control specifications. The model allows for both ClockWise and Counter-ClockWise main rotor rotation, and is valid for a range of flight conditions including autorotation and the Vortex-Ring-State (VRS). Further, this model has been compared with an equivalent FLIGHTLAB nonlinear model. Simulation results show that the match between the model and FLIGHTLAB is very good for static (trim) conditions, is good to very good for dynamic conditions from hover to medium speed flight $u = 5\text{m/s}$, and is fair to good for dynamic conditions at high speed $u = 10\text{ m/s}$. While keeping in mind the model's accuracy reduction at high speed, this model could potentially be used to simulate and investigate the flight dynamics of a flybarless small-scale UAV helicopter, including in autorotation and VRS conditions, as well as provide a basis for model-based control design. Indeed, future work will focus on the development of nonlinear and linear control schemes. In particular, we have currently used an adapted version of this model, based on closed-form expressions, to obtain optimal helicopter flight trajectories, by solving constrained nonlinear optimal control problems. This topic will be elaborated upon in future publications.

Appendix A: Nomenclature

Vectors in this document are printed in boldface \mathbf{X} and are defined in three-dimensional space \mathbb{R}^3 . A vector is qualified by its subscript while its superscript denotes the projection frame: for example \mathbf{V}_a^I represents the aerodynamic velocity projected on frame F_I . Further matrices are written in outline type \mathbb{M} . Finally transformation matrices are denoted as \mathbb{T}_{ij} , with the two suffices signifying from frame F_j to frame F_i .

Kinematics

- Time
 - T_s Sample period (also called sample interval)
- Position
 - x_N, x_E, x_Z Coordinates of CG position vector in F_o frame
- Altitude
 - $h_H = -x_Z - z_H$ Hub position above ground
 - $h_G = -x_Z$ CG position above ground
- Angles
 - ψ Azimuth angle (yaw angle, heading)
 - θ Inclination angle (pitch angle, or elevation)
 - ϕ Bank angle (roll angle)
- Linear velocities are denoted \mathbf{V} and their components u, v, w
 - $\mathbf{V}_{k,G}$ Kinematic velocity of the vehicle center of mass
 - $\mathbf{V}_{a,G}$ Aerodynamic velocity of the vehicle center of mass
 - $u_k^o = V_N$ x component of $\mathbf{V}_{k,G}$ on F_o , V_N North velocity
 - $v_k^o = V_E$ y component of $\mathbf{V}_{k,G}$ on F_o , V_E East velocity
 - $w_k^o = V_Z$ z component of $\mathbf{V}_{k,G}$ on F_o , V_Z Vertical velocity
 - $u_k^b = u$ x component of $\mathbf{V}_{k,G}$ on body frame F_b
 - $v_k^b = v$ y component of $\mathbf{V}_{k,G}$ on body frame F_b
 - $w_k^b = w$ z component of $\mathbf{V}_{k,G}$ on body frame F_b
 - Vz_{Lmax} Max. vertical velocity at touchdown
- Angular velocities are denoted $\mathbf{\Omega}$ and their components p, q, r
 - $\mathbf{\Omega}_k = \mathbf{\Omega}_{bo}$ Kinematic angular velocity of the vehicle relative to the earth
 - $p_k^b = p$ Roll velocity (roll rate) of the vehicle relative to the earth
 - $q_k^b = q$ Pitch velocity (pitch rate) of the vehicle relative to the earth
 - $r_k^b = r$ Yaw velocity (yaw rate) of the vehicle relative to the earth

-
- Atmosphere
 - \mathbf{V}_w Wind linear velocity in F_o , of an atmospheric particle which could have been located at the vehicle center of mass
 - u_w Wind x-velocity in F_o
 - v_w Wind y-velocity in F_o
 - w_w Wind z-velocity in F_o
 - Ψ_w Wind azimuthal angular position
 - ρ Air density
 - T Static temperature
 - γ Specific heat ratio (air)
 - R Gas constant (air)
 - a speed of sound
 - Mass & Inertia
 - m Vehicle total mass
 - m_{ZeroF} Vehicle zero fuel mass
excluding fuel and additional payload
 - m_{PL} Additional payload mass
 - m_{Fus} Fuselage mass
 - $A = I_{xx}$ Vehicle inertia moment wrt x_b
 - $B = I_{yy}$ Vehicle inertia moment wrt y_b
 - $C = I_{zz}$ Vehicle inertia moment wrt z_b
 - $D = I_{yz}$ Vehicle inertia product wrt x_b
 - $E = I_{xz}$ Vehicle inertia product wrt y_b
 - $F = I_{xy}$ Vehicle inertia product wrt z_b

And the vehicle inertia matrix is given by

$$\mathbb{I} = \begin{pmatrix} A & 0 & -E \\ 0 & B & 0 \\ -E & 0 & C \end{pmatrix}$$

We further denote the fuselage inertia matrix as \mathbb{I}_{Fus}

- Other
 - M Mach number
 - g Gravity constant

Main rotor and blade dynamics

- Position
 - x_H, y_H, z_H Position of main rotor Hub center wrt vehicle CG
 - $x_{G_{bl}}, y_{G_{bl}}, z_{G_{bl}}$ Position of blade CG G_{bl} wrt flap hinge
- Angles
 - β_P Rotor precone angle
 - α_{bl} Blade section angle of attack
 - ψ_{bl} Azimuthal angular position of blade
 - ζ_{bl} Blade lag angle
 - β_{bl} Blade flap angle
 - β_0 Rotor TPP coning angle
 - β_{1c} Longitudinal rotor TPP tilt (positive forward)
 - β_{1s} Lateral rotor TPP tilt (positive towards retreating side)
 - θ_{bl} Blade pitch outboard of flap hinge (feathering) angle
 - ψ_{PA} Swashplate phase angle
 - θ_0 Blade root collective pitch
 - θ_{1c} Lateral cyclic pitch
 - θ_{1s} Longitudinal cyclic pitch
 - β_{TPPw} Sideslip angle between TPP frame and TPPw frame (dynamic inflow model)
 - χ Main rotor wake skew angle (always positive)

$$\chi = \arctan\left(\frac{\sqrt{\mu_1^2 + \mu_2^2}}{|\lambda_m + \mu_3|}\right)$$
- Linear velocities
 - v_i Rotor induced velocity, normal to the TPP and positive when oriented downwards (produced by a positive rotor thrust)
 - v_h Rotor induced velocity in hover

$$v_h = \sqrt{\frac{m \cdot g}{2 \cdot \rho \cdot \pi \cdot R_{rot}^2}}$$
 - V_{ref} Reference velocity

$$V_{ref} = \Omega_{MR} \cdot R_{rot}$$
 - U_P Flow velocity perpendicular to the reference ($x_{F_{ref}}, y_{F_{ref}}$) plane
 - U_T Flow velocity tangential to the reference ($x_{F_{ref}}, y_{F_{ref}}$) plane
- Angular velocities
 - $\Omega_{MR100\%}$ Nominal (100%) main rotor angular velocity
 - Ω_{MR} Instantaneous main rotor angular velocity
- Main rotor properties

Γ	Direction of rotation, <i>CCW</i> : $\Gamma = 1$ <i>CW</i> : $\Gamma = -1$
N_b	Main rotor number of blades
M_{bl}	Blade 0th mass moment (blade mass from flap hinge)
I_β	Blade 2nd mass moment (inertia about flap hinge)
r_{dm}	Distance between flap hinge and blade element dm
R_{rot}	Rotor radius measured from hub center
R_{bl}	Blade radius measured from flap hinge
c_{bl}	Blade chord
c_{hub}	Hub arm chord
$K_{S\beta}$	Hub spring restraint coefficient (due to flap)
$K_{S\zeta}$	Hub spring restraint coefficient (due to lag)
$K_{D\beta}$	Hub spring damping coefficient (due to flap)
$K_{D\zeta}$	Hub spring damping coefficient (due to lag)
$K_{(\theta\beta)}$	Pitch-flap coupling ratio
$K_{(\theta\zeta)}$	Pitch-lag coupling ratio
K_p	Off-axis coefficient (roll)
K_q	Off-axis coefficient (pitch)
μ	Advance ratio
μ_1	Non-dimensional forward flight air velocity
μ_2	Non-dimensional sideways flight air velocity
$\mu = \sqrt{\mu_1^2 + \mu_2^2}$	Non-dimensional in-plane (rotor disk) air velocity
μ_3	Non-dimensional vertical flight air velocity (normal to the TPP)
$\bar{\mu} = \frac{\mu}{\lambda_h}$	Normalizing advance ratio
$f(\bar{\mu})$	Advance ratio correction (fitting function)
$\bar{\lambda} = \frac{\lambda_m + \mu_3}{\lambda_h}$	Normalizing total inflow
$g(\bar{\lambda})$	VRS correction factor
$\dot{g}(\bar{\lambda}) = \partial g(\bar{\lambda}) / \partial \bar{\lambda}$	
$\lambda = \frac{v_i}{V_{ref}}$	Induced inflow due to rotor thrust (TPP)
λ_m	Momentum theory induced inflow due to rotor thrust (TPP)
λ_0	Uniform inflow due to rotor thrust (TPP)
λ_s	Lateral inflow due to rotor thrust (TPP)
λ_c	Longitudinal inflow due to rotor thrust (TPP)
λ_h	Rotor induced inflow in hover
$\lambda_h = \sqrt{\frac{C_{TMR}}{2}} = v_h / V_{ref}$	
G_{eff}	Ground effect corrective factor
V_T	Non-dimensional total velocity at the rotor disk center
V_M	Mass flow parameter
$c_{l_{bl}}$	Blade section lift coefficient
$c_{d_{bl}}$	Blade section drag coefficient
c_M	Blade section pitching moment due to airfoil camber
B	Tip loss factor, expressed as percentage of blade length R_{bl}
K_{defic}	Lift deficiency factor
$K_{(\beta, defic)}$	Lift due to flap deficiency factor

- Forces/moments
 - \mathbf{F}_{MR} Main rotor forces
 - \mathbf{Mom}_{MR} Main rotor moments
 - L_{MR} Main rotor roll moment
 - M_{MR} Main rotor pitch moment
 - T_{MR} Main rotor thrust
 - C_{TMR} Main rotor thrust coefficient
 $C_{TMR} = T_{MR}/(\rho \cdot \pi \cdot R_{rot}^2 \cdot V_{ref}^2)$
 - C_{LMR} Main rotor roll moment coefficient
 $C_{LMR} = L_{MR}/(\rho \cdot \pi \cdot R_{rot}^3 \cdot V_{ref}^2)$
 - C_{MMR} Main rotor pitch moment coefficient
 $C_{MMR} = M_{MR}/(\rho \cdot \pi \cdot R_{rot}^3 \cdot V_{ref}^2)$

Tail rotor

- Position vector components
 - x_{TR}, y_{TR}, z_{TR} Position of tail rotor hub wrt vehicle CG
- Angles
 - β_{0TR} Tail rotor coning angle
 - θ_{TR} Blade pitch angle
 - θ_{0TR} Blade root collective pitch
 - θ_{biasTR} Preset collective pitch bias
 - δ_{3TR} Hinge skew angle for pitch-flap coupling
- Linear velocities
 - $\mathbf{V}_{a,TR}$ Aerodynamic velocity of the tail rotor hub
 - v_{bl} Transitions velocity (vertical fin blockage)
 - V_{refTR} Reference velocity
 $V_{refTR} = \Omega_{MR} \cdot R_{rotTR}$
- Angular velocities
 - $\Omega_{TR100\%}$ Nominal (100%) tail rotor angular velocity
 - Ω_{TR} Instantaneous tail rotor angular velocity

- Tail rotor properties

$N_{b_{TR}}$	Tail rotor number of blades
$R_{rot_{TR}}$	Rotor radius measured from tail rotor shaft
c_{TR}	Blade chord
$\sigma_{TR} = \frac{N_{b_{TR}} \cdot c_{TR}}{\pi \cdot R_{rot_{TR}}}$	Tail rotor solidity
$\mu_{x_{TR}}$	x-component of tail rotor advance ratio
$\mu_{y_{TR}}$	y-component of tail rotor advance ratio
	$\mu_{xy_{TR}}^2 = \mu_{x_{TR}}^2 + \mu_{y_{TR}}^2$
$\mu_{z_{TR}}$	z-component of tail rotor advance ratio
λ_{TR}	Tail rotor inflow
λ_{dw}	Main rotor downwash at tail rotor
$t_1 \quad t_2 \quad t_3$	Bailey coefficients
k_{bl}	Blockage factor due to vertical fin
b_{t_1}	Tail blockage constant
$K_{TR_{corr}}$	Correction factor
$c_{l(0,TR)}$	Blade section lift curve slope
$c_{d_{TR}}$	Blade drag coefficient
B_{TR}	Tip loss factor, expressed as percentage of blade length

- Forces/moments

T_{TR}	Tail rotor thrust
C_{TTR}	Tail rotor thrust coefficient
$F_{x_{TR}}$	Tail rotor x-force
$F_{y_{TR}}$	Tail rotor y-force
$F_{z_{TR}}$	Tail rotor z-force
L_{TR}	Tail rotor roll moment
M_{TR}	Tail rotor pitch moment
N_{TR}	Tail rotor yaw moment

Appendix B: Physical Parameters

	Name	Parameter	Value	Unit
Environment	Air density	ρ	1.2367	kg/m^3
	Static temperature	T	273.15 + 15	K
	Specific heat ratio (air)	γ	1.4	
	Gas constant (air)	R	287.05	$J/kg.K$
	Gravity constant	g	9.812	m/s^2
Vehicle	Zero fuel mass	m_{Zero}	18	kg
	Fuel mass	m_{fuel}	2	kg
	Payload mass	m_{PL}	0	kg
	Fuselage mass	m_{Fus}	19.446	kg
	Total inertia moment wrt x_b	A	1.2	$kg.m^2$
	Total inertia moment wrt y_b	B	1.5	$kg.m^2$
	Total inertia moment wrt z_b	C	1	$kg.m^2$
	Total inertia product wrt x_b	D	0	$kg.m^2$
	Total inertia product wrt y_b	E	0	$kg.m^2$
	Total inertia product wrt z_b	F	0	$kg.m^2$
	Fuselage inertia moment wrt x_b	A	0.9516	$kg.m^2$
	Fuselage inertia moment wrt y_b	B	1.2515	$kg.m^2$
	Fuselage inertia moment wrt z_b	C	0.7263	$kg.m^2$
	Fuselage inertia product wrt x_b	D	0	$kg.m^2$
	Fuselage inertia product wrt y_b	E	0	$kg.m^2$
	Fuselage inertia product wrt z_b	F	0	$kg.m^2$
	X-pos. of fus. CG wrt total CG	x_H	0	m
	Y-pos. of fus. CG wrt total CG	y_H	0	m
	Z-pos. of fus. CG wrt total CG	z_H	0.015	m
	X-pos. of MR hub wrt total CG	x_H	0	m
	Y-pos. of MR hub wrt total CG	y_H	0	m
	Z-pos. of MR hub wrt total CG	z_H	-0.36	m
	X-pos. of TR hub wrt total CG	x_{TR}	-1.150	m
Y-pos. of TR hub wrt total CG	y_{TR}	0.040	m	
Z-pos. of TR hub wrt total CG	z_{TR}	-0.070	m	
Max. vertical vel (landing)	Vz_{Lmax}	0.25	m/s	
Main	Direction of rotation	Γ	-1	
	Number of blades	N_b	3	
	Nominal angular velocity	$\Omega_{MR_{100\%}}$	151.843	rad/s
	Rotor radius from hub	R_{rot}	0.944	m
	Swashplate phase angle	ψ_{PA}	0	rad
	Precone angle	β_P	0	rad
	Pitch-flap coupling ratio	$K_{(\theta\beta)}$	0	
	Pitch-lag coupling ratio	$K_{(\theta\zeta)}$	0	
Spring restraint coef. due to flap	$K_{S\beta}$	271.1635	$N.m/rad$	

Rotor MR	Spring damping coef. due to flap	$K_{D\beta}$	0	$N.m.s/rad$
	Spring restraint coef. due to lag	$K_{S\zeta}$	0	$N.m/rad$
	Spring damping coef. due to lag	$K_{D\zeta}$	24.4047	$N.m.s/rad$
	Off-axis roll coef.	K_p	0	
	Off-axis pitch coef.	K_q	0	
	Offset distance	e_P	0.035	m
	Offset distance	e_L	0.049	m
	Offset distance	e_F	0.010	m
	Blade mass	M_{bl}	0.277	kg
	Blade twist at tip	θ_{wash}	0	rad
	Blade chord	c_{bl}	0.076	m
	Hub arm chord	c_{hub}	0.015	m
	Root cutout from flap hinge	r_c	0.006	m
	Y-pos. blade CG wrt flap hinge	$y_{G_{bl}}$	0.8932	m
	Tip loss factor	B	0.97	
	Airfoil lift coef.	$c_{l_{bl}}$	NACA0012	
	Airfoil drag coef.	$c_{d_{bl}}$	NACA0012	
	Airfoil pitching moment coef.	c_M	NACA0012	
	Lift deficiency factor	K_{defic}	0.89	
	Lift deficiency (due to flap)	$K_{(\beta, defic)}$	1	
Transmission	Gearbox transmission ratio	GB	4.67	
Tail Rotor TR	Number of blades	$N_{b_{TR}}$	2	
	Rotor radius from hub	$R_{rot_{TR}}$	0.18	m
	Pitch-flap coupling	$\delta_{3_{TR}}$	0	rad
	Preset collective pitch bias	$\theta_{bias_{TR}}$	0	rad
	Partial coning angle wrt thrust	$\beta_{0_{TR}}$	0	rad/N
	Tail blockage constant	b_{t1}	1	
	Transition velocity	v_{bl}	0	m/s
	Blockage due to vertical fin	k_{bl}	1	
	Correction factor	$K_{TR_{corr}}$	1/1.270	
	Blade chord	c_{TR}	0.035	m
	Tip loss factor	B_{TR}	0.92	
	Airfoil lift curve slope	$c_{l_{(0, TR)}}$	5.73	rad^{-1}
Blade drag coef.	$c_{d_{TR}}$	0.035		
Actuators	MR collective range	θ_0	$[-3,10].\pi/180$	rad
	MR lateral cyclic range	θ_{1c}	$[-5,5].\pi/180$	rad
	MR longitudinal cyclic range	θ_{1s}	$[-5,5].\pi/180$	rad
	TR collective range	$\theta_{0_{TR}}$	$[6,18].\pi/180$	rad
	Max. rate	$\frac{d}{dt}\theta_i$	$80.\pi/180$	rad/s

Table 3: Physical Parameters

Appendix C: Frames and rotations

All frames are three-dimensional orthogonal and right-handed.

Kinematic frames

Regarding kinematic frames, we adopt here the notation used in [34].

The inertial frame $F_I (A, \mathbf{x}_I, \mathbf{y}_I, \mathbf{z}_I)$

The inertial frame F_I , is a Galilean²⁵ frame, a geocentric inertial axis system. The origin of the frame A being the center of the earth, the axis south-north \mathbf{z}_I is carried by the axis of the earth's rotation²⁶, while axes \mathbf{x}_I and \mathbf{y}_I are keeping a fixed direction in space, with the axis \mathbf{x}_I lying in the equatorial plane and oriented towards the vernal equinox point or "point γ " [34].

Vehicle-carried normal earth frame $F_o (O, \mathbf{x}_o, \mathbf{y}_o, \mathbf{z}_o)$

The origin O is a fixed point relative to the earth. The axis \mathbf{z}_o is oriented towards the descending direction of the local gravity attraction, in vehicle CG. The axis \mathbf{x}_o is directed towards the geographical north. The earth is assumed spherical.

Body frame $F_b (G, \mathbf{x}_b, \mathbf{y}_b, \mathbf{z}_b)$

This frame is linked to the vehicle body. The fuselage axis \mathbf{x}_b is oriented towards the front and belongs to the symmetrical plane of the vehicle. The axis \mathbf{z}_b is in the symmetrical plane of the vehicle and oriented downward relative to the vehicle. This definition assumes the existence of a symmetrical plane.

Blade frames

The following main rotor frames have been defined:

- Blade frame $F_{ref} (F, \mathbf{x}_{ref}, \mathbf{y}_{ref}, \mathbf{z}_{ref})$
- Blade frame $F_{bl} (F, \mathbf{x}_{bl}, \mathbf{y}_{bl}, \mathbf{z}_{bl})$
- $F_1 (F, \mathbf{x}_1, \mathbf{y}_1, \mathbf{z}_1)$
- $F_2 (L, \mathbf{x}_2, \mathbf{y}_2, \mathbf{z}_2)$

²⁵This frame is only Galilean when used in relationship with the accuracy searched for in flight dynamics

²⁶Note however that the axis \mathbf{z}_I , also called polar-axis, is animated by a movement of precession and nutation wrt a stellar frame, for further details see [115]

-
- $F_3 (L, \mathbf{x}_3, \mathbf{y}_3, \mathbf{z}_3)$
 - $F_4 (P, \mathbf{x}_4, \mathbf{y}_4, \mathbf{z}_4)$
 - $F_5 (P, \mathbf{x}_5, \mathbf{y}_5, \mathbf{z}_5)$
 - $F_6 (H, \mathbf{x}_6, \mathbf{y}_6, \mathbf{z}_6)$
 - Hub-Body frame $F_{HB} (H, \mathbf{x}_{HB}, \mathbf{y}_{HB}, \mathbf{z}_{HB})$. The Hub-Body axes are defined wrt the main rotor hub, remaining fixed relative to the rigid body of the helicopter
 - Tip-Path-Plane (TPP) F_{TPP} . The Tip Path Plane axes are defined wrt the motion described by the main rotor blade tips. The TPP has a longitudinal and lateral tilt wrt the F_{HB}
 - Tip-Path-Plane Wind (TPPw) F_{TPPw} . Here the x-axis of the TPP frame has been rotated to be aligned with the incoming flow

The frames are shown in Fig. 2, Fig. 3, Fig. 4, Fig. 5, and Fig. 6.

Note that Fig. 3 shows the case of a CCW main rotor, when seen from above. If the helicopter were in forward flight mode then the blade shown in Fig. 3 would be the advancing blade.

With the following blade angle conventions, as in [98]

- Blade flap angle β_{bl} is defined to be positive for upward motion of the blade (as produced by the thrust force on the blade)
- Blade lag angle ζ_{bl} is defined to be positive when opposite the direction of rotation of the rotor (as produced by the blade drag forces)
- Blade pitch angle θ_{bl} is defined to be positive for nose-up rotation of the blade

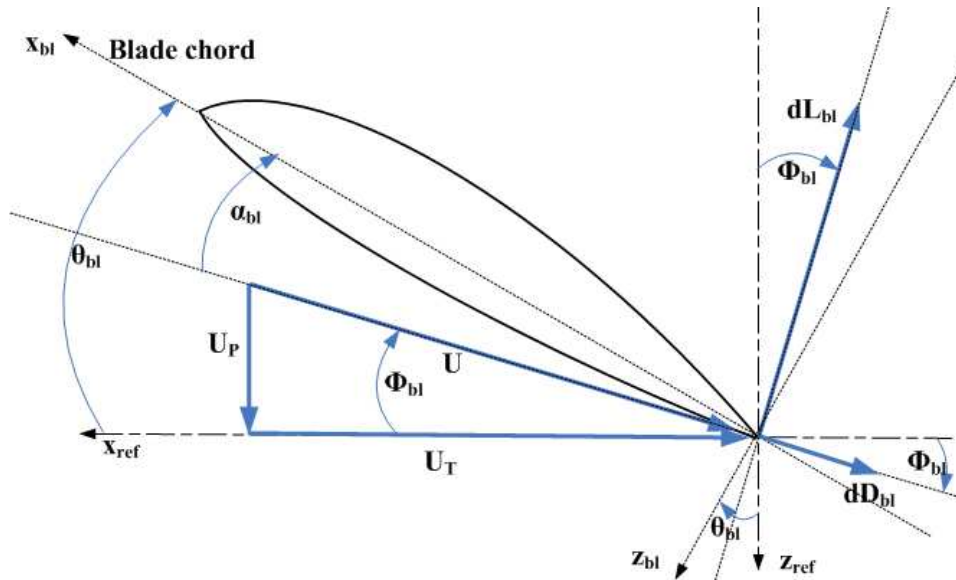


Figure 2: Elemental aerodynamic forces. View from an observer positioned on rotor shaft, and looking outboard at an advancing blade for the case of CCW rotation

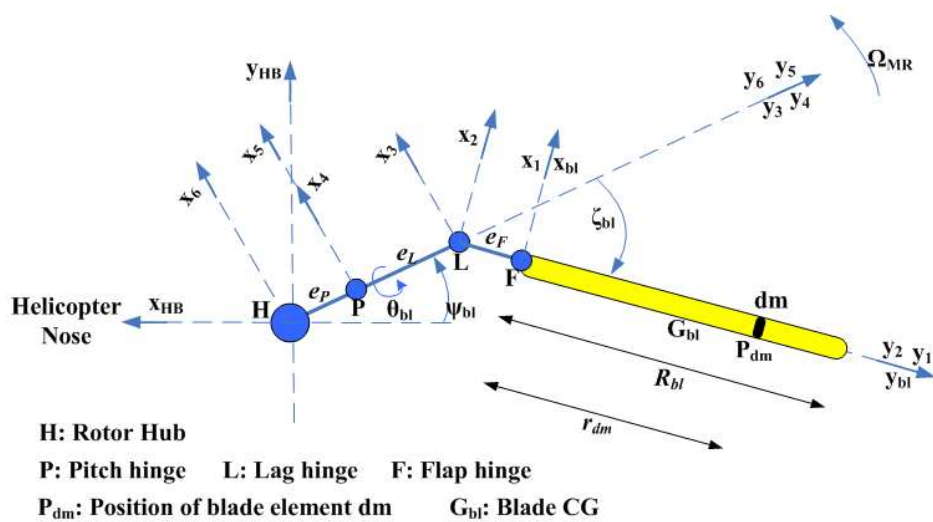


Figure 3: Main rotor frames (top-view)

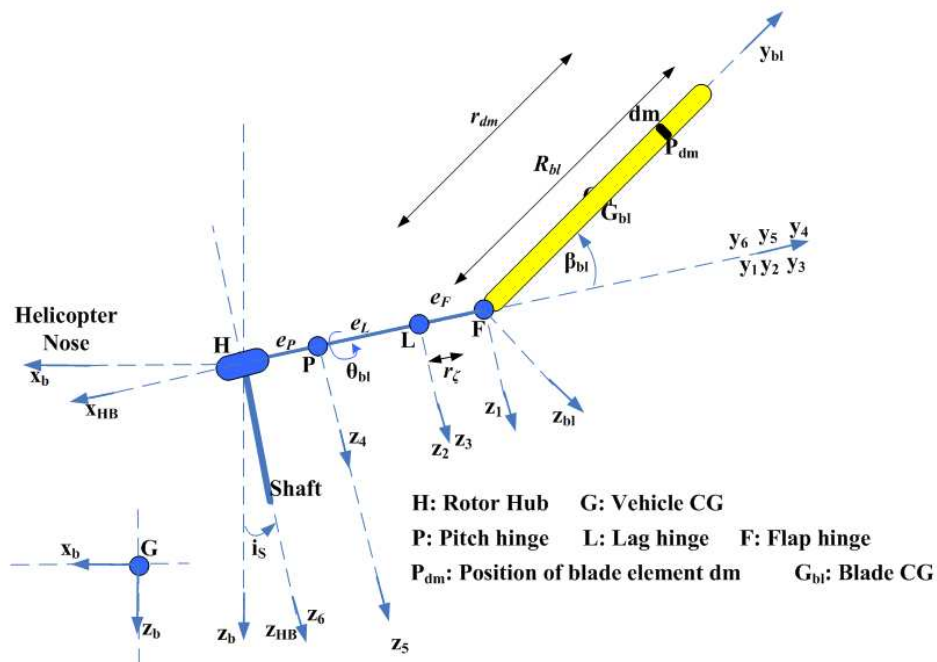


Figure 4: Main rotor frames (side-view)

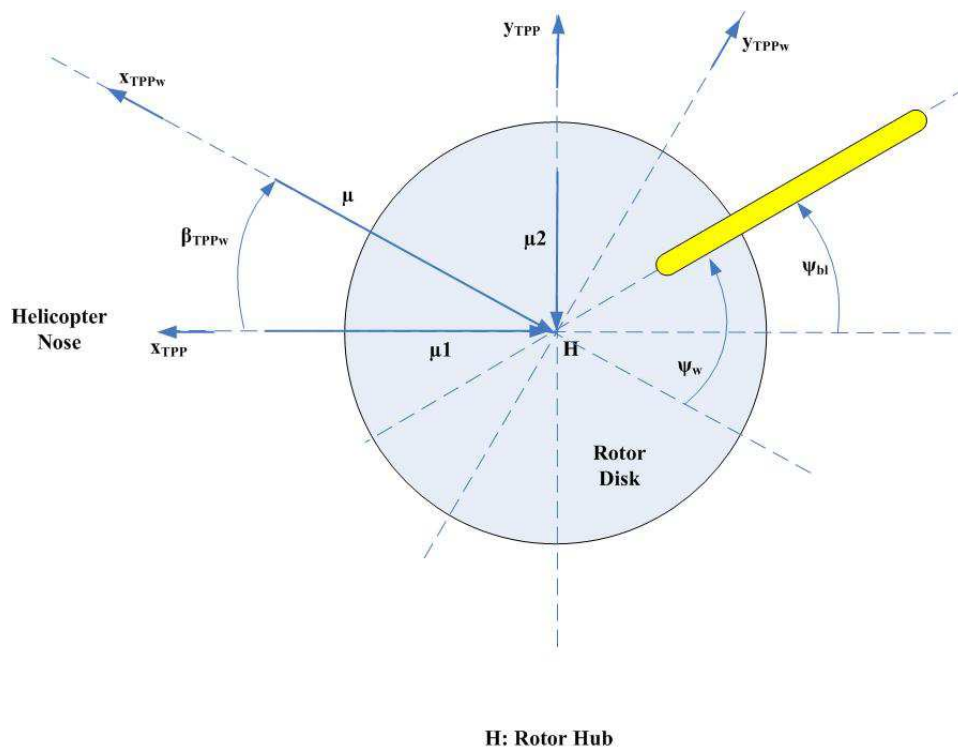


Figure 5: Helicopter velocities in TPP and TPPw (top view)

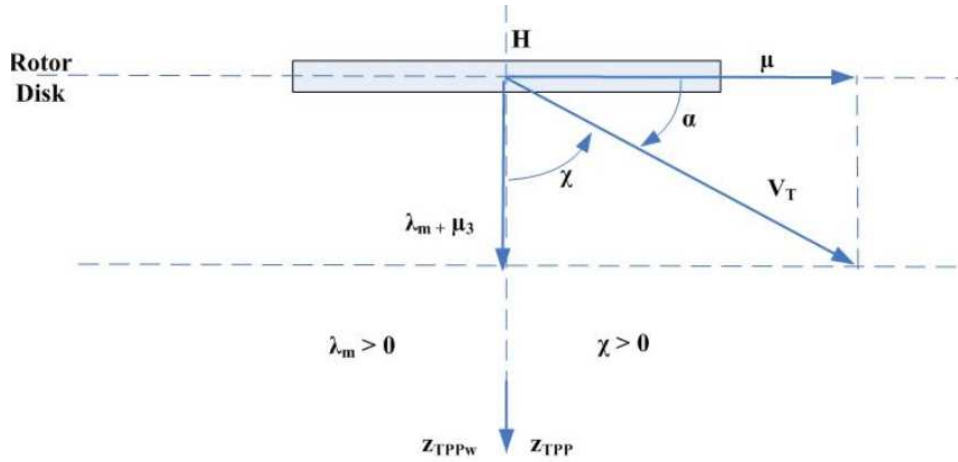


Figure 6: Main rotor wake skew angle (forward flight)

Frame transformations

We only explicitly give here two relevant transformation matrices \mathbb{T}_{ob} and $\mathbb{T}_{(TPP)(HB)}$, all other transformations matrices $\mathbb{T}_{(ref)(bl)}$, $\mathbb{T}_{1(bl)}$, \mathbb{T}_{32} , \mathbb{T}_{54} , $\mathbb{T}_{(HB)6}$, and $\mathbb{T}_{(TPPw)(TPP)}$ are standard rotation matrices, which may involve the CW/CWW toggle Γ . For the tail coordinate system see [15].

Transformation from F_b to F_o

First rotation	ψ azimuth angle	$-\pi < \psi \leq \pi$
Second rotation	θ inclination angle	$-\frac{\pi}{2} \leq \theta \leq \frac{\pi}{2}$
Third rotation	ϕ bank angle	$-\pi < \phi \leq \pi$

$$\mathbb{T}_{ob} = \begin{pmatrix} \cos \theta \cos \psi & \sin \theta \sin \phi \cos \psi - \sin \psi \cos \phi & \cos \psi \sin \theta \cos \phi + \sin \phi \sin \psi \\ \sin \psi \cos \theta & \sin \theta \sin \phi \sin \psi + \cos \psi \cos \phi & \sin \theta \cos \phi \sin \psi - \sin \phi \cos \psi \\ -\sin \theta & \cos \theta \sin \phi & \cos \theta \cos \phi \end{pmatrix} \quad (106)$$

Since \mathbb{T}_{ob} is an orthogonal matrix, we have $\mathbb{T}_{bo} = \mathbb{T}_{ob}^{-1} = \mathbb{T}_{ob}^T$

Transformation from F_{HB} to F_{TPP}

β_{1c} Longitudinal rotor TPP tilt	$-\frac{\pi}{2} < \beta_{1c} < \frac{\pi}{2}$
β_{1s} Lateral rotor TPP tilt	$-\frac{\pi}{2} < \beta_{1s} < \frac{\pi}{2}$

REMARK 1 In case of CW rotation we need to do the following change of variable

- $\beta_{1sbl} \longleftarrow -\beta_{1sbl}$
- We use the following convention CCW : $\Gamma = 1$ and CW : $\Gamma = -1$

$$\mathbb{T}_{(TPP)(HB)} = \begin{pmatrix} \cos \beta_{1c} & 0 & \sin \beta_{1c} \\ 0 & \cos \beta_{1s} & -\Gamma \sin \beta_{1s} \\ -\sin \beta_{1c} & \Gamma \sin \beta_{1s} & \cos \beta_{1c} \cos \beta_{1s} \end{pmatrix} \quad (107)$$

Here it is important to realize that $\mathbb{T}_{(TPP)(HB)}$ is not an orthogonal matrix, i.e. $\mathbb{T}_{(TPP)(HB)}^T \neq \mathbb{T}_{(TPP)(HB)}^{-1}$

Transformation from F_{TPP} to F_{HB}

$$\mathbb{T}_{(HB)(TPP)} = \begin{pmatrix} \cos \beta_{1c} & 0 & -\sin \beta_{1c} \\ 0 & \cos \beta_{1s} & \Gamma \sin \beta_{1s} \\ \sin \beta_{1c} & -\Gamma \sin \beta_{1s} & \cos \beta_{1c} \cos \beta_{1s} \end{pmatrix} \quad (108)$$

Here too $\mathbb{T}_{(HB)(TPP)}$ is not an orthogonal matrix.

Appendix D: Useful integrals

We assume here that the main rotor blade has a constant mass distribution per unit length ρ_{bl} .

$$\begin{aligned}
 M_{bl} &= \int_0^{R_{bl}} dm \\
 C_0 &= \int_0^{R_{bl}} r_{dm} \cdot dm = M_{bl} \cdot y_{G_{bl}} \\
 I_\beta &= \int_0^{R_{bl}} r_{dm}^2 \cdot dm = \rho_{bl} \int_0^{R_{bl}} r_{dm}^2 \cdot dr_{dm} = \rho_{bl} \cdot \frac{R_{bl}^3}{3} = M_{bl} \cdot \frac{R_{bl}^2}{3} \\
 C_1 &= \int_0^{R_{bl}} r_{dm}^3 \cdot dm = \rho_{bl} \int_0^{R_{bl}} r_{dm}^3 \cdot dr_{dm} = \rho_{bl} \cdot \frac{R_{bl}^4}{4} = M_{bl} \cdot \frac{R_{bl}^3}{4}
 \end{aligned}$$

Appendix E: Flap-Lag expressions

We provide here expressions for the B_{12} , B_{21} , F_1 , F_2 terms defined in eq (37) and eq (39), obtained with the MATLAB symbolic toolbox. Here to decrease computational load, we have assumed small angles in blade flap, lag and pitch angles.

$$\begin{aligned}
B_{12} = & \left(\beta_{bl} I_\beta + e_F \beta_{bl} C_0 \right) \dot{\zeta}_{bl} + \left(\left(\left(2\Omega_{MR} - 3\Gamma r \right) \theta_{bl} + 3q \cos \psi_{bl} + 3p\Gamma \sin \psi_{bl} \right) \zeta_{bl} \right. \\
& + \left(\left(3q \cos \psi_{bl} + 3p\Gamma \sin \psi_{bl} \right) \theta_{bl} + 3\Gamma r - 2\Omega_{MR} \right) \beta_{bl} - 3q \sin \psi_{bl} + 3p\Gamma \cos \psi_{bl} \Big) I_\beta \\
& + \left(\left(\left(-3\Gamma r e_F + 2\Omega_{MR} e_F \right) \theta_{bl} + 3q e_F \cos \psi_{bl} + 3p\Gamma \sin \psi_{bl} e_F \right) \zeta_{bl} \right. \\
& \left. + \left(\left(3q e_F \cos \psi_{bl} + 3p\Gamma \sin \psi_{bl} e_F \right) \theta_{bl} + 3\Gamma r e_F - 2\Omega_{MR} e_F \right) \beta_{bl} + 3p\Gamma e_F \cos \psi_{bl} - 3q e_F \sin \psi_{bl} \right) C_0
\end{aligned} \tag{109}$$

$$\begin{aligned}
B_{21} = & -2 \left(\beta_{bl} I_\beta + e_F \beta_{bl} C_0 \right) \dot{\zeta}_{bl} + \left(\left(\left(-3p\Gamma \sin \psi_{bl} - 3q \cos \psi_{bl} \right) \theta_{bl} + 2\Omega_{MR} - 3\Gamma r \right) \beta_{bl} \right. \\
& + \left(\left(-2\Omega_{MR} + 3\Gamma r \right) \theta_{bl} - 3p\Gamma \sin \psi_{bl} - 3q \cos \psi_{bl} \right) \zeta_{bl} + 3q \sin \psi_{bl} - 3p\Gamma \cos \psi_{bl} \Big) I_\beta \\
& + \left(\left(\left(-3q e_F \cos \psi_{bl} - 3p\Gamma \sin \psi_{bl} e_F \right) \theta_{bl} + 2\Omega_{MR} e_F - 3\Gamma r e_F \right) \beta_{bl} \right. \\
& \left. + \left(\left(3\Gamma r e_F - 2\Omega_{MR} e_F \right) \theta_{bl} - 3q e_F \cos \psi_{bl} - 3p\Gamma \sin \psi_{bl} e_F \right) \zeta_{bl} + 3q e_F \sin \psi_{bl} - 3p\Gamma e_F \cos \psi_{bl} \right) C_0
\end{aligned} \tag{110}$$

$$\begin{aligned}
F_1 = & \left(\left(\left(\left(\left(-3\Gamma\Omega_{MR} + 4r \right) p \cos \psi_{bl} + \left(3\Omega_{MR} - 4\Gamma r \right) q \sin \psi_{bl} \right) \theta_{bl} \right. \right. \right. \\
& \left. \left. \left. - 8qp\Gamma \cos^2 \psi_{bl} + \left(4q^2 - 4p^2 \right) \sin \psi_{bl} \cos \psi_{bl} + 4qp\Gamma \right) \beta_{bl} + \right. \right. \\
& \left. \left(\left(-2p^2 + 2q^2 \right) \cos^2 \psi_{bl} + 4qp\Gamma \cos \psi_{bl} \sin \psi_{bl} - \Omega_{MR}^2 + 3r\Gamma\Omega_{MR} - 2r^2 + 2p^2 \right) \theta_{bl} \right. \\
& \left. + \left(\left(2\Gamma r - 3\Omega_{MR} \right) q + \Gamma \dot{p} \right) \cos \psi_{bl} + \left(\left(2r - 3\Gamma\Omega_{MR} \right) p - \dot{q} \right) \sin \psi_{bl} \right) \zeta_{bl} \\
& + \left(\left(\left(4\Gamma r - 3\Omega_{MR} \right) q \cos \psi_{bl} + \left(-3\Gamma\Omega_{MR} + 4r \right) p \sin \psi_{bl} \right) \theta_{bl} \right. \\
& \left. + \left(-2p^2 + 2q^2 \right) \cos^2 \psi_{bl} + 4qp\Gamma \cos \psi_{bl} \sin \psi_{bl} - 3r\Gamma\Omega_{MR} + 2r^2 + \Omega_{MR}^2 - 2q^2 \right) \beta_{bl} \\
& + \left(4qp\Gamma \cos^2 \psi_{bl} + \left(2p^2 - 2q^2 \right) \sin \psi_{bl} \cos \psi_{bl} - \dot{\Omega}_{MR} - 2qp\Gamma + \Gamma \dot{r} \right) \theta_{bl} \\
& + \left(\left(2r - 3\Gamma\Omega_{MR} \right) p - \dot{q} \right) \cos \psi_{bl} + \left(\left(3\Omega_{MR} - 2\Gamma r \right) q - \Gamma \dot{p} \right) \sin \psi_{bl} \right) I_\beta \\
& + \left(\left(\left(\left(\left(\left(2e_P + 2e_L + 4e_F \right) r + \left(-3e_F - 3e_P - 3e_L \right) \Gamma\Omega_{MR} \right) p \right. \right. \right. \right. \right. \\
& \left. \left. \left. - \dot{q}e_P - \dot{q}e_L \right) \cos \psi_{bl} + \left(\left(\left(-2e_L - 2e_P - 4e_F \right) \Gamma r + \left(3e_P + 3e_F + 3e_L \right) \Omega_{MR} \right) q \right. \right. \right. \\
& \left. \left. \left. + \left(-\dot{p}e_P - \dot{p}e_L \right) \Gamma \right) \sin \psi_{bl} + 2p^2 z_H + \left(-2v - 2rx_H \right) p \right. \right. \\
& \left. + 2q^2 z_H + \left(2u - 2ry_H \right) q - \dot{w} - \dot{p}y_H + \dot{q}x_H \right) \theta_{bl} + \left(-4e_L - 8e_F - 4e_P \right) \Gamma qp \cos^2 \psi_{bl} \\
& + \left(\left(\left(-2e_L - 2e_P - 4e_F \right) p^2 + \left(2e_P + 2e_L + 4e_F \right) q^2 \right) \sin \psi_{bl} \right. \\
& \left. \left. - 2\Gamma p^2 y_H + \left(2\Gamma qx_H - 2\Gamma w \right) p + 2\Gamma r q z_H - 2\Gamma r^2 y_H + 2\Gamma ru \right. \right.
\end{aligned}$$

$$\begin{aligned}
& + \left(\dot{v} - \dot{p}z_H + \dot{r}x_H \right) \Gamma \cos \psi_{bl} + \left(\left(2qy_H + 2rz_H \right) p \right. \\
& \quad \left. + \dot{q}z_H - \dot{r}y_H + 2qw - 2q^2x_H - 2r^2x_H + \dot{u} - 2rv \right) \sin \psi_{bl} \\
& + \left(2e_P + 2e_L + 4e_F \right) \Gamma qp + \left(e_P + e_L \right) \dot{\Omega}_{MR} + \left(-\dot{r}e_P - \dot{r}e_L \right) \Gamma \beta_{bl} \\
& + \left(\left(-2p^2e_F + 2q^2e_F \right) \cos^2 \psi_{bl} + 4qp\Gamma \cos \psi_{bl} e_F \sin \psi_{bl} - 2r^2e_F - \Omega_{MR}^2 e_F + 2p^2e_F \right. \\
& \quad \left. + 3\Gamma r e_F \Omega_{MR} \right) \theta_{bl} + \left(\left(-3\Omega_{MR} e_F + 2\Gamma r e_F \right) q + \Gamma \dot{p}e_F \right) \cos \psi_{bl} \\
& \quad + \left(\left(-3\Gamma \Omega_{MR} e_F + 2r e_F \right) p - \dot{q}e_F \right) \sin \psi_{bl} \zeta_{bl} \\
& + \left(\left(\left(-2e_L - 2e_F - 2e_P \right) p^2 + \left(2e_L + 2e_F + 2e_P \right) q^2 \right) \cos^2 \psi_{bl} \right. \\
& + \left(\left(4e_F + 4e_L + 4e_P \right) \Gamma qp \sin \psi_{bl} + \left(2qy_H + 2rz_H \right) p + \dot{q}z_H - \dot{r}y_H + 2qw - 2q^2x_H \right. \\
& \quad \left. - 2r^2x_H + \dot{u} - 2rv \right) \cos \psi_{bl} + \left(2\Gamma p^2 y_H + \left(2\Gamma w - 2\Gamma q x_H \right) p \right. \\
& \quad \left. - 2\Gamma r q z_H + 2\Gamma r^2 y_H - 2\Gamma r u + \left(-\dot{r}x_H + \dot{p}z_H - \dot{v} \right) \Gamma \right) \sin \psi_{bl} \\
& + \left(2e_L + 2e_F + 2e_P \right) p^2 + \left(2e_L + 2e_F + 2e_P \right) r^2 + \left(-3e_F - 3e_P - 3e_L \right) \Gamma \Omega_{MR} r \\
& \quad + \left(e_F + e_P + e_L \right) \Omega_{MR}^2 \beta_{bl} + \left(\left(4e_F + 4e_L + 4e_P \right) \Gamma qp \cos^2 \psi_{bl} \right. \\
& + \left(\left(\left(2e_L + 2e_F + 2e_P \right) p^2 + \left(-2e_L - 2e_F - 2e_P \right) q^2 \right) \sin \psi_{bl} + 2\Gamma p^2 y_H \right. \\
& \quad \left. + \left(2\Gamma w - 2\Gamma q x_H \right) p - 2\Gamma r q z_H + 2\Gamma r^2 y_H - 2\Gamma r u + \left(-\dot{r}x_H + \dot{p}z_H \right. \right. \\
& \quad \left. \left. - \dot{v} \right) \Gamma \right) \cos \psi_{bl} + \left(\left(-2qy_H - 2rz_H \right) p - 2qw - \dot{u} - \dot{q}z_H + \dot{r}y_H \right. \\
& + 2q^2x_H + 2rv + 2r^2x_H \left. \right) \sin \psi_{bl} + \left(-2e_L - 2e_F - 2e_P \right) \Gamma qp + \left(-e_F - e_L - e_P \right) \dot{\Omega}_{MR} \\
& \quad + \left(\dot{r}e_L + \dot{r}e_P + \dot{r}e_F \right) \Gamma \theta_{bl} + \left(\left(\left(2e_L + 2e_F + 2e_P \right) r + \left(-3e_F - 3e_P \right. \right. \right. \\
& \quad \left. \left. - 3e_L \right) \Gamma \Omega_{MR} \right) p - \dot{q}e_F - \dot{q}e_P - \dot{q}e_L \left. \right) \cos \psi_{bl} + \left(\left(\left(-2e_L - 2e_F - 2e_P \right) \Gamma r \right. \right. \\
& + \left(3e_P + 3e_F + 3e_L \right) \Omega_{MR} \left. \right) q + \left(-\dot{p}e_P - \dot{p}e_L - \dot{p}e_F \right) \Gamma \sin \psi_{bl} + 2p^2z_H \\
& \quad + \left(-2v - 2rx_H \right) p + 2q^2z_H + \left(2u - 2ry_H \right) q - \dot{w} - \dot{p}y_H + \dot{q}x_H \left. \right) C_0
\end{aligned}$$

$$\begin{aligned}
F_2 = & \left(\left(\left(\left(-4qp\Gamma \cos^2 \psi_{bl} + \left(-2p^2 + 2q^2 \right) \sin \psi_{bl} \cos \psi_{bl} \right. \right. \right. \right. \\
& \left. \left. \left. + 2qp\Gamma + \Gamma \dot{r} - \dot{\Omega}_{MR} \right) \theta_{bl} + \left(-\dot{q} - 2rp \right) \cos \psi_{bl} \right. \right. \\
& \left. \left. + \left(2\Gamma r q - \Gamma \dot{p} \right) \sin \psi_{bl} \right) \zeta_{bl} + \left(\left(-2p^2 + 2q^2 \right) \cos^2 \psi_{bl} \right. \right. \\
& \left. \left. + 4qp\Gamma \cos \psi_{bl} \sin \psi_{bl} - \Omega_{MR}^2 + 3r\Gamma\Omega_{MR} - 2r^2 + 2p^2 \right) \theta_{bl} \right. \\
& \left. + \left(2\Gamma r q - \Gamma \dot{p} \right) \cos \psi_{bl} + \left(2rp + \dot{q} \right) \sin \psi_{bl} \right) \beta_{bl} \\
& + \left(\left(\left(\left(3\Omega_{MR} - 4\Gamma r \right) q \cos \psi_{bl} + \left(3\Gamma\Omega_{MR} - 4r \right) p \sin \psi_{bl} \right) \theta_{bl} \right. \right. \\
& \left. \left. + \left(4q^2 - 4p^2 \right) \cos^2 \psi_{bl} + 8qp\Gamma \cos \psi_{bl} \sin \psi_{bl} - 2q^2 + 2p^2 \right) \zeta_{bl} \right. \\
& \left. + \left(\left(\left(3\Gamma\Omega_{MR} - 2r \right) p + \dot{q} \right) \cos \psi_{bl} + \left(2\Gamma r - 3\Omega_{MR} \right) q \right. \right. \\
& \left. \left. + \Gamma \dot{p} \right) \sin \psi_{bl} \right) \theta_{bl} + 4qp\Gamma \cos^2 \psi_{bl} + \left(2p^2 - 2q^2 \right) \sin \psi_{bl} \cos \psi_{bl} \\
& - \dot{\Omega}_{MR} - 2qp\Gamma + \Gamma \dot{r} \Big) I_\beta + \left(\left(\left(\left(-4qp\Gamma \cos^2 \psi_{bl} e_F + \left(-2p^2 e_F \right. \right. \right. \right. \right. \\
& \left. \left. \left. + 2q^2 e_F \right) \sin \psi_{bl} \cos \psi_{bl} + \Gamma \dot{r} e_F - \dot{\Omega}_{MR} e_F + 2qp\Gamma e_F \right) \theta_{bl} \right. \right. \\
& \left. \left. + \left(-\dot{q} e_F - 2rpe_F \right) \cos \psi_{bl} + \left(2\Gamma r q e_F - \Gamma \dot{p} e_F \right) \sin \psi_{bl} \right) \zeta_{bl} \right. \\
& \left. + \left(\left(-2p^2 e_F + 2q^2 e_F \right) \cos^2 \psi_{bl} + 4qp\Gamma \cos \psi_{bl} e_F \sin \psi_{bl} \right. \right. \\
& \left. \left. - 2r^2 e_F - \Omega_{MR}^2 e_F + 2p^2 e_F + 3\Gamma r e_F \Omega_{MR} \right) \theta_{bl} + \left(2\Gamma r q e_F - \Gamma \dot{p} e_F \right) \cos \psi_{bl} \right. \\
& \left. + \left(2rpe_F + \dot{q} e_F \right) \sin \psi_{bl} \right) \beta_{bl} + \left(\left(\left(-8\Gamma r e_F \right. \right. \right. \\
& \left. \left. + 6\Omega_{MR} e_F \right) q \cos \psi_{bl} + \left(-8r e_F + 6\Gamma\Omega_{MR} e_F \right) p \sin \psi_{bl} \right) \theta_{bl}
\end{aligned}$$

$$\begin{aligned}
& + \left(\left(-2e_P - 2e_L - 8e_F \right) p^2 + \left(2e_P + 2e_L + 8e_F \right) q^2 \right) \cos^2 \psi_{bl} \\
& + \left(\left(4e_P + 16e_F + 4e_L \right) \Gamma q p \sin \psi_{bl} + \left(2qy_H + 2rz_H \right) p - 2rv \right. \\
& \quad \left. + \dot{u} + \dot{q}z_H + 2qw - 2r^2x_H - 2q^2x_H - \dot{r}y_H \right) \cos \psi_{bl} \\
& + \left(2\Gamma p^2y_H + \left(2\Gamma w - 2\Gamma qx_H \right) p - 2\Gamma r qz_H + 2\Gamma r^2y_H \right. \\
& \quad \left. - 2\Gamma ru + \left(-\dot{r}x_H + \dot{p}z_H - \dot{v} \right) \Gamma \right) \sin \psi_{bl} \\
& + \left(2e_P + 2e_L + 4e_F \right) p^2 - 4q^2e_F + \left(2e_P + 2e_L \right) r^2 + \left(-3e_P - 3e_L \right) \Gamma \Omega_{MR} r \\
& \quad + \left(e_P + e_L \right) \Omega_{MR}^2 \zeta_{bl} + \left(\left(\left(\left(-2e_L - 2e_P - 4e_F \right) r \right. \right. \right. \\
& \quad \left. \left. + \left(3e_L + 3e_P + 6e_F \right) \Gamma \Omega_{MR} \right) p + 2\dot{q}e_F + \dot{q}e_P + \dot{q}e_L \right) \cos \psi_{bl} \\
& + \left(\left(\left(2e_P + 2e_L + 4e_F \right) \Gamma r + \left(-3e_L - 6e_F - 3e_P \right) \Omega_{MR} \right) q \right. \\
& \quad \left. + \left(2\dot{p}e_F + \dot{p}e_P + \dot{p}e_L \right) \Gamma \right) \sin \psi_{bl} - 2p^2z_H + \left(2rx_H + 2v \right) p \\
& \quad - 2q^2z_H + \left(-2u + 2ry_H \right) q + \dot{w} + \dot{p}y_H - \dot{q}x_H \theta_{bl} \\
& + \left(4e_P + 8e_F + 4e_L \right) \Gamma q p \cos^2 \psi_{bl} + \left(\left(\left(2e_P + 2e_L + 4e_F \right) p^2 \right. \right. \\
& \quad \left. \left. + \left(-2e_L - 2e_P - 4e_F \right) q^2 \right) \sin \psi_{bl} + 2\Gamma p^2y_H + \left(2\Gamma w \right. \right. \\
& \quad \left. \left. - 2\Gamma qx_H \right) p - 2\Gamma r qz_H + 2\Gamma r^2y_H - 2\Gamma ru + \left(-\dot{r}x_H + \dot{p}z_H \right. \right. \\
& \quad \left. \left. - \dot{v} \right) \Gamma \right) \cos \psi_{bl} + \left(\left(-2qy_H - 2rz_H \right) p - \dot{u} \right. \\
& \quad \left. - \dot{q}z_H + 2q^2x_H + 2rv + \dot{r}y_H - 2qw + 2r^2x_H \right) \sin \psi_{bl} \\
& + \left(-2e_L - 2e_P - 4e_F \right) \Gamma q p + \left(-e_P - 2e_F - e_L \right) \dot{\Omega}_{MR} + \left(\dot{r}e_L \right. \\
& \quad \left. + \dot{r}e_P + 2\dot{r}e_F \right) \Gamma C_0 + M_{bl} \left(\left(\left(\left(3e_F^2 \Omega_{MR} \right. \right. \right. \right. \\
& \quad \left. \left. - 4\Gamma r e_F^2 \right) q \cos \psi_{bl} + \left(3\Gamma e_F^2 \Omega_{MR} - 4r e_F^2 \right) p \sin \psi_{bl} \right) \theta_{bl} \\
& + \left(\left(-2e_L e_F - 4e_F^2 - 2e_P e_F \right) p^2 + \left(4e_F^2 + 2e_L e_F + 2e_P e_F \right) q^2 \right) \cos^2 \psi_{bl}
\end{aligned}$$

$$\begin{aligned}
& + \left(\left(4e_{LeF} + 4e_{PeF} + 8e_F^2 \right) \Gamma q p \sin \psi_{bl} + \left(2rz_{HeF} + 2qy_{HeF} \right) p \right. \\
& \quad - 2q^2 x_{HeF} + 2qwe_F - 2r^2 x_{HeF} - 2rve_F + \left(-\dot{r}y_H + \dot{u} \right. \\
& \quad \quad \left. \left. + \dot{q}z_H \right) e_F \right) \cos \psi_{bl} + \left(2\Gamma p^2 y_{HeF} + \left(2\Gamma we_F \right. \right. \\
& \quad \left. \left. - 2\Gamma qx_{HeF} \right) p - 2\Gamma rqz_{HeF} + 2\Gamma r^2 y_{HeF} - 2\Gamma rue_F + \left(-\dot{r}x_H \right. \right. \\
& \quad \left. \left. + \dot{p}z_H - \dot{v} \right) e_F \Gamma \right) \sin \psi_{bl} + \left(2e_F^2 + 2e_{PeF} + 2e_{LeF} \right) p^2 \\
& \quad - 2q^2 e_F^2 + \left(2e_{PeF} + 2e_{LeF} \right) r^2 + \left(-3e_{LeF} - 3e_{PeF} \right) \Gamma \Omega_{MR} \\
& \quad + \left(e_{LeF} + e_{PeF} \right) \Omega_{MR}^2 \zeta_{bl} + \left(\left(\left(\left(-2e_F^2 - 2e_{LeF} \right. \right. \right. \right. \\
& \quad \left. \left. \left. - 2e_{PeF} \right) r + \left(3e_F^2 + 3e_{PeF} + 3e_{LeF} \right) \Gamma \Omega_{MR} \right) p + \dot{q}e_{PeF} + \dot{q}e_F^2 \right. \\
& \quad \left. \left. + \dot{q}e_{LeF} \right) \cos \psi_{bl} + \left(\left(\left(2e_F^2 + 2e_{PeF} + 2e_{LeF} \right) \Gamma r \right. \right. \right. \\
& \quad \left. \left. \left. + \left(-3e_F^2 - 3e_{LeF} - 3e_{PeF} \right) \Omega_{MR} \right) q + \left(\dot{p}e_{LeF} + \dot{p}e_F^2 \right. \right. \\
& \quad \left. \left. + \dot{p}e_{PeF} \right) \Gamma \right) \sin \psi_{bl} - 2p^2 z_{HeF} + \left(2ve_F + 2rx_{HeF} \right) p \\
& \quad - 2q^2 z_{HeF} + \left(-2ue_F + 2ry_{HeF} \right) q + \left(\dot{w} + \dot{p}y_H \right. \\
& \quad \left. - \dot{q}x_H \right) e_F \theta_{bl} + \left(4e_{LeF} + 4e_F^2 + 4e_{PeF} \right) \Gamma q p \cos^2 \psi_{bl} \\
& \quad + \left(\left(\left(\left(2e_F^2 + 2e_{PeF} + 2e_{LeF} \right) p^2 + \left(-2e_F^2 - 2e_{LeF} \right. \right. \right. \right. \\
& \quad \left. \left. \left. - 2e_{PeF} \right) q^2 \right) \sin \psi_{bl} + 2\Gamma p^2 y_{HeF} + \left(2\Gamma we_F \right. \right. \\
& \quad \left. \left. - 2\Gamma qx_{HeF} \right) p - 2\Gamma rqz_{HeF} + 2\Gamma r^2 y_{HeF} - 2\Gamma rue_F + \left(-\dot{r}x_H \right. \right. \\
& \quad \left. \left. + \dot{p}z_H - \dot{v} \right) e_F \Gamma \right) \cos \psi_{bl} + \left(\left(-2qy_{HeF} - 2rz_{HeF} \right) p \right. \\
& \quad \left. + 2q^2 x_{HeF} - 2qwe_F + 2r^2 x_{HeF} + 2rve_F + \left(-\dot{u} - \dot{q}z_H \right. \right. \\
& \quad \left. \left. + \dot{r}y_H \right) e_F \right) \sin \psi_{bl} + \left(-2e_F^2 - 2e_{LeF} - 2e_{PeF} \right) \Gamma q p \\
& \quad + \left(-e_F^2 - e_{LeF} - e_{PeF} \right) \dot{\Omega}_{MR} + \left(\dot{r}e_{PeF} + \dot{r}e_F^2 + \dot{r}e_{LeF} \right) \Gamma \right) \quad (112)
\end{aligned}$$

Appendix F: Simulation results

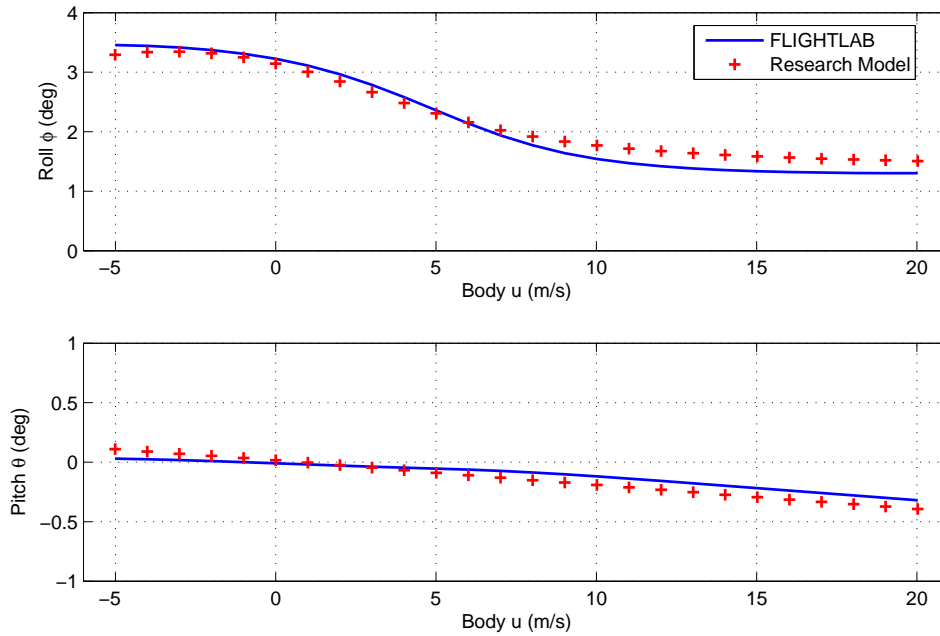


Figure 7: Trim: roll and pitch angles as a function of body longitudinal velocity u

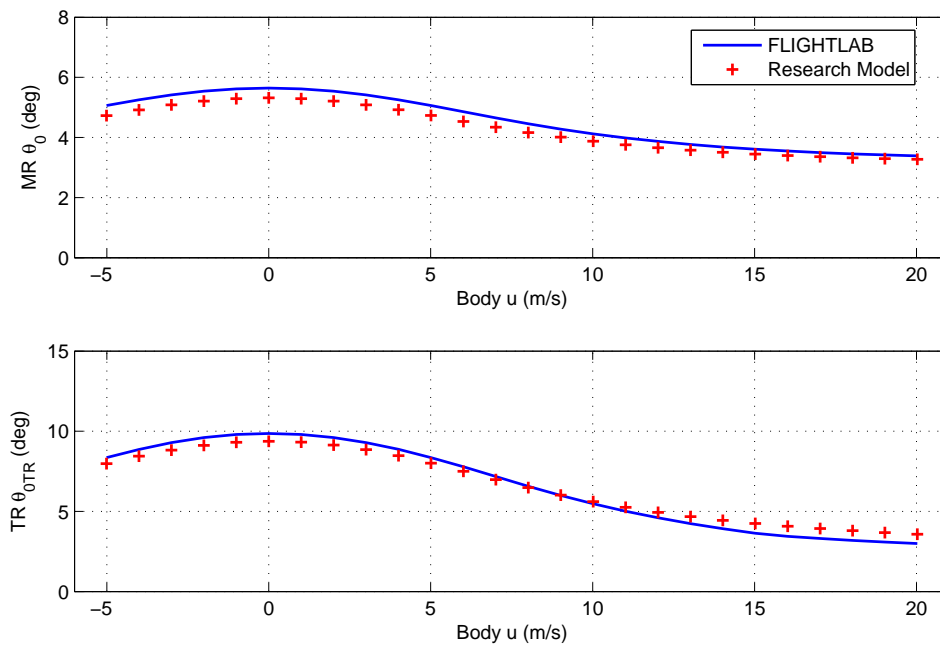


Figure 8: Trim: main and tail rotor collective pitch angles as a function of body longitudinal velocity u

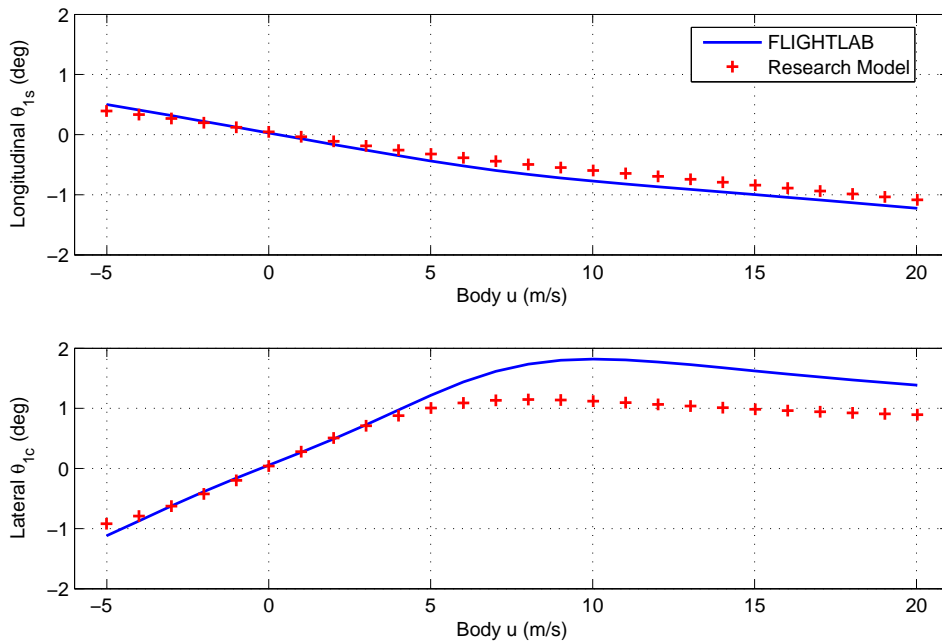


Figure 9: Trim: main rotor longitudinal and lateral pitch angles as a function of body longitudinal velocity u

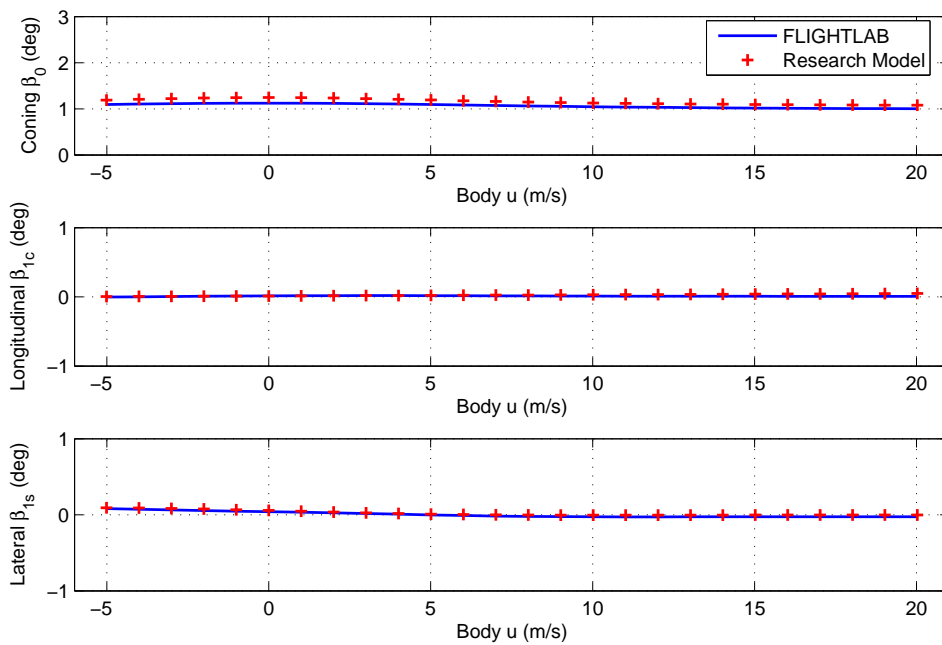


Figure 10: Trim: Tip-Path-Plane coning, longitudinal and lateral angles as a function of body longitudinal velocity u

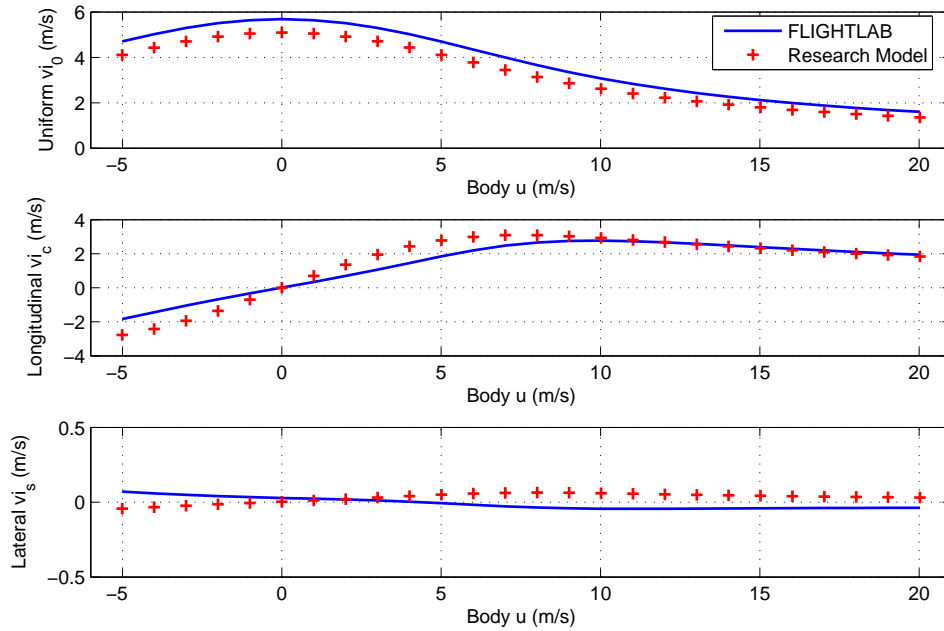


Figure 11: Trim: main rotor uniform, longitudinal and lateral inflow velocities as a function of body longitudinal velocity u

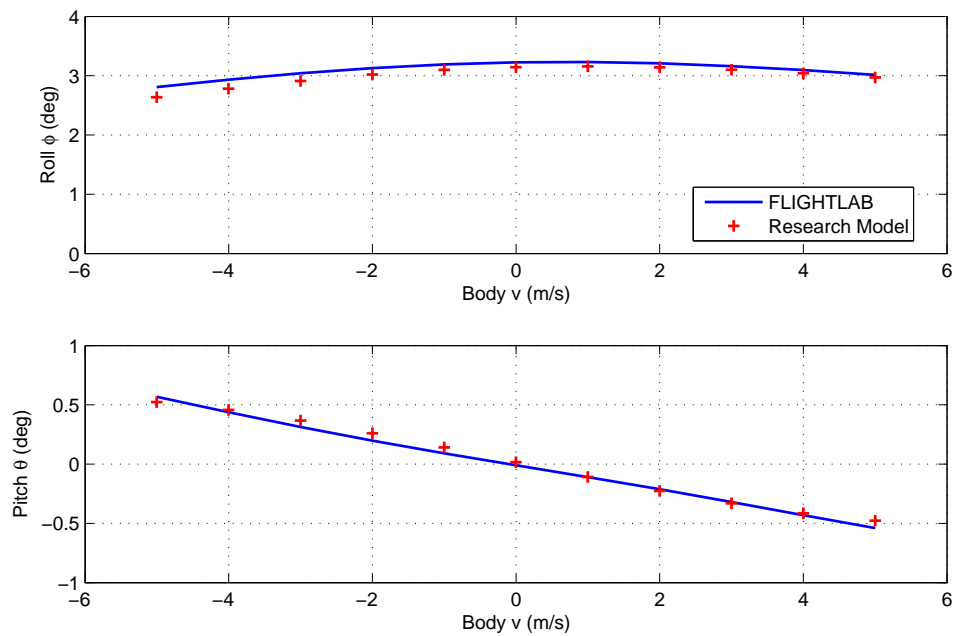


Figure 12: Trim: roll and pitch angles as a function of body lateral velocity v

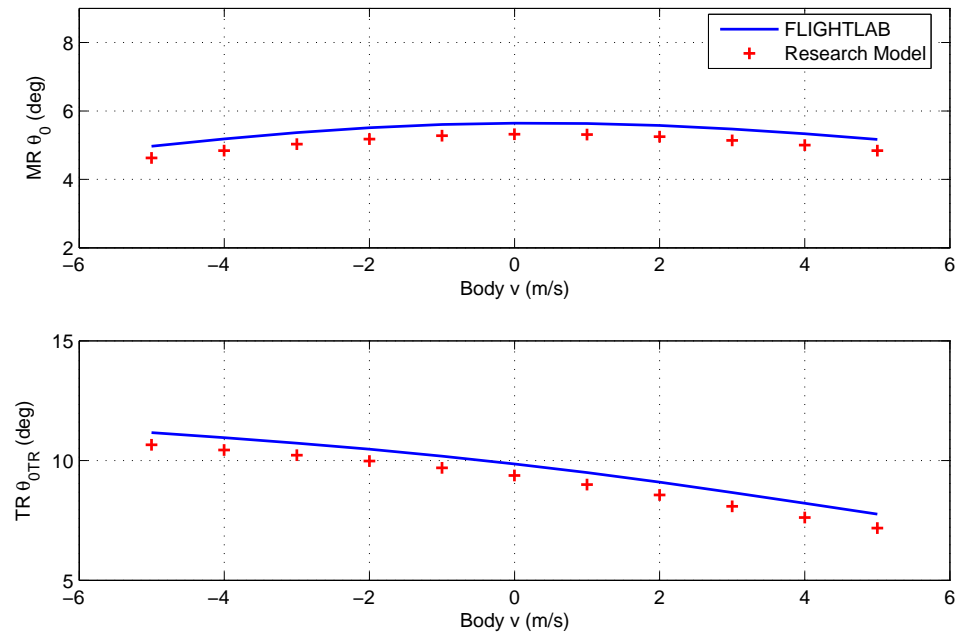


Figure 13: Trim: main and tail rotor collective pitch angles as a function of body lateral velocity v

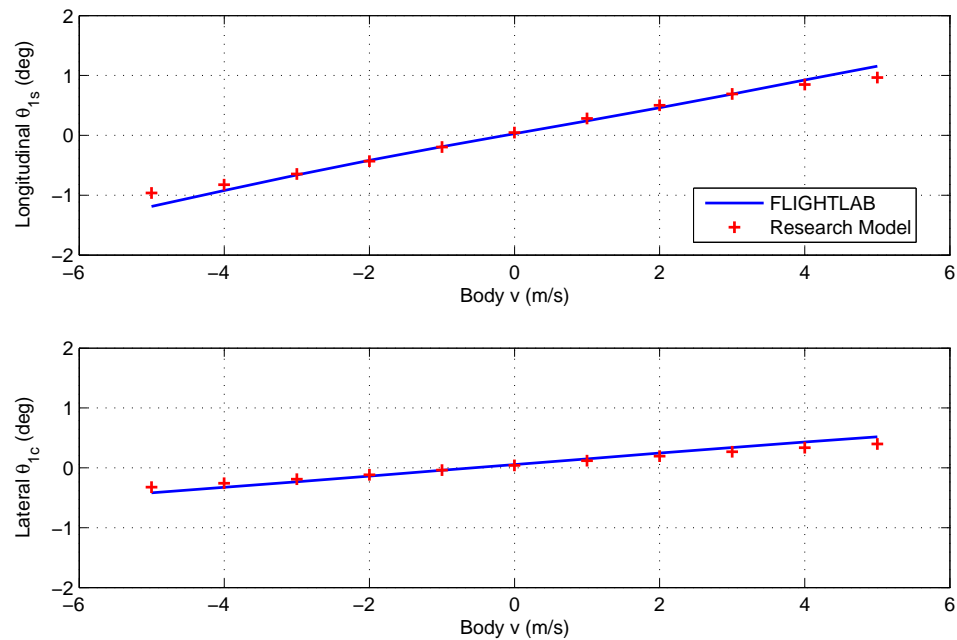


Figure 14: Trim: main rotor longitudinal and lateral pitch angles as a function of body lateral velocity v

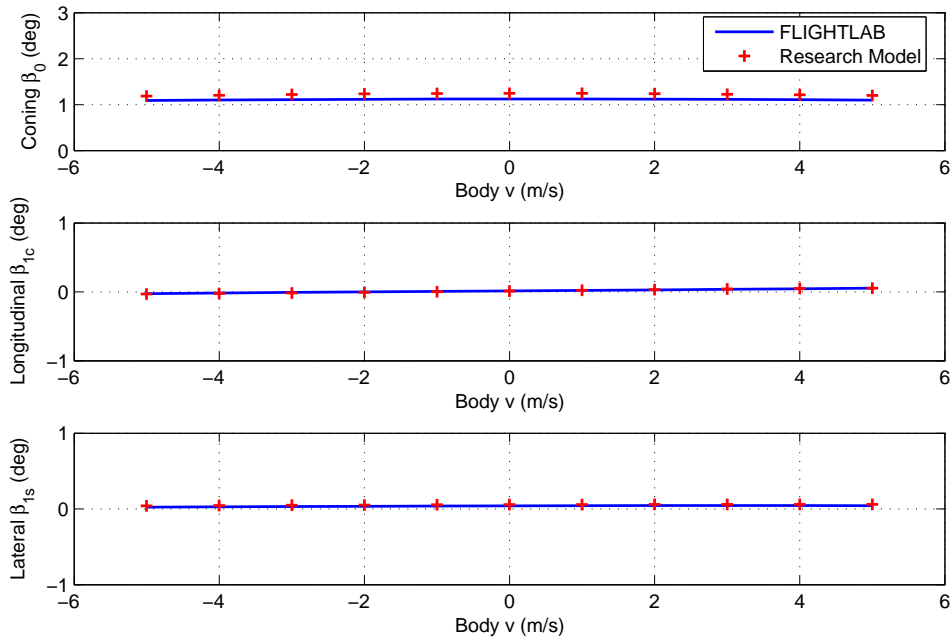


Figure 15: Trim: Tip-Path-Plane coning, longitudinal and lateral angles as a function of body lateral velocity v

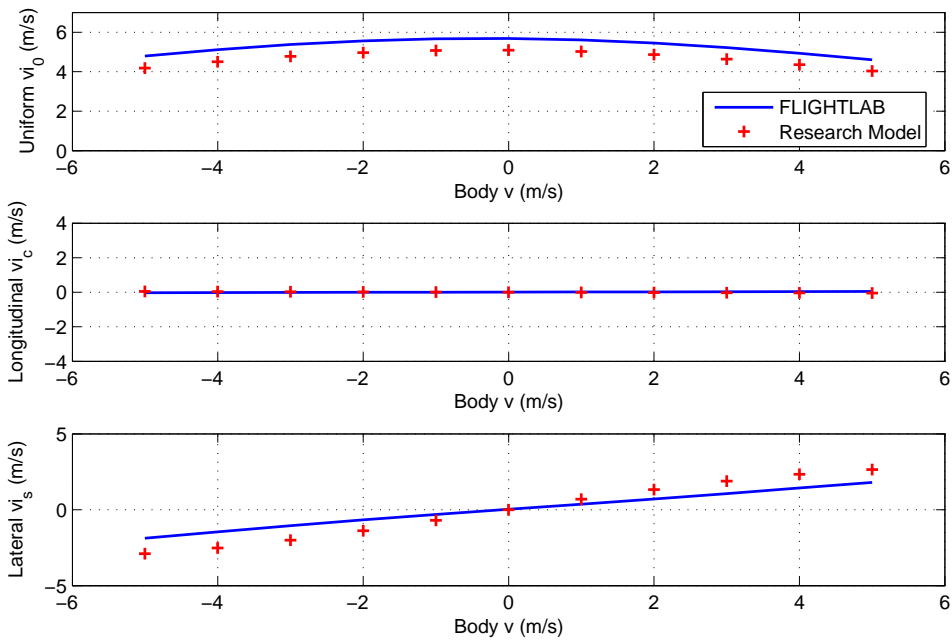


Figure 16: Trim: main rotor uniform, longitudinal and lateral inflow velocities as a function of body lateral velocity v

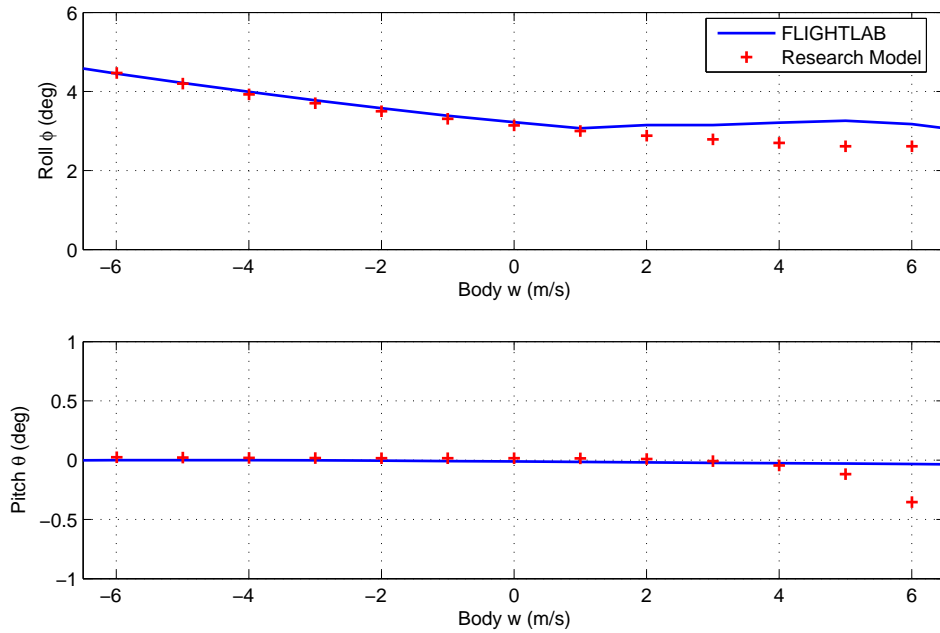


Figure 17: Trim: roll and pitch angles as a function of body vertical velocity w

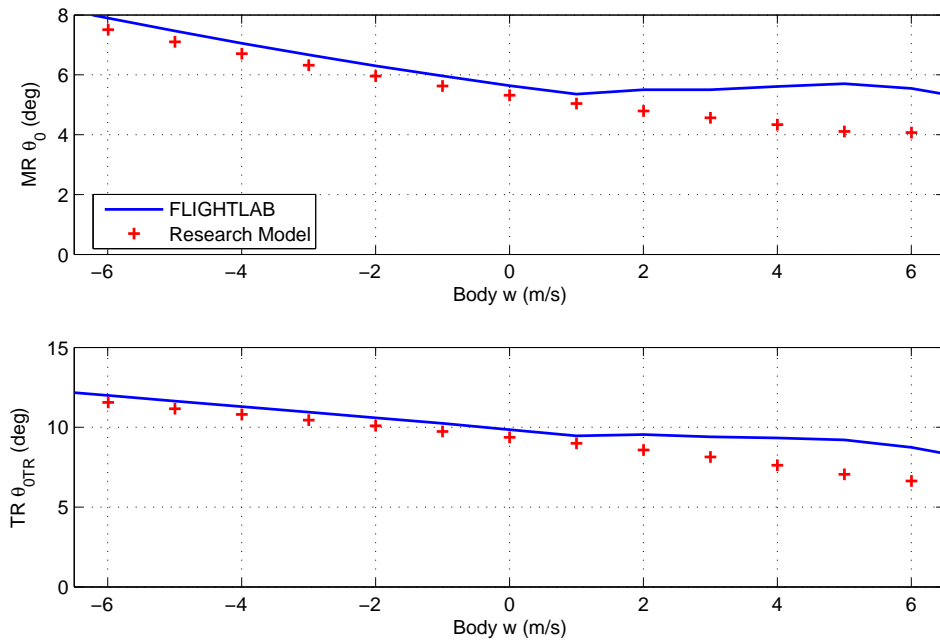


Figure 18: Trim: main and tail rotor collective pitch angles as a function of body vertical velocity w

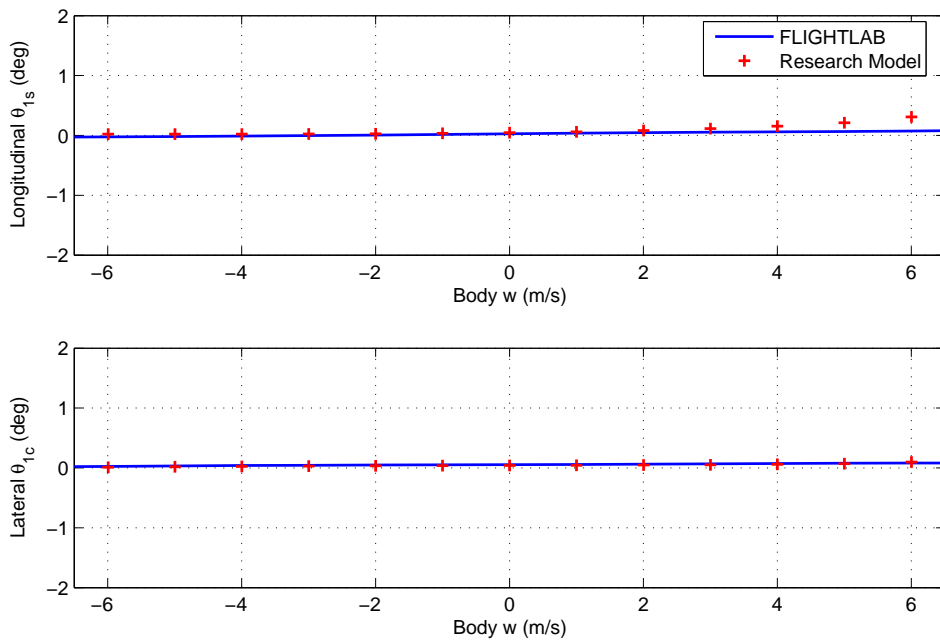


Figure 19: Trim: main rotor longitudinal and lateral pitch angles as a function of body vertical velocity w

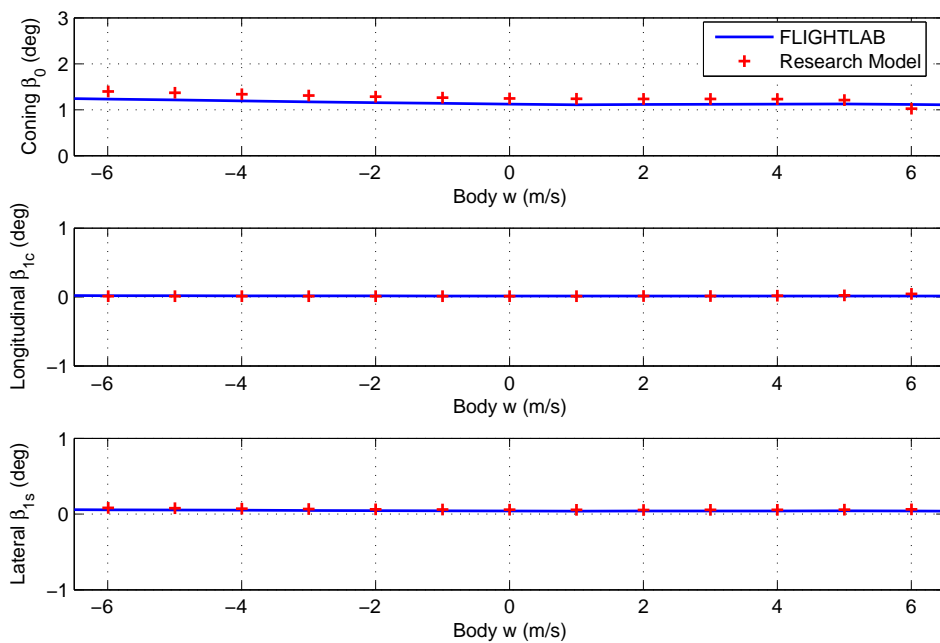


Figure 20: Trim: Tip-Path-Plane coning, longitudinal and lateral angles as a function of body vertical velocity w

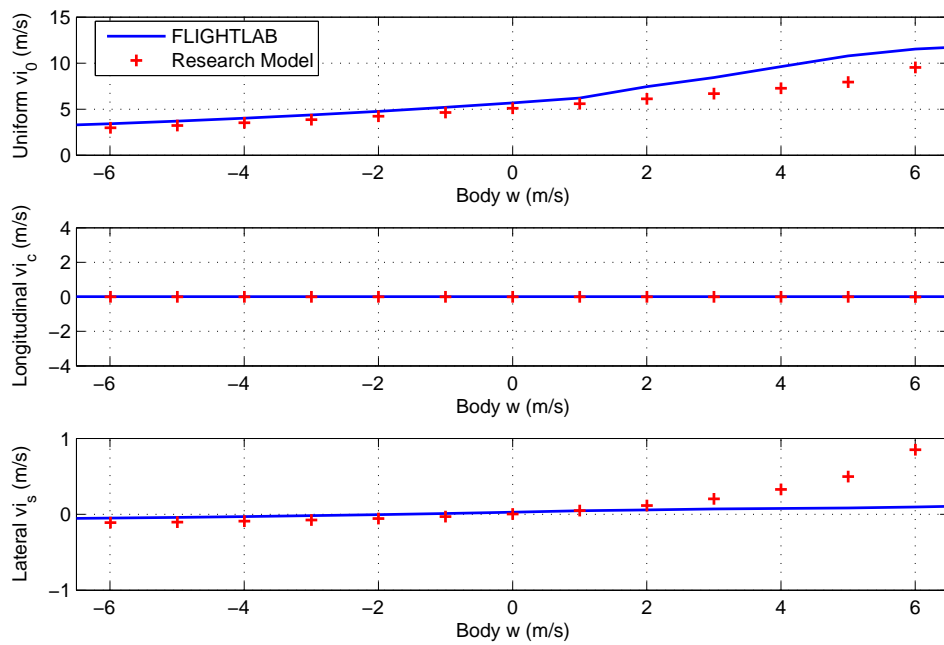


Figure 21: Trim: main rotor uniform, longitudinal and lateral inflow velocities as a function of body vertical velocity w

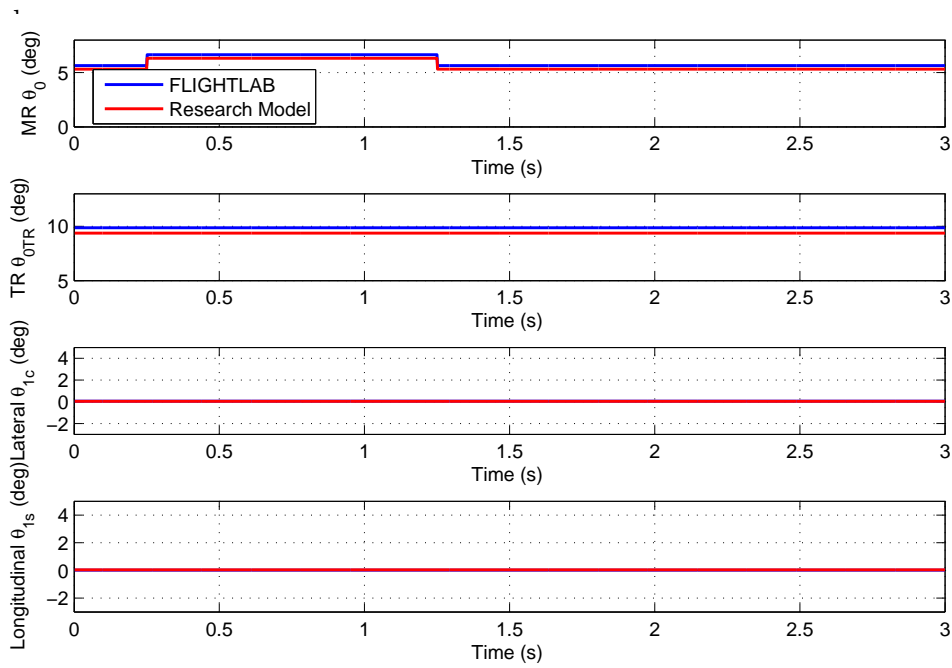


Figure 22: Control inputs

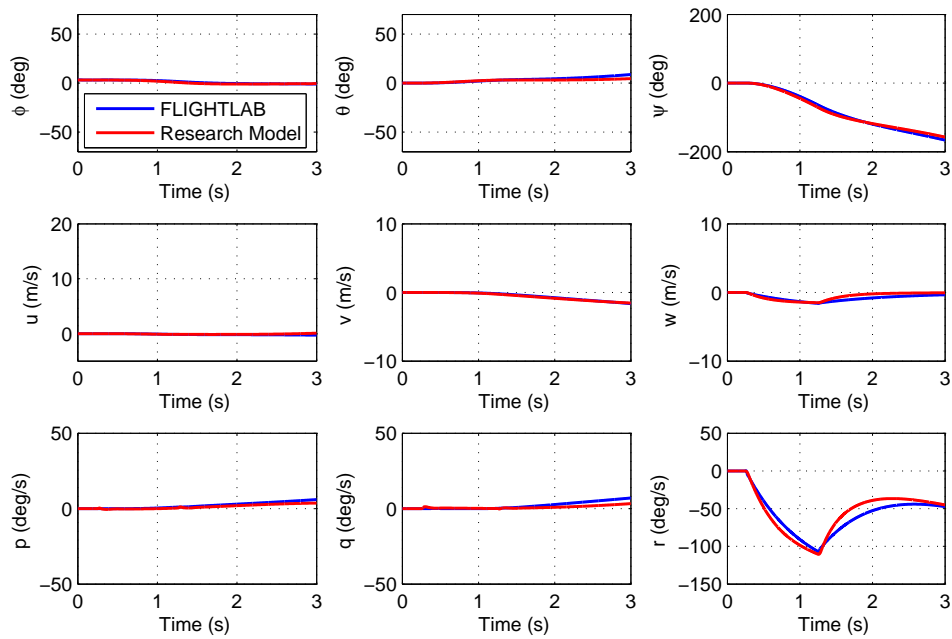


Figure 23: Vehicle motion: response to main rotor collective pitch input (at hover)

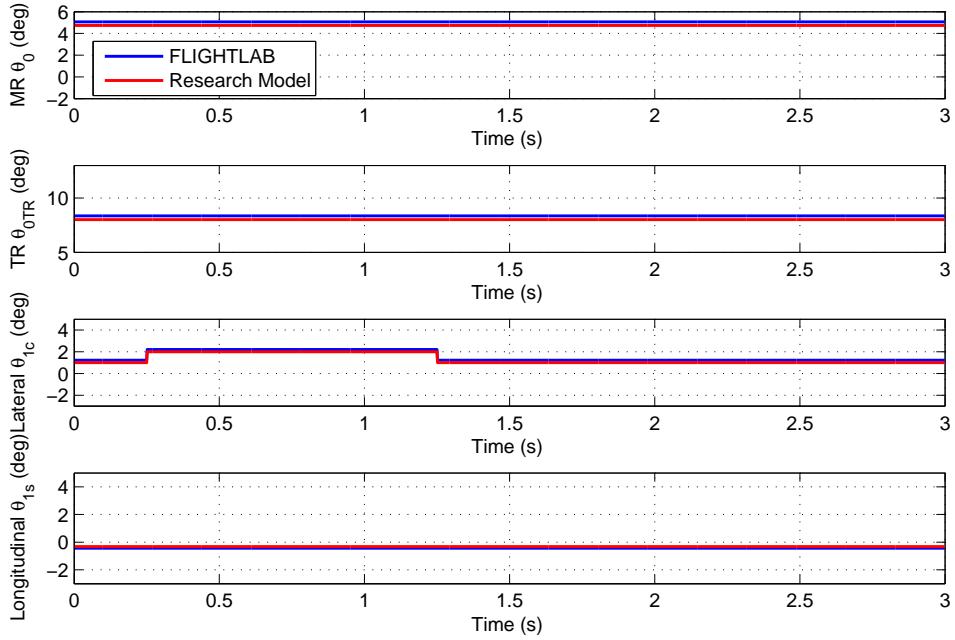


Figure 24: Control inputs

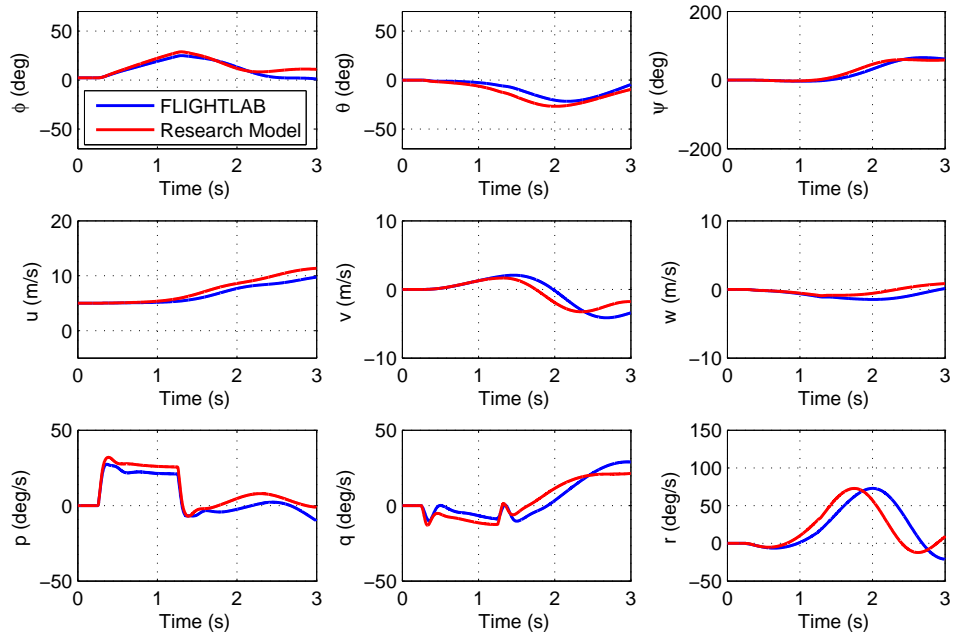


Figure 25: Vehicle motion: response to main rotor lateral cyclic pitch input (at $u = 5 \text{ m/s}$)

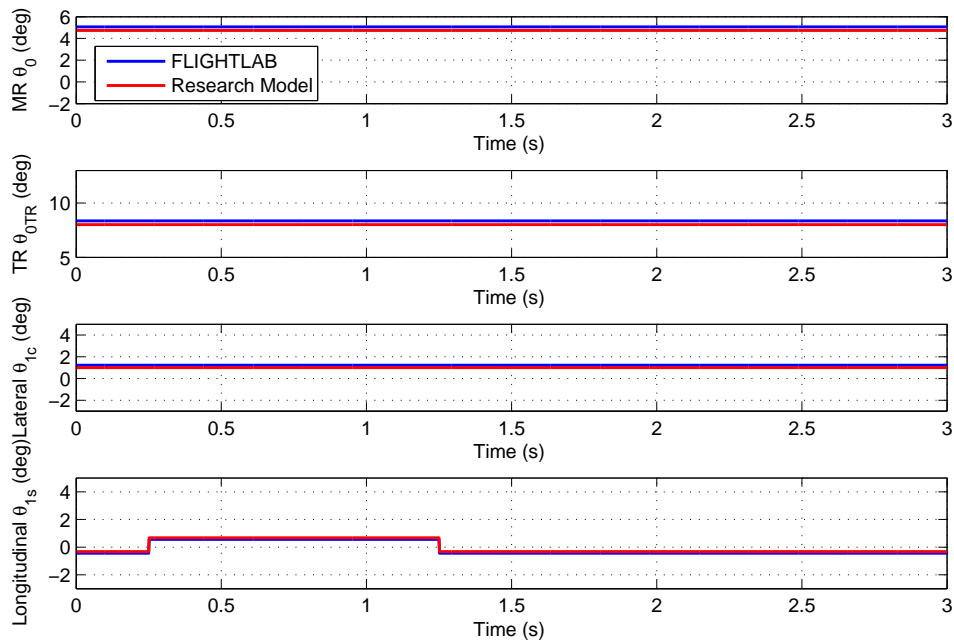


Figure 26: Control inputs

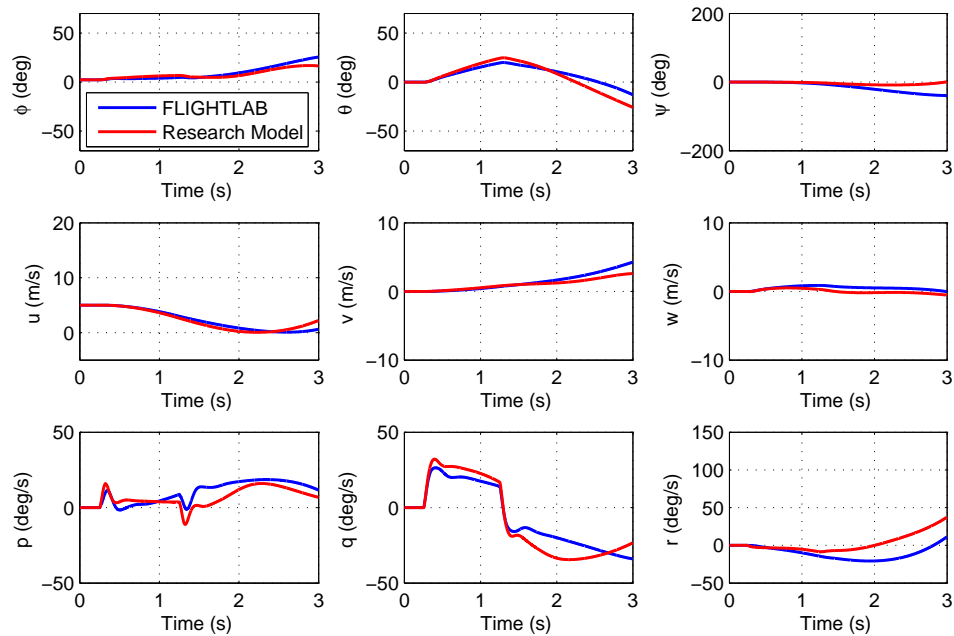


Figure 27: Vehicle motion: response to main rotor longitudinal cyclic pitch input (at $u = 5 \text{ m/s}$)

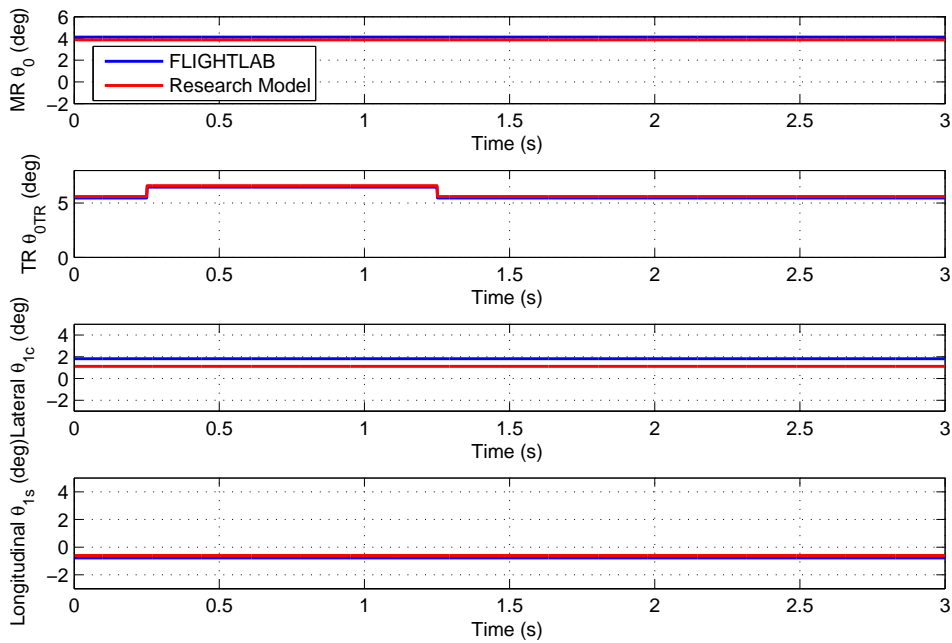


Figure 28: Control inputs

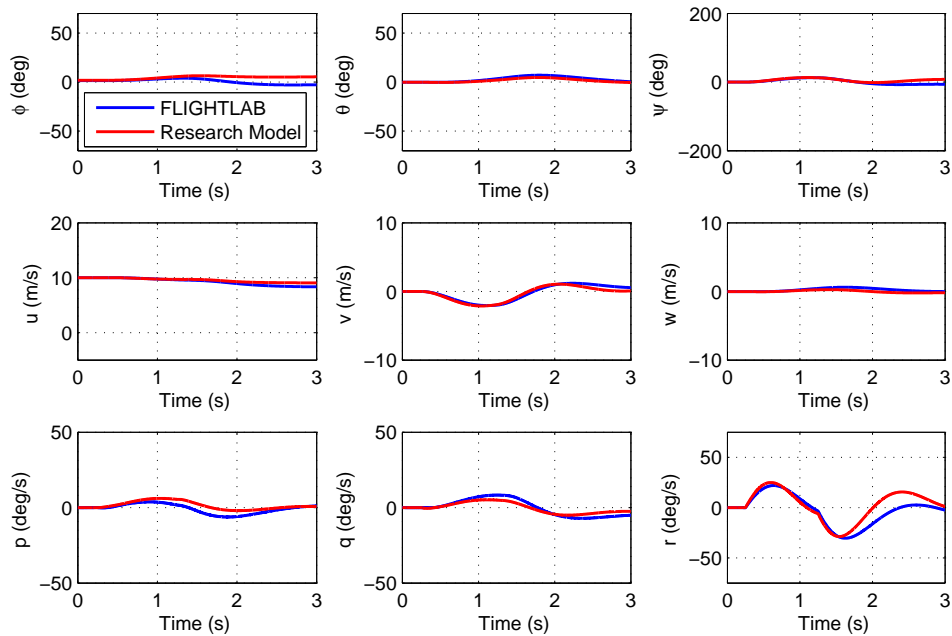


Figure 29: Vehicle motion: response to tail rotor collective pitch input (at $u = 10 \text{ m/s}$)

References

- [1] http://en.wikipedia.org/wiki/Gaussian_quadrature.
- [2] <http://en.wikipedia.org/wiki/Helicopter>.
- [3] Aeronautical design standard-33e-prf. Technical report, U.S. Army Material Command, 1999.
- [4] P. Abbeel, A. Coates, T. Hunter, and A. Y. Ng. Autonomous autorotation of an rc helicopter. In *11th International Symposium on Experimental Robotics (ISER)*, 2008.
- [5] P. Abbeel, A. Coates, M. Quigley, and A. Y. Ng. An application of reinforcement learning to aerobatic helicopter flight. In *NIPS 19*, 2007.
- [6] N. S. Achar and G. H. Gaonkar. Helicopter trim analysis by shooting and finite element methods with optimally damped newton iterations. *AIAA Journal*, 31(2), 1993.
- [7] E. W. Aiken. A mathematical representation of an advanced helicopter for piloted simulator investigations of control-system and display variations. Technical Report TM-81203, NASA, 1980.
- [8] K. B. Amer. Theory of helicopter damping in pitch or roll and comparison with flight measurements. Technical Report TN 2136, NASA Langley Research Center, 1948.
- [9] O. Amidi. *An Autonomous Vision-Guided Helicopter*. PhD thesis, Carnegie Mellon University, 1996.
- [10] T. L. Andersen, D. F. Lauritzen, J. T. Madsen, M. M. Sorensen, and B. A. Mertz. Autonomous inverted hover of a small scale helicopter. Technical report, Project Report, Aalborg University, 2008.
- [11] J. D. Anderson. *Fundamentals of Aerodynamics. Third Ed.* McGraw-Hill Higher Education, NY, 2001.
- [12] Anonymous. Handling qualities requirements for military rotorcrafts. Technical Report ADS-33D-PRF, United States Army and Troop Command, Aviation Research and Development Center, St Louis, Missouri, 1996.
- [13] U. T. P. Arnold, J. D. Keller, H. C. Curtiss, and G. Reichert. The effect of inflow models on the predicted response of helicopters. *Journal of the American Helicopter Society*, pages 25–36, 1998.
- [14] ART. <http://www.flightlab.com/>, Mountain View CA., U.S.A.

-
- [15] ART. *FLIGHTLAB Theory Manual (Vol. One & Two)*. Advanced Rotorcraft Technology, Inc., Mountain View CA, 2006.
- [16] A. Bagai, J. G. Leishman, and J. Park. A free-vortex rotor wake model for maneuvering flight. In *AHS Technical Specialist Meeting on Rotorcraft Acoustics and Aerodynamics*, 1997.
- [17] A. Bagai, J. G. Leishman, and J. Park. Aerodynamic analysis of a helicopter in steady maneuvering flight using a free-vortex rotor wake model. *Journal of the American Helicopter Society*, pages 109–120, 1999.
- [18] J. Bagnell and J. Schneider. Autonomous helicopter control using reinforcement learning policy search methods. In *International Conference on Robotics and Automation*, 2001.
- [19] F. J. Bailey. A simplified theoretical method of determining the characteristics of a lifting rotor in forward flight. Technical Report RNo. 716, NACA, 1941.
- [20] M. G. Ballin. Validation of a real-time engineering simulation of the uh-60a helicopter. Technical Report TM 88360, NASA Ames Research Center, 1987.
- [21] M. G. Ballin and M. A. Dalang-Secrtan. Validation of the dynamic response of a blade-element uh-60 simulation model in hovering flight. In *46th Forum of the American Helicopter Society*, 1990.
- [22] A. E. Barabanov, N. Y. Vazhinsky, and D. V. Romaev. Full autopilot for small electrical helicopter. In *33th European Rotorcraft Forum*, 2007.
- [23] E. Barocela, D. A. Peters, and K. R. Krothapalli. The effect of wake distortion on rotor inflow gradients and off-axis coupling. In *AIAA Atmospheric Flight Mechanics Conference*, 1997.
- [24] P. M. Basset. Modeling of the dynamic inflow on the main rotor and the tail components in helicopter flight mechanics. In *22nd European Rotorcraft Forum*, 1996.
- [25] P. M. Basset and A. Elomari. A rotor vortex wake model for helicopter flight mechanics and its applications to the prediction of the pitch-up phenomena. In *25th European Rotorcraft Forum*, 1999.
- [26] P. M. Basset, O. Heuze, J. V. R. Prasad, and M. Hamers. Finite state rotor induced flow model for interferences and ground effect. In *57th Annual Forum of the American Helicopter Society*, 2001.

-
- [27] P. M. Basset and F. Tchen-Fo. Study of the rotor wake distortion effects on the helicopter pitch-roll cross-couplings. In *24th European Rotorcraft Forum*, 1998.
- [28] P. Bendotti and J. C. Morris. Robust hover control for a model helicopter. In *American Control Conference*, 1995.
- [29] B. Benoit, A. M. Dequin, K. Kampa, W. von Grunhagen, P. M. Basset, and B. Gimonet. Host a general helicopter simulation tool for germany and france. In *56th Annual Forum of the American Helicopter Society*, 2000.
- [30] S. Bhandari and R. Colgren. 6-dof dynamic model for a raptor 50 uav helicopter including stabilizer bar dynamics. In *AIAA Modeling and Simulation Technologies Conference*, 2006.
- [31] G. S. Bir, I. Chopra, and K. Nguyen. Development of umarc (university of maryland advanced rotorcraft code). In *46th Annual Forum of the American Helicopter Society*, 1990.
- [32] B. B. Blake and I. B. Alansky. Stability and control of the yuh-61a. In *31st Forum of the American Helicopter Society*, 1975.
- [33] B. B. Blake and K. Lunn. Helicopter stability and control test methodology. In *AIAA Atmospheric Flight Mechanics Conference*, 1980.
- [34] J. L. Boiffier. *The Dynamics of Flight The Equations*. John Wiley & Sons, Chichester, England, 1998.
- [35] C. R. Brackbill. *Helicopter Rotor Aeroelastic Analysis Using a Refined Elastomeric Damper Model*. PhD thesis, Pennsylvania State University, 2000.
- [36] A. R. S. Bramwell. *Bramwell's Helicopter Dynamics, Second Edition*. AIAA Inc., Reston VA, USA, 2001.
- [37] P. R. Brinson. Towards higher bandwidth in helicopter flight control systems. In *Royal Aeronautical Society Conference on Helicopter Handling Qualities and Control*, 1988.
- [38] G. Buskey, O. Roberts, P. Corke, P. Ridley, and G. Wyeth. *Sensing and Control for a Small-Size Helicopter. in Experimental Robotics VIII, pp. 476-486*. Springer, Berlin/Heidelberg, 2003.
- [39] G. Cai, B. M. Chen, T. H. Lee, and K. Y. Lum. Comprehensive nonlinear modeling of an unmanned-aerial-vehicle helicopter. In *AIAA Guidance, Navigation and Control Conference*, 2008.

-
- [40] G. Cai, B. M. Chen, K. Peng, M. Dong, and T. H. Lee. Modeling and control system design for a uav helicopter. In *Proceedings of the 14th Mediterranean Conference on Control and Automation*, 2006.
- [41] P. J. Carpenter and B. Fridovitch. Effect of a rapid blade pitch increase on the thrust and induced velocity response of a full scale helicopter rotor. Technical Report TN 3044, NASA Langley Research Center, 1953.
- [42] I. C. Cheeseman and N. E. Bennett. The effect of the ground on a helicopter rotor in forward flight. Technical Report 3021, British A.R.C., 1955.
- [43] R. T. N. Chen. A simplified rotor system mathematical model for piloted flight dynamics simulation. Technical Report NTM 78575, NASA Ames Research Center, 1979.
- [44] R. T. N. Chen. Effects of primary rotor parameters on flapping dynamics. Technical Report NTP 1431, NASA Ames Research Center, 1980.
- [45] R. T. N. Chen. Flap-lag equations of motion of rigid, articulated rotor blades with three hinge sequences. Technical Report NTM 100023, NASA Ames Research Center, 1987.
- [46] R. T. N. Chen. A survey of nonuniform inflow models for rotorcraft flight dynamics and control applications. Technical Report NTM 102219, NASA Ames Research Center, 1989.
- [47] R. T. N. Chen. An exploratory investigation of the flight dynamics effects of rotor rpm variations and rotor state feedback in hover. Technical Report TM 103968, NASA Ames Research Center, 1992.
- [48] R. T. N. Chen and W. S. Hindson. Influence of dynamic inflow on the helicopter vertical response. Technical Report NTM 88327, NASA Ames Research Center, 1986.
- [49] R. T. N. Chen and W. S. Hindson. Influence of high-order dynamics on helicopter flight control system bandwidth. *AIAA Journal of Guidance, Control, and Dynamics*, 9(2):190–197, 1986.
- [50] R. T. N. Chen, J. V. Lebacqz, E. W. Aiken, and M. B. Tischler. Helicopter mathematical models and control law development for handling qualities research. Technical Report NCR 2495, NASA Ames Research Center, 1988.
- [51] M. La Civita. *Integrated Modeling and Robust Control for Full-Envelope Flight of Robotic Helicopters*. PhD thesis, Carnegie Mellon University, 2002.

-
- [52] A. Conway. *Autonomous Control of an Unstable Helicopter Using Carrier Phase GPS Only*. PhD thesis, Stanford University, 1995.
- [53] R. Cunha and C. Silvestre. Dynamic modeling and stability analysis of model-scale helicopters with bell-hiller stabilizing bar. In *AIAA Guidance, Navigation, and Control Conference*, 2003.
- [54] H. C. Curtiss. Stability and control modeling. In *12th European Rotorcraft Forum*, 1986.
- [55] H. C. Curtiss. Physical aspects of rotor body coupling in stability and control. In *46th Annual Forum of the American Helicopter Society*, 1990.
- [56] H. C. Curtiss. Aerodynamic models and the off-axis response. In *55th Annual Forum of the American Helicopter Society*, 1999.
- [57] H. C. Curtiss. Rotorcraft stability and control, past, present, and future. the 20th annual alexander a. nikolsky lecture. *Journal of the American Helicopter Society*, 2003.
- [58] H. C. Curtiss and N. K. Shupe. A stability and control theory for hingeless rotors. In *27th Annual Forum of the American Helicopter Society*, 1971.
- [59] R. Czyba. Modelling of unmanned model-scale helicopter dynamics for needs of the simulator. In *11th IFAC Symposium on Large Scale Complex Systems Theory and Applications*, 2007.
- [60] A. de Jong. Helicopter uav control using classical control. Technical report, Master Thesis, Delft University of Technology, 2004.
- [61] DoD. Flying qualities of piloted v/stol aircraft. Technical Report Specification MIL-F-83300, 1970.
- [62] DoD. Unmanned aircraft systems (uas) roadmap 2005-2030. Technical report, U.S.A. DoD, 2005.
- [63] C. W. Ellis. Effects of rotor dynamics on helicopter automatic control system requirements. *Aeronautical Engineering Review*, 1953.
- [64] R. W. Empey and R. A. Ormiston. Tail rotor thrust on a 5.5-foot helicopter model in ground effect. In *30th Forum of the American Helicopter Society*, 1974.
- [65] J. M. Engel. Reinforcement learning applied to uav helicopter control. Technical report, Master Thesis, Delft University of Technology, 2005.

-
- [66] J. W. Fletcher and M. B. Tischler. Improving helicopter flight mechanics models with laser measurements of blade flapping. In *53rd Annual Forum of the American Helicopter Society*, 1997.
- [67] C. Friedman, A. Fertman, and O. Rand. A generic rotorcraft simulation using matlab/simulink. In *65th Annual Forum of the American Helicopter Society*, 2009.
- [68] K. Furuta, Y. Ohyama, and O. Yamano. Dynamics of rc helicopter and control. *Mathematics and Computers in Simulation*, 26:148–159, 1984.
- [69] G. H. Gaonkar and D. A. Peters. Effectiveness of current dynamic-inflow models in hover and forward flight. *Journal of the American Helicopter Society*, 31(2), 1986.
- [70] G. H. Gaonkar and D. A. Peters. Review of dynamic inflow modeling for rotorcraft flight dynamics. *Vertica*, pages 213–242, 1988.
- [71] V. Gavrillets, B. Mettler, and E. Feron. Nonlinear model for a small-size acrobatic helicopter. In *AIAA Guidance, Navigation and Control Conference*, 2001.
- [72] A. Gessow and G. C. Myers. *Aerodynamics of the Helicopter*. College Park Pr, 1999.
- [73] N. B. Grady, M. T. Frye, and C. Qian. The instrumentation and flight testing of a rotorcraft vehicle for undergraduate flight control research. In *AIAA Modeling and Simulation Technologies Conference and Exhibit*, 2006.
- [74] W. E. Hackett, T. S. Gernett, and B. V. Borek. Mathematical model for the ch-47b helicopter capable of real-time simulation of the full flight envelope. Technical Report CR 166458, NASA, 1983.
- [75] U. B. Hald, M. V. Hesselbaek, and M. Siegumfeldt. Nonlinear modeling and optimal control of a miniature autonomous helicopter. Technical report, Master Thesis, Aalborg University, 2006.
- [76] W. E. Hall and A. E. Bryson. Inclusion of rotor dynamics in controller design for helicopters. *AIAA Journal of Aircraft*, 10(4):200–206, 1973.
- [77] M. Hamers and P. M. Basset. Application of the finite state unsteady wake model in helicopter flight dynamic simulation. In *26th European Rotorcraft Forum*, 2000.
- [78] M. Hamers and W. von Grunhagen. Nonlinear helicopter model validation applied to realtime simulations. In *53rd Annual Forum of the American Helicopter Society*, 1997.

-
- [79] J. M. Harrison and P. Shanthakumaran. Ah-64 apache engineering simulation - flyrt engineering manual. Technical Report TR 90-A-011, USAAVSCOM, 1990.
- [80] J. M. Harrison and P. Shanthakumaran. A helicopter flight model suitable for aggressive maneuvers. Technical Report RTTN-91-004, MDHC, 1991.
- [81] C. He, C. S. Lee, and W. Chen. Rotorcraft simulation model enhancement to support design, testing and operational analysis. *Journal of the American Helicopter Society*, pages 284–292, 2000.
- [82] C. He, C. S. Lee, and W. Chen. Technical notes - finite state induced flow model in vortex ring state. *Journal of the American Helicopter Society*, pages 318–320, 2000.
- [83] C. J. He. *Development and Application of a Generalized Dynamic Wake Theory for Lifting Rotors*. PhD thesis, Georgia Institute of Technology, 1989.
- [84] R. K. Heffley and M. A. Mnich. Minimum-complexity helicopter simulation math model. Technical Report NCR 177476, NASA Ames Research Center, 1988.
- [85] H. H. Heyson. Linearized theory of wind-tunnel jet-boundary corrections and ground effect for vtol-stol aircraft. Technical Report TR R-124, NASA Langley Research Center, 1962.
- [86] H. H. Heyson. Theoretical study of the effect of the ground proximity on the induced efficiency of helicopter rotors. Technical Report TM X-71951, NASA Ames Research Center, 1977.
- [87] H. H. Heyson. A brief survey of rotary wing induced velocity theory. Technical Report TM 78741, NASA Langley Research Center, 1978.
- [88] K. B. Hilbert. A mathematical model of the uh-60 helicopter. Technical Report TM-85890, NASA Ames Research Center, 1984.
- [89] S. W. Hong and H. C. Curtiss. An analytic modeling and system identification study of rotor fuselage dynamics at hover. Technical Report CR-192303, NASA, 1993.
- [90] J. A. Houck, F. L. Moore, J. J. Howlett, K. S. Pollock, and M. M. Browne. Rotor systems research aircraft simulation mathematical model. Technical Report NTM 78629, NASA Langley Research Center, 1977.

-
- [91] S. S. Houston. Analysis of rotorcraft flight dynamics in autorotation. *AIAA Journal of Guidance, Control, and Dynamics*, 25(1):33–39, 2002.
- [92] J. Howlett. Uh-60a black hawk engineering simulation program: Volume i - mathematical model. Technical Report CR-166309, NASA, 1981.
- [93] J. J. Howlett. Rsra simulation model—vol. i. mathematical model equations. Technical Report SER-72009, Sikorsky Aircraft, 1974.
- [94] R. J. Huston and C. E. K. Morris. A wind-tunnel investigation of helicopter directional control in rearward flight in ground effect. Technical Report TN D-6118, NASA Langley Research Center, 1965.
- [95] J. Jimenez, A. Desopper, A. Taghizad, and L. Binet. Induced velocity model in steep descent and vortex ring state prediction. In *27th European Rotorcraft Forum*, 2001.
- [96] E. N. Johnson and P. A. DeBitetto. Modeling and simulation for small autonomous helicopter development. In *AIAA Modeling and Simulation Technologies Conference*, 1997.
- [97] W. Johnson. Helicopter optimal descent and landing after power loss. Technical Report TM 73-244, NASA Ames Research Center, 1977.
- [98] W. Johnson. *Helicopter Theory*. Dover Publications Inc., NY, USA, 1994.
- [99] J. D. Keller. An investigation of helicopter dynamic coupling using an analytical model. *Journal of the American Helicopter Society*, 41(4):322330, 1996.
- [100] S. P. Khaligh, F. Fahimi, and M. Saffarian. Comprehensive aerodynamic modeling of a small autonomous helicopter rotor at all flight regimes. In *AIAA Modeling and Simulation Technologies Conference*, 2009.
- [101] F. D. Kim, R. Celi, and M. B. Tischler. Forward flight trim and frequency response validation of a helicopter simulation model. *Journal of Aircraft*, 30(6), 1993.
- [102] S. K. Kim and T. M. Tilbury. Mathematical modeling and experimental identification of a model helicopter. In *AIAA Modeling and Simulation Technologies Conference*, 1998.
- [103] B. D. Kothmann, Y. Lu, E. DeBrun, and J. Horn. Perspectives on rotorcraft aerodynamic modeling for flight dynamics applications. In *4th Decennial Specialists Conference on Aeromechanics*, 2004.

-
- [104] K. R. Krothapalli, J. V. R. Prasad, and D. A. Peters. Development of a comprehensive wake theory for lifting rotors. In *AIAA Atmospheric Flight Mechanics Conference*, 1996.
- [105] K. R. Krothapalli, J. V. R. Prasad, and D. A. Peters. Helicopter rotor dynamic inflow modeling for maneuvering flight. *Journal of the American Helicopter Society*, pages 129–139, 2001.
- [106] D. L. Kunz. Comprehensive rotorcraft analysis: Past, present, and future. In *AIAA/ASME/ASCE/AHS/ASC Structures, Structural Dynamics & Materials Conference*, 2005.
- [107] G. J. Leishman. *Principles of Helicopter Aerodynamics*. Cambridge University Press, Cambridge, UK, 2000.
- [108] B. Manimala, D. Walker, and G. Padfield. Rotorcraft simulation modeling and validation for control design and load prediction. In *31st European Rotorcraft Forum*, 2005.
- [109] M. H. Mansur and M. B. Tischler. An empirical correction method for improving off-axes response prediction in component type flight mechanics helicopter models. Technical Report TM 110406, NASA Ames Research Center, 1997.
- [110] M. H. Mansur, M. B. Tischler, M. Chaimovich, A. Rosen, and O. Rand. Modeling methods for high-fidelity rotorcraft flight mechanics simulation. Technical Report TM 103842, NASA Ames Research Center, 1992.
- [111] L. Marconi and R. Naldi. Robust nonlinear control for a miniature helicopter for aerobatic maneuvers. In *32nd European Rotorcraft Forum*, 2006.
- [112] J. S. G. McVicar and G. Bradley. Engineering notes - robust and efficient trimming algorithm for application to advanced mathematical models of rotorcraft. *AIAA Journal of Aircraft*, 32(2), 1995.
- [113] B. Mettler. *Identification Modelling and Characteristics of Miniature Rotorcraft*. Kluwer Academic Publishers, Norwell Mass, USA, 2003.
- [114] D. G. Miller and F. White. A treatment of the impact of rotor-fuselage coupling on helicopter handling qualities. In *43rd Annual Forum of the American Helicopter Society*, 1987.
- [115] P. Misra and P. Enge. *Global Positioning System: Signals, Measurements and Performance, Second Edition*. Ganga-Jamuna Press, Lincoln MA, USA, 2006.

-
- [116] K. Miyajima. Analytical design of a high performance stability and control augmentation system for a hingeless rotor helicopter. *Journal of the American Helicopter Society*, 1979.
- [117] J. C. Morris, M. van Nieuwstadt, and P. Bendotti. Identification and control of a model helicopter in hover. In *American Control Conference*, 1994.
- [118] C. Munzinger. Development of a real-time flight simulator for an experimental model helicopter. Technical report, Master Thesis, Georgia Institute of Technology, 1998.
- [119] A. Y. Ng, A. Coates, M. Diel, V. Ganapathi, J. Schulte, B. Tse, E. Berger, and E. Liang. Autonomous inverted helicopter flight via reinforcement learning. In *International Symposium on Experimental Robotics*, 2004.
- [120] A. Y. Ng, H. J. Kim, M. Jordan, and S. Sastry. Autonomous helicopter flight via reinforcement learning. In *Neural Information Processing Systems (NIPS)*, 2004.
- [121] G. D. Padfield. *Helicopter Flight Dynamics*. Blackwell Science Ltd, Oxford, UK, 1996.
- [122] T. J. Pallett and S. Ahmad. Real-time helicopter flight control: Modelling and control by linearization and neural networks. Technical Report TR-EE 91-35, Purdue University School of Electrical Engineering, 1991.
- [123] D. A. Peters and D. Barwey. A general theory of rotorcraft trim. In *AIAA*, 1995.
- [124] D. A. Peters, D. D. Boyd, and C. J. He. Finite-state induced-flow model for rotors in hover and forward flight. *Journal of the American Helicopter Society*, pages 5–17, 1989.
- [125] D. A. Peters, M. Chouchane, and M. Fulton. Helicopter trim with flap-lag-torsion and stall by an optimized controller. *AIAA Journal of Guidance*, 13(5), 1990.
- [126] D. A. Peters and N. HaQuang. Technical notes - dynamic inflow for practical applications. *Journal of the American Helicopter Society*, pages 64–68, 1988.
- [127] D. A. Peters and C. He. Technical note: Modification of mass-flow parameter to allow smooth transition between helicopter and windmill states. *Journal of the American Helicopter Society*, pages 275–278, 2006.

-
- [128] D. A. Peters and C. J. He. Correlation of measured induced velocities with a finite-state wake model. *Journal of the American Helicopter Society*, 36(3), 1991.
- [129] D. A. Peters and C. J. He. Finite state induced flow models part ii: Three-dimensional rotor disk. *AIAA Journal of Aircraft*, 32(2):323–333, 1995.
- [130] D. A. Peters and A. P. Izadpanah. Helicopter trim by periodic shooting with newton-raphson iteration. In *37th Annual Forum of the American Helicopter Society*, 1981.
- [131] D. A. Peters and B. S. Kim. Control settings for a trimmed stalled rotor by an automatic feedback system. In *AIAA*, 1981.
- [132] D. A. Peters, J. A. Morillo, and A. M. Nelson. New developments in dynamic wake modeling for dynamics applications. *Journal of the American Helicopter Society*, pages 120–127, 2003.
- [133] J. D. Phillips. Mathematical model of the 34-3g helicopter. Technical Report TM 84316, NASA, 1982.
- [134] D. M. Pitt and D. A. Peters. Theoretical prediction of dynamic-inflow derivatives. In *6th European Rotorcraft Forum*, 1980.
- [135] D. M. Pitt and D. A. Peters. Theoretical prediction of dynamic-inflow derivatives. *Vertica*, 5:21–34, 1981.
- [136] J. V. R. Prasad, T. Fanciullo, J. Zhao, and D. A. Peters. Towards a high fidelity inflow model for maneuvering and in-ground effect flight simulation. In *57th Annual Forum of the American Helicopter Society*, 2001.
- [137] J. V. R. Prasad, H. Zhang, and D. A. Peters. Finite state in-ground effect inflow models for lifting rotors. In *53rd Annual Forum of the American Helicopter Society*, 1997.
- [138] J. V. R. Prasad, J. Zhao, and D. A. Peters. Modeling of rotor dynamic wake distortion during maneuvering flight. In *AIAA Atmospheric Flight Mechanics Conference*, 2001.
- [139] R. W. Prouty. Ground effect and the helicopter - a summary. In *AIAA Aircraft Design Systems and operations Meeting*, 1985.
- [140] R. W. Prouty. *Helicopter Performance, Stability, and Control*. Krieger Publishing Company, Malabar, Florida USA, 1995.

-
- [141] W. F. Putman. An experimental investigation of ground effect on a four-propeller tilt-wing v/stol model. Technical Report TR 68-45, USAAVLABS, 1968.
- [142] O. Rand and S. M. Barkai. Numerical evaluation of the equations of motion of helicopter blades and symbolic exactness. *Journal of the American Helicopter Society*, 1995.
- [143] J. M. Roberts, P. I. Corke, and G. Buskey. Low-cost flight control system for a small autonomous helicopter. In *Australian Conference on Robotics and Automation*, 2002.
- [144] A. Rosen and A. Isser. A new model of rotor dynamics during pitch and roll of a hovering helicopter. *Journal of the American Helicopter Society*, 1995.
- [145] S. Saripalli, J. F. Montgomery, and G. S. Sukhatme. Visually-guided landing of an autonomous aerial vehicle. *IEEE Transactions on Robotics and Automation*, 19(3):371–381, 2003.
- [146] S. Saripalli and G. Sukhatme. Landing on a moving target using an autonomous helicopter. In *International Conference on Field and Service Robotics*, 2003.
- [147] G. J. Schulein, M. B. Tichler, M. H. Mansur, and A. Rosen. Validation of cross-coupling modeling improvements for uh-60 flight mechanics simulations. *Journal of the American Helicopter Society*, 47(3):209–213, 2002.
- [148] E. Seckel and H. C. Curtiss. Aerodynamic characteristics of helicopter rotors. Technical Report No. 659, Department of Aerospace and Mechanical Engineering, Princeton University, 1962.
- [149] O. Shakernia, C. S. Sharp, R. Vidal, D. H. Shim, Y. Ma, and S. Sastry. Multiple view motion estimation and control for landing an unmanned aerial vehicle. In *International Conference on Robotics and Automation*, 2002.
- [150] R. S. Shevell. *Fundamentals of Flight*. Prentice Hall, Upper Saddle River NJ, 1989.
- [151] D. H. Shim. *Hierarchical Control System Synthesis for Rotorcraft-based Unmanned Aerial Vehicles*. PhD thesis, University of California at Berkeley, 2000.
- [152] G. J. Sissingh. The effect of induced velocity variation on helicopter rotor damping pitch or roll. Technical Report 101, British A.R.C., 1952.

-
- [153] T. Sudiyanto, A. Budiyo, and H. Y. Sutarto. Hardware in-the-loop simulation for control system designs of model helicopter. In *Aerospace Indonesia Meeting, Bandung*, 2005.
- [154] S. Taamallah. A qualitative introduction to the vortex-ring-state, autorotation, and optimal autorotation. In *36th European Rotorcraft Forum*, 2010.
- [155] S. Taamallah. Small-scale helicopter blade flap-lag equations of motion for a flybarless pitch-lag-flap main rotor (submitted for publication). In *AIAA Modeling and Simulation Technologies Conference*, 2011.
- [156] M. D. Takahashi. A flight-dynamic helicopter mathematical model with a single flap-lag-torsion main rotor. Technical Report TM 102267, NASA Ames Research Center, 1990.
- [157] M. D. Takahashi, J. W. Fletcher, and M. B. Tischler. Development of a model following control law for inflight simulation using analytical and identified models. In *51st Forum of the American Helicopter Society*, 1995.
- [158] P. D. Talbot, B. E. Tinling, W. A. Decker, and R. T. N. Chen. A mathematical model of a single main rotor helicopter for piloted simulation. Technical Report NTM 84281, NASA Ames Research Center, 1982.
- [159] O. Tanner. *Modeling, Identification, and Control of Autonomous Helicopters*. PhD thesis, ETH Zurich, 2003.
- [160] C. Theodore and R. Celi. Prediction of the off-axis response to cyclic pitch using a maneuvering free wake model. In *25th European Rotorcraft Forum*, 1999.
- [161] M. B. Tischler. System identification requirements for high bandwidth rotorcraft flight control system design. In *AGARD LS-178 Rotorcraft System Identification*, 1991.
- [162] M. B. Tischler. Identification of bearingless main rotor dynamic characteristics from frequency-response wind-tunnel test data. *Journal of the American Helicopter Society*, 1999.
- [163] UAVS. Brentford, U.K., 1998.
- [164] T. van Holten. Upgrading of classical lifting-line theory to obtain accurate flight mechanical helicopter models: Improved correction for sweep effects. In *Advances in Rotorcraft Technology AGARD-FVP*, 1996.

-
- [165] W. R. M. van Hoydonck, H. Haverdings, and M. D. Pavel. A review of rotorcraft wake modeling methods for flight dynamics applications. In *35th European Rotorcraft Forum*, 2009.
- [166] W. R. M. van Hoydonck and M. Pavel. Development of a modular, generic helicopter flight dynamics model for real-time simulations. In *AIAA Modeling and Simulation Technologies Conference and Exhibit*, 2007.
- [167] C. M. Velez, A. Agudelo, and J. Alvarez. Modeling, simulation and rapid prototyping of an unmanned mini-helicopter. In *AIAA Modeling and Simulation Technologies Conference and Exhibit*, 2006.
- [168] W. von Grunhagen. Dynamic inflow modeling for helicopter rotors and its influence on the prediction of cross-couplings. In *AHS Aeromechanics Specialists Conference*, 1995.
- [169] G. M. Voorsluijs. A modular generic helicopter model. Technical report, Master Thesis, Delft University of Technology, 2002.
- [170] J. M. Weber, T. Y. Liu, and W. Chung. A mathematical simulation model of a ch-47b helicopter. Technical Report TM 84351, NASA, 1984.
- [171] M. F. Weilenmann and H. P. Geering. Test bench for rotorcraft hover control. *AIAA Journal of Guidance, Control, and Dynamics*, 17(4):729–736, 1994.
- [172] D. A. Wells. *Lagrangian Dynamics*. McCraw-Hill Co., 1967.
- [173] H. Xin and Z. Gao. An experimental investigation of model rotors operating in vertical descent. In *19th European Rotorcraft Forum*, 1993.
- [174] W.T. Yeager, W. H. Young, and W. H. Mantay. A wind-tunnel investigation of parameters affecting helicopter directional control in ground effect. Technical Report TN D-7694, NASA Langley Research Center, 1974.
- [175] J. Zhao. *Dynamic Wake Distortion Model for Helicopter Maneuvering Flight*. PhD thesis, Georgia Institute of Technology, 2005.
- [176] J. Zhao, J. V. R. Prasad, and D. A. Peters. Rotor dynamic wake distortion model for helicopter maneuvering flight. *Journal of the American Helicopter Society*, pages 414–424, 2004.
- [177] L. Zhao and V. R. Murthy. Optimal controller for an autonomous helicopter in hovering and forward flight. In *47th AIAA Aerospace Sciences Meeting*, 2009.

-
- [178] X. Zhao and H. C. Curtiss. A linearized model of helicopter dynamics including correlation with flight test. In *2nd International Conference on Rotorcraft Basic Research*, 1988.
- [179] X. Zhao and H. C. Curtiss. A study of helicopter stability and control including blade dynamics. Technical Report TR 1823T, NASA Ames Research Center, 1988.
- [180] Y. Zhao, A. A. Jhemi, and R. T. N. Chen. Optimal vtol operation of a multiengine helicopter in the event of one engine failure. In *AIAA Guidance, Navigation and Control Conference*, 1995.